Substrate use and climate structure chemical signal composition across Australia's most diverse gecko radiation

Running title: Substrate, climate and chemical signals

Scott A. Macor[1*], Stephen M. Zozaya[2], Conrad J. Hoskin[1], Wesley J. Read[2], Craig Moritz[2], Megan Higgie[1]

1 *College of Science and Engineering, James Cook University, Townsville, Queensland, Australia*

2 *Division of Ecology and Evolution, Research School of Biology, The Australian National University, Canberra, Australian Capital Territory, Australia*

*Corresponding author: Scott A. Macor (scott.macor@my.jcu.edu.au)

Abstract

Sensory drive theory predicts that communication signals coevolve with sensory systems and the local transmission environment, generating divergence in signals across environmental gradients. Understanding how signalling traits evolve in response to environmental conditions is central to explaining patterns of phenotypic divergence and ecological specialisation, given their potential roles in social interactions, mate choice, and species recognition. Here, we investigate how the abiotic environment shapes the evolution of chemical signalling in Australia's most speciose gecko genus, *Gehyra*. We analysed male epidermal pore secretions from 754 individuals, representing 58 species and species-level lineages across climatic gradients spanning the Australian monsoonal tropics and arid zone. Chemical blends were characterised using gas chromatography, and multivariate phylogenetic comparative analyses tested for associations between chemical composition and the abiotic environment. Composition varied along two axes: substrate use, with saxicoline lineages showing blends distinct from arboreal and generalist lineages; and climate, primarily vapour pressure, with some evidence that moisture effects on blend composition are stronger under hotter conditions. Results were robust to sensitivity analyses considering within-lineage variation. These findings are consistent with sensory drive theory and indicate that substrate use and climate are both associated with variation in chemical communication signals at macroevolutionary scales.

Keywords: sensory drive, *Gehyra*, lizard, epidermal pore secretion, phylogenetic comparative methods, pheromones

Introduction

Understanding how signalling traits evolve in response to abiotic conditions is central to explaining patterns of phenotypic divergence, ecological specialisation, and premating isolation. Signals used in mate choice, territoriality, and other social interactions must be effectively transmitted, detected, and interpreted within the environments in which organisms live. Sensory drive theory predicts that environmental conditions shape signal design by favouring signal properties that maximise efficacy and reliability under local climatic and ecological constraints (Endler, 1992; Boughman, 2002; Seehausen et al., 2008). Classic examples include adaptive shifts in visual signals of fishes across differing light environments (Maan et al., 2017; Torres-Dowdall et al., 2017) and divergence in acoustic signals of frogs and birds across structurally complex or noisy habitats (Boeckle et al., 2009; Hoskin & Goosem, 2010; Goutte et al., 2016; To et al., 2021). Under this framework, signalling traits are expected to diverge rapidly across environmental gradients and may play a disproportionate role in ecological specialisation and premating isolation. Because environmentally driven signal divergence can disrupt mate recognition between populations, sensory drive provides a mechanistic link between environmental gradients and speciation (Boughman, 2002; Maan & Seehausen, 2011).

Chemical signals—such as pheromones—are particularly well suited for examining environment–signal relationships. Pheromones mediate a wide range of behaviours, including mate recognition, territoriality, and social signalling (Wyatt, 2003; Barbosa et al., 2006; Müller-Schwarze, 2006; Symonds & Elgar, 2008; Mason & Parker, 2010; Martín & López, 2011). In many vertebrates, these signals are produced in specialised skin or cloacal glands and are emitted into the environment, where they function in within- and between-species communication (Alberts, 1993; Müller-Schwarze, 2006; Weldon et al., 2008; Martín & López, 2014). Because chemical signals are largely free of structural constraints, they can respond rapidly to selection imposed by environmental conditions, sexual selection, and social interactions (Smadja & Butlin, 2009; Baeckens et al., 2018). As a result, chemical traits may capture ecological and behavioural divergence that is not yet reflected

in other phenotypic axes, facilitating premating isolation and speciation even in the absence of obvious morphological change. This pattern has been observed in several morphologically cryptic species complexes of lizards (Barbosa et al., 2006; Scott et al., 2015; Doughty et al., 2018a; Zozaya et al., 2019b) as well as in many other groups with non-visual signalling modalities (Hopkins & Bass, 1981; Higgie et al., 2000; Hoskin & Higgie, 2010; Weber et al., 2016, 2018).

Squamate reptiles (lizards and snakes) are well suited for studying the evolution of chemical signals. With over 12,000 currently described species, squamates are the most diverse group of terrestrial vertebrates, occupying nearly every habitat type except the high polar regions (Uetz et al., 2026). Many squamates possess a well-developed vomeronasal system and rely heavily on chemical cues for social and reproductive interactions (Cooper et al., 1996; Halpern & Martínez-Marcos, 2003; Martín & López, 2014). There are multiple sources of chemical signals in squamates, with compounds exuded from epidermal pores, cloacal glands, and other skin surfaces (Martín & López, 2014; García-Roa et al., 2017). These secretions often contain a mix of lipophilic molecules and proteins, with lipids in particular showing high diversity and potential for environmental and behavioural modulation (Weldon et al., 2008; Zozaya et al., 2022).

Environmental conditions are expected to exert strong selective pressures on chemical signal composition (Alberts, 1992; Baeckens et al., 2018; Zozaya et al., 2022). Many chemical signals function in external environments—sometimes persisting on substrates for extended periods—and their structure and stability must therefore withstand local temperature and humidity, which govern evaporation and degradation rates, and rainfall, which can wash deposited signals from substrates altogether (Endler, 1992; Martín & López, 2013; Apps et al., 2015). Consistent with these pressures, lizards in hotter, more arid habitats tend to produce more stable, high molecular weight compounds that resist evaporation, whereas species in mesic environments produce richer blends of more volatile compounds suited to airborne transmission (Baeckens et al., 2018). Substrate use also influences signal selection, partly through its effect on local microclimate but also through two

pathways that climate alone does not capture. First, substrates differ in their chemical background: vegetation produces volatile compounds against which arboreal signals must be detected, whereas rock surfaces are comparatively inert (Wilson et al., 2015). Second, substrates differ in their physical and chemical properties: porous, absorbent bark retains different compound classes than smooth, non-absorbent rock (Regnier & Goodwin, 1977; Apps et al., 2015). Because vegetation and rock occur across many climatic zones, these substrate-specific selective pressures can act partly independently of broad climate. Empirically, ground-dwelling *Podarcis* lizards deposit waxier scent marks than saxicoline congeners, interpreted as an adaptation to the persistence challenges of warm, humid vegetated ground (García-Roa et al., 2016), and broad-scale comparative work in geckos and lacertids shows that investment in chemical signalling itself tracks substrate use (Baeckens et al., 2015; Agashe et al., 2025), with arboreal and saxicoline species possessing more pores than terrestrial generalists (Agashe et al., 2025). Together, these patterns illustrate the central prediction of sensory drive theory: that environmental conditions shape signal design to maximise efficacy of transmission and perception (Endler, 1992; Boughman, 2002; Seehausen et al., 2008).

Broad comparative studies of chemical signal evolution remain rare across animals, particularly in vertebrates, where most work has been limited to single species or small clades (Roberts et al., 2010; Khannoon et al., 2011; delBarco-Trillo et al., 2012; García-Roa et al., 2016; Van Bocxlaer et al., 2016; Ibáñez et al., 2017; Joshi et al., 2022). Recent comparative analyses have begun to identify environmental correlates of chemical signal variation (Baeckens et al., 2018; Mangiacotti et al., 2021; Zozaya et al., 2022), but which environmental factors predict chemical signal composition, and whether they act consistently across large radiations once shared ancestry is accounted for, remain poorly resolved. These questions are especially pressing in morphologically conservative radiations, where behavioural traits—including chemical signals—may be a major axis along which divergence proceeds. Here, we address these gaps using the Australian gecko genus *Gehyra*, a radiation of more than 60 described and candidate species distributed across much of the Australian continent. The genus shows high levels of cryptic diversity (e.g., Doughty et al., 2018a,

2018b; Oliver et al., 2020; Read et al., 2026), and previous work on another Australian gekkonid genus, *Heteronotia*, suggests the potential for species-specificity in chemical traits despite conservative morphologies (Zozaya et al., 2019b, 2023). We sampled epidermal pore secretions from 790 male individuals from 58 lineages spanning a wide range of climatic conditions and using several broad substrate types. Using gas chromatography, we quantified multivariate variation in chemical signal composition and applied phylogenetic comparative methods to test whether chemical signal composition is associated with substrate use and key environmental variables, including vapour pressure and temperature. By integrating individual-level data, a phylogenomic framework and multiple abiotic axes, this study provides a broad comparative test of sensory drive predictions for chemical signal evolution in a vertebrate radiation.

Methods

Field sampling

We collected epidermal pore secretions from 58 genetically distinct lineages of the Australian gecko genus *Gehyra* across two sampling trips. We did field sampling from September–December in 2021 and 2022, spanning ca. 3,450 km east–west and 1,600 km north–south, collecting epidermal pore secretions from 790 individuals from across the Australian monsoonal tropics and arid zone (Fig. 1). We aimed to sample at least ten adult male geckos per lineage, with individuals collected from one or more sites depending on the extent of their geographic distributions, site accessibility, and species detection. Sample sizes varied among lineages due to differences in geographic range and local abundance. We located the geckos at night using a head torch, captured them by hand, and processed them within 1–2 hours. We recorded GPS coordinates, assigned each gecko a unique ID, sampled epidermal pore secretions, measured snout-to-vent length (SVL), collected a tissue sample (~5 mm of the tail-tip), and released the animal at the point of capture after processing. We used the

methods of Zozaya et al. (2019b) to sample epidermal secretions from male geckos. Briefly, we used sterilised tweezers to gently apply pressure around the pre-cloacal epidermal pores (Fig. 2), to exude the waxy secretions. We then used a sterilised stainless-steel probe to remove the secretions and place them into individual glass microvials. We sealed each vial with a PTFE-lined cap. At each site, we prepared a control sample by following this procedure without collecting secretions, allowing us to later identify possible contaminants and remove them prior to statistical analysis. We placed both secretions and control samples in a car freezer set to −20°C, then stored at −22°C upon return to the laboratory at James Cook University, Townsville. All procedures were approved by the Australian National University Animal Ethics Committee (approval no. A2019/15 & A2022/07). Fieldwork was conducted under permits from Queensland Department of Environment, Tourism, Science and Innovation (WISP18597517 & WA0036387); Northern Territory Parks and Wildlife Commission (69132); Western Australian Department of Biodiversity, Conservation and Attractions (FO25000338-3).

Lineage Identification and Phylogenomics

Because many *Gehyra* are difficult to identify to species or lineage from morphology, we obtained mitochondrial NADH dehydrogenase subunit 2 (*ND2*) sequences for 460 of the 754 analysed individuals and inferred a maximum-likelihood phylogeny. Sequencing and phylogenetic methods and results are given in Methods S1 (Table S1; Fig. S1).

To provide a phylogenetic framework for comparative analyses of chemical signal evolution, we inferred a species-level phylogeny for *Gehyra* using Anchored Hybrid Enrichment (AHE; Lemmon et al., 2012) data generated through the Australian Amphibian and Reptile Genomics (AusARG) initiative (via BioPlatforms Australia: https://data.bioplatforms.com/organization/ausarg). This sampling includes near-complete coverage of described and putative Australian *Gehyra* species (49 described species; 28 putative taxa, i.e., deeply divergent candidate species). We also incorporated an additional sample for non-Australian *Gehyra* (*Gehyra insulana* LSUMZ95873) and three outgroup

159 taxa for calibration in subsequent dating analyses (*Lucasium iris* QM J96406 [SMZ1328], Tiatragul et
160 al., 2026; *Lepidodactylus pumilus* LSUMZ97473 and *Gymnodactylus amarali* CHUNB5200, Singhal et
161 al., 2021). Sequences were aligned using the pipesnake workflow (Brennan et al., 2024b), followed
162 by gene tree and species tree estimation. Briefly, this involves alignment with MAFFT (Katoh &
163 Standley, 2013), removal of uninformative sites at threshold of 0.80 using ClipKIT (Steenwyk et al.,
164 2020), and then estimation of gene trees under maximum-likelihood in IQ-TREE 2 (Minh et al., 2020),
165 using ModelFinder (Kalyaanamoorthy et al., 2017) to identify the best substitution model. Gene trees
166 are then passed to hybrid weighted-ASTRAL (wASTRAL; Zhang & Mirarab, 2022) to estimate a species
167 tree (Fig. S2).

168 We estimated divergence times using MCMCTree implemented in PAML (Rannala & Yang,
169 2007), using the weighted-ASTRAL species-tree topology as the input (Fig. S3). Due to the absence of
170 relevant primary fossil calibrations (Daza et al., 2014), we applied a set of four secondary node
171 calibrations derived from a densely sampled squamate phylogeny (Brennan et al., 2024a), generated
172 using the Squamate Conserved Loci (SqCL) marker set (Singhal et al., 2017). Secondary calibrations
173 were applied using Skew-T distributions to accommodate uncertainty in node ages. Using AMAS
174 (Borowiec, 2016) we split the alignment (total 538,641 bp) into four quartiles based on the full
175 distribution of previous rate estimates for the AHE loci, before removing the third codon position. We
176 then used baseml to estimate branch lengths, gradient and the Hessian for each of the four
177 partitions, before running MCMCTree on the concatenated outputs (gradient and Hessian [in.BV file])
178 and the concatenated alignment for four independent analyses. Finally, we combined output mcmc
179 files using LogCombiner (Bouckaert et al., 2014) and reran using option “print = -1” in the .ctl file,
180 before checking convergence (ESS > 200) using Tracer v1.7.2 (Rambaut et al., 2018).

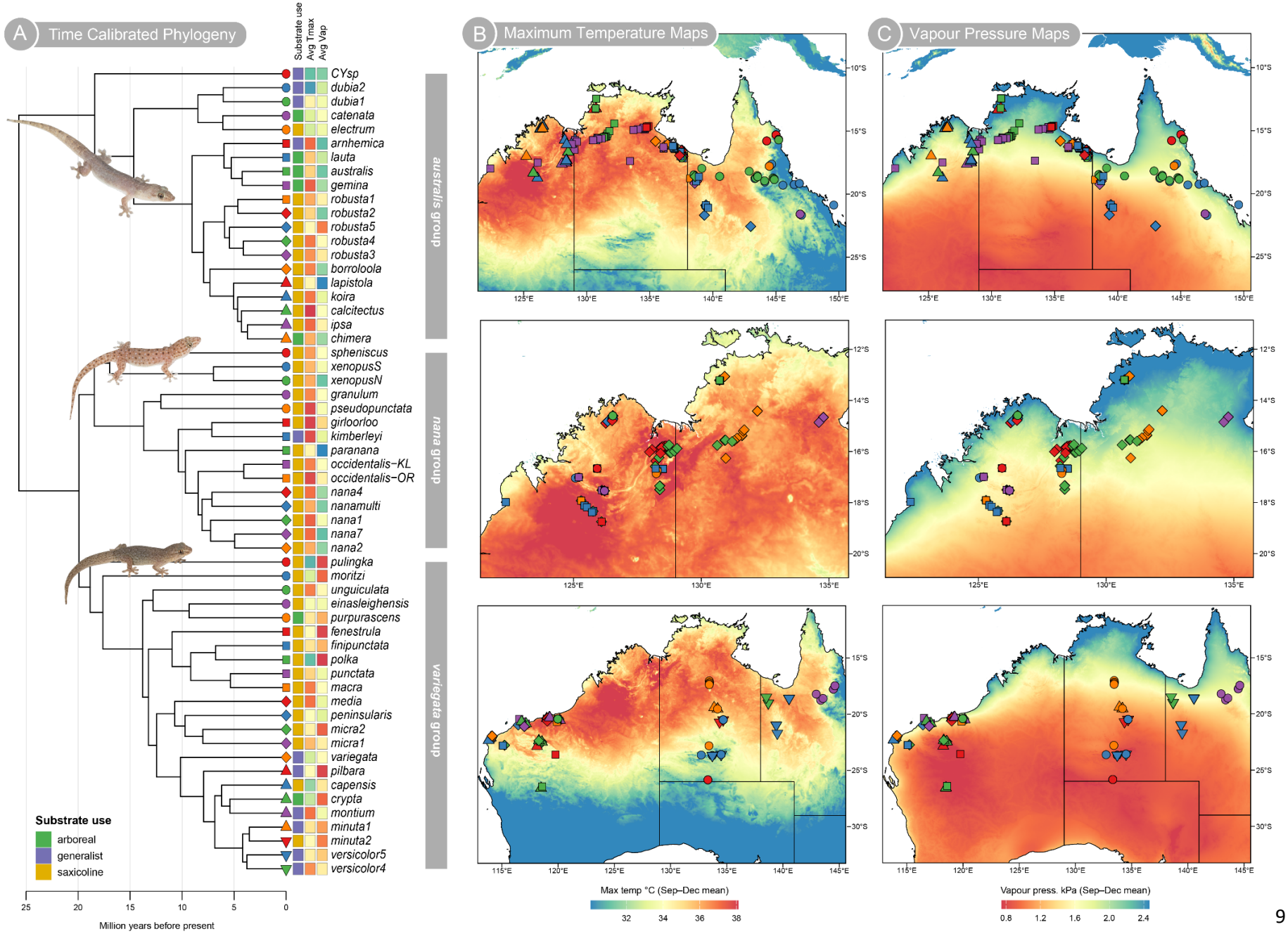

A Time Calibrated Phylogeny
Substrate use
Avg Tmax
Avg Vap
CYsp
dubia2
dubia1
catenata
electrum
arnhemica
lauta
australis
gemina
robusta1
robusta2
robusta5
robusta4
robusta3
borroloola
lapistola
koira
calcitectus
ipsa
chimera
spheniscus
xenopusS
xenopusN
granulum
pseudopunctata
girloorloo
kimberleyi
paranana
occidentalis−KL
occidentalis−OR
nana4
nanamulti
nana1
nana7
nana2
pulingka
moritzi
unguiculata
einasleighensis
purpurascens
fenestrula
finipunctata
polka
punctata
macra
media
peninsularis
micra2
micra1
variegata
pilbara
capensis
crypta
montium
minuta1
minuta2
versicolor5
versicolor4
australis group
nana group
variegata group
Substrate use
arboreal
generalist
saxicoline
25
20
15
10
5
0
Million years before present
B Maximum Temperature Maps
C Vapour Pressure Maps
Max temp °C (Sep–Dec mean)
32
34
36
38
Vapour press. kPa (Sep–Dec mean)
0.8
1.2
1.6
2.0
2.4

Figure 1. Phylogenetic and climatic context of the sampled *Gehyra* lineages. (A) Time-calibrated phylogeny pruned to lineages with chemical signal data (from Fig. S3). Symbols (shape and colour) identify lineages in B and C; they are unique within groups but reused across groups. Tip columns show substrate use, maximum temperature and vapour pressure, coloured on the map scales. Geckos, top to bottom: *G. australis*, *G. nana* (nana4) and *G. variegata*. (B) Maximum temperature and (C) vapour pressure (WorldClim September–December means) across the sampling region, in rows for the *australis*, *nana* and *variegata* groups; each symbol is one individual.

Gas Chromatography – Flame Ionisation Detector

We prepared all epidermal secretion samples in a randomised order under a fume hood. We added 95 µL of *n*-Hexane and 5 µL of BSTFA (*N,O*-bis(trimethylsilyl)trifluoroacetamide) to each vial. n-Hexane acts as a solvent, while BSTFA reacts with polar compounds, replacing active hydrogens with a $–Si(CH_3)_3$ (trimethylsilyl) group, to yield silyl derivatives that are more volatile, less polar, and more thermally stable, allowing polar compounds (e.g., fatty acids, alcohols, sterols) to elute reliably from the GC column. We then vortexed each sample for 30 seconds and incubated it on a 70°C heat block for 60 minutes to promote derivatisation. After heating, we vortexed the samples again for 30 seconds. We then chemically characterised the samples using an Agilent 6890N gas chromatograph equipped with a Flame Ionisation Detector (FID) and an Agilent HP-5MS column (30 m × 0.25 mm × 0.1 µm), using hydrogen as the carrier gas at a constant flow of 1 mL/min and nitrogen as the FID makeup gas. We injected 1 µL of each sample in pulsed splitless mode, with the front inlet set to 250°C and the detector at 370°C. The oven temperature program began at 100°C, increased to 165°C at 25°C/min, then to 280°C at 10°C/min, to 310°C at 5°C/min, then to 350°C at 20°C/min (held for 1 minute), before reducing to 325°C at 25°C/min and holding for 5 minutes. The total run time per sample was 29.1 minutes. We cleaned the autosampler syringe before and after each injection with four washes of analytical-grade n-hexane. We manually integrated chromatograms using Agilent OpenLab software. Figure 2 shows an example of a manually integrated chromatogram, where each

peak represents a specific chemical or group of chemicals with similar retention times. We excluded any contaminants detected in control vial samples or blank n-hexane runs and consistently integrated the same peaks across all individuals. The processed epidermal pore secretions are hereafter referred to as chemical signals.

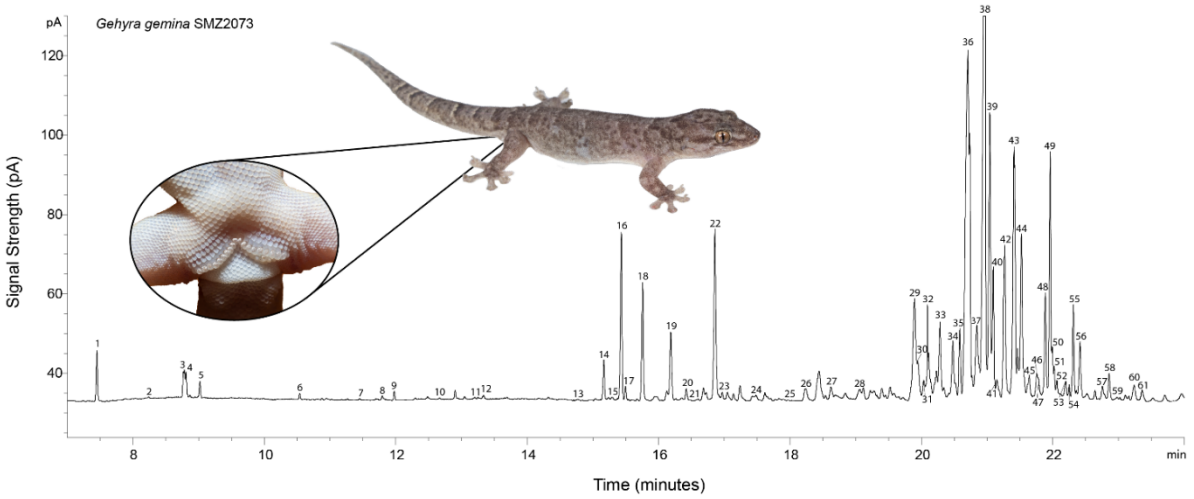


Figure 2. Example gas chromatograph trace produced using a flame ionisation detector, with photos of a male *Gehyra gemina* (top-centre) and the location of the pre-cloacal pores (left). Each peak represents a chemical compound or co-eluting chemicals with similar retention properties. The peaks are numbered from 1–61, representing the compounds used in this study. The same 61 peaks were analysed for every individual gecko for every lineage.

Chemical data processing

Our initial collection comprised chemical signal samples from 790 male *Gehyra* across 58 divergent lineages. Chemical signals from 22 individuals could not be successfully integrated due to insufficient signal or GC errors and were removed. An additional 14 individuals were removed as extreme outliers in pairwise plots and principal component analysis, likely caused by mislabelling, field contamination, or sample preparation issues. The final chemical signal dataset consisted of 754 individuals, with lineage-level sample sizes ranging from 2 to 37 (mean = 13.0, median = 11; all except 4 lineages had ≥ 5 samples, and 37 of 58 lineages had ≥ 10 samples; see Table S2).

Chemical blends were characterised from GC-FID chromatograms. One peak was removed from the original 62-peak dataset due to its irregular occurrence and suspected origin as a contaminant; the remaining 61 peaks represent chemically distinct compounds or co-eluting compounds with similar retention properties. Individual compounds were not chemically identified, which was beyond the scope of this study; peaks are therefore treated as traits defined by retention time, allowing comparison of blend composition across lineages. Peak areas reflect the abundance of each compound within the blend. Peak areas were converted to proportions of each individual's summed peak area (the summed area of all 61 integrated peaks), yielding compositional data where all traits sum to one within a sample. We applied a centred log-ratio transformation and corrected for variation in summed peak area prior to analysis (RRPP; Collyer & Adams, 2018). Because CLR values sum to zero within each individual, one peak (peak 46) was excluded, leaving 60 peaks. Full details of these transformations and corrections are given in the supplement (Methods S2, Fig. S4 and Table S3; Methods S3 and Figs S5–S6). Individual-level profiles were aggregated to lineage means for phylogenetic analyses. Lineage means were then standardised to zero mean and unit variance for each peak, so that abundant compounds did not dominate the analyses.

Testing predictors of chemical signal composition

To visualise divergence in chemical signal composition among lineages, we ran a principal component analysis (PCA) on the standardised lineage means using rda() in vegan (Oksanen et al., 2026). We then projected the time-calibrated tree onto the first two principal components, estimating ancestral node positions with fastAnc in phytools (Revell, 2012). The resulting phylomorphospace shows lineage divergence in chemical space in the context of shared ancestry. Prior to fitting environmental models, we estimated phylogenetic signal in the chemical signal data using K_{mult} (Blomberg et al., 2003; Adams, 2014; physignal function in geomorph, Adams & Otárola-Castillo, 2013), and estimated Pagel's λ (Pagel, 1999) using an intercept-only multivariate phylogenetic generalised least squares (mvGLS) model.

We tested the effects of substrate use and climatic variables on lineage-level chemical signal composition. We used all 60 CLR-transformed peaks simultaneously as the multivariate response, with mvGLS models implemented in mvMORPH (Clavel et al., 2015; Clavel & Morlon, 2020). This penalised-likelihood framework accommodates high-dimensional multivariate data while accounting for phylogenetic non-independence. To characterise each lineage's substrate use, we broadly categorised lineages into three substrate use types (arboreal, generalist, or saxicoline) based on our own observations and published information (Ashman et al., 2018; Doughty et al., 2018a, 2018b; Kealley et al., 2018; Oliver et al., 2019; Wilson & Swan, 2025). Arboreal lineages were those found predominantly on trees, saxicoline lineages predominantly on rock, and generalist lineages those that are mostly arboreal but also regularly use rock and human structures such as walls, particularly where saxicoline congeners are absent. The two termite-mound specialists (*G. kimberleyi* and *G. pilbara*) fit none of these categories and, being too few to analyse as a separate group, were conservatively classified as generalists; *G. kimberleyi* is also occasionally found on trees. Substrate use was treated as a categorical variable. For climatic conditions experienced during the period of peak chemical activity (September–December), we extracted monthly climatic data from WorldClim v2.1 at 30 arc-second (~1 km) resolution (Fick & Hijmans, 2017). Using geographic coordinates for each sampling location, we extracted long-term (1970–2000) monthly values for minimum, mean and maximum temperature (°C), precipitation (mm), vapour pressure (kPa), and solar radiation (kJ m^{-2} day^{-1}), and then calculated seasonal means for each individual. These values capture local climatic conditions during the primary breeding period for *Gehyra* in northern Australia (Fig. 1).

To avoid multicollinearity among predictors, we examined pairwise Pearson correlations among seasonal means for all six climatic variables across all lineages (Fig. S7). Average, minimum, and maximum temperatures were highly correlated ($r > 0.90$), therefore we retained maximum temperature (T_{max}) as the most ecologically relevant metric, given the expected disproportionate influence of extreme heat on chemical volatility and persistence. Solar radiation was subsequently excluded because it was negatively correlated with both precipitation ($r = -0.85$) and vapour

277 pressure (r = −0.66). Although vapour pressure (Vap) and precipitation (Prec) were moderately
278 correlated (r = 0.71), we retained both variables for model evaluation because they capture distinct
279 hydric processes. All environmental variables were standardised to mean zero and unit variance
280 across lineages prior to analysis.

281 All mvGLS models were fitted using the time-calibrated tree pruned to the relevant lineages
282 and assumed Pagel's λ trait evolution model with RidgeArch penalisation (Clavel et al., 2019).
283 Statistical significance was assessed using permutation-based MANOVA (Pillai's trace, 10,000
284 permutations). Substrate use was analysed as a single-predictor model with substrate use as a three-
285 level factor, treating it as a structural axis distinct from continuous climatic variables. Following a
286 significant overall effect of substrate use, all pairs of substrate categories were compared using
287 general linear hypothesis tests (pairwise.glh in mvMORPH, Clavel et al., 2015; 10,000 permutations)
288 with Holm-adjusted p-values (Holm, 1979). To assess whether substrate use had changed repeatedly
289 across the phylogeny, rather than differing between a few clades, we calculated the minimum
290 number of transitions required to explain its distribution using Fitch parsimony (Fitch, 1971) in
291 phangorn (Schliep, 2011), and estimated its history by stochastic character mapping under an equal-
292 rates Mk model (make.simmap in phytools; Huelsenbeck et al., 2003; Revell, 2012; Fig. S8). For
293 climatic predictors, rather than fitting single-predictor models, we evaluated a set of candidate Type
294 III mvGLS models including all pairwise combinations of T_{max}, Vap, and Prec, with interaction terms
295 included to reflect the joint nature of climatic gradients. Because GIC has not been validated for
296 penalised mvGLS models with multiple predictors, we used the candidate models to select the
297 moisture variable (Vap or Prec), based on permutation tests, effect sizes and which variable
298 remained significantly associated with the chemical signal when both were included in the same
299 model. Inference on the selected model was treated as a single planned test of whether the moisture
300 effect depended on T_{max}. For transparency, p-values corrected across the three candidate models
301 (Benjamini & Hochberg, 1995; separately for each term) are reported in Table S4. To confirm that the
302 associations with substrate use and climate were not confounded, we also fitted a joint model

including both (substrate use + Vap × T_{max}; Type III MANOVA; Table S5). We did not model interactions between substrate use and climate because arboreal (7) and generalist (11) lineages were too few to estimate category-specific climate responses reliably.

We extracted regression coefficients to quantify the direction and magnitude of association between predictors and individual chemical peaks (Table S6). For substrate use, because saxicoline lineages differed from both other categories, which did not differ from each other, we summarised the substrate effect as the contrast between saxicoline lineages and the mean of arboreal and generalist lineages. We visualised this contrast at the lineage level by calculating composition-weighted scores, multiplying each lineage's chemical profile by the contrast coefficient vector, and compared these among arboreal, generalist and saxicoline lineages using boxplots. Peak-level coefficients for this contrast were plotted as a ranked bar chart, with coefficients retaining their original sign, indicating whether each peak was higher or lower in saxicoline lineages, and we highlighted peaks ≥ 70% of the maximum absolute coefficient to identify dominant contributors (Mardia et al., 1979).

We explored the Vap × T_{max} interaction in several ways. Because the interaction was significant in the selected model but not after correction across candidate models (see Results), these summaries are descriptive. As predictors were standardised, each peak's Vap coefficient is its response at mean T_{max}, and its response at any other temperature is that coefficient plus the interaction coefficient multiplied by T_{max} in standard deviation units. We evaluated this at one standard deviation below the mean T_{max} (33.3°C), the mean (35.3°C), and one standard deviation above (37.3°C). The 60 per-peak values at a given temperature form an effect vector describing how the whole blend shifts per one standard deviation increase in Vap. We summarised each vector by its Euclidean length, the overall strength of the response; by the angle between vectors from different temperatures, which distinguishes a response that is reorganised across peaks from one that is

merely rescaled; and by the cumulative proportion of squared length in the highest-ranking peaks, the degree to which the response is concentrated in a few compounds.

The lineage-level mvGLS models above do not account for intraspecific variation. To assess the robustness of results to within-lineage variation, we conducted two complementary validation analyses: (i) a resampling procedure that re-ran the mvGLS analyses 10,000 times after randomly selecting one individual per lineage, and (ii) Bayesian multivariate mixed models that explicitly modelled individual-level variance and phylogenetic non-independence. Full details are provided in Supplementary Methods S4 and Figures S9–S29, and Methods S5 and Figures S30–S31.

Results

Phylogenetic relationships

Phylogenetic relationships inferred using weighted ASTRAL and the AHE dataset were broadly consistent with previous phylogenetic studies of the group (Ashman et al., 2018; Moritz et al., 2018; Oliver et al., 2019; Lau et al., 2025; Oliver et al., 2026; Fig. S2). Australian *Gehyra* form two major clades: the large-bodied *australis* group (Sistrom et al., 2009; Oliver et al., 2020) and the generally smaller-bodied *punctata-variegata* group (including the *nana* group). Divergence times estimated using MCMCTree (Fig. S3) align with those produced by Oliver et al. (2026) using an exon capture dataset. These phylogenetic and divergence time estimates, while not the focus of this study, provide a phylogenetic framework spanning both shallow and deep splits within the genus and enable macroevolutionary analyses of chemical signal divergence, substrate use, and climate gradients.

Substrate use and climate are associated with chemical signal composition

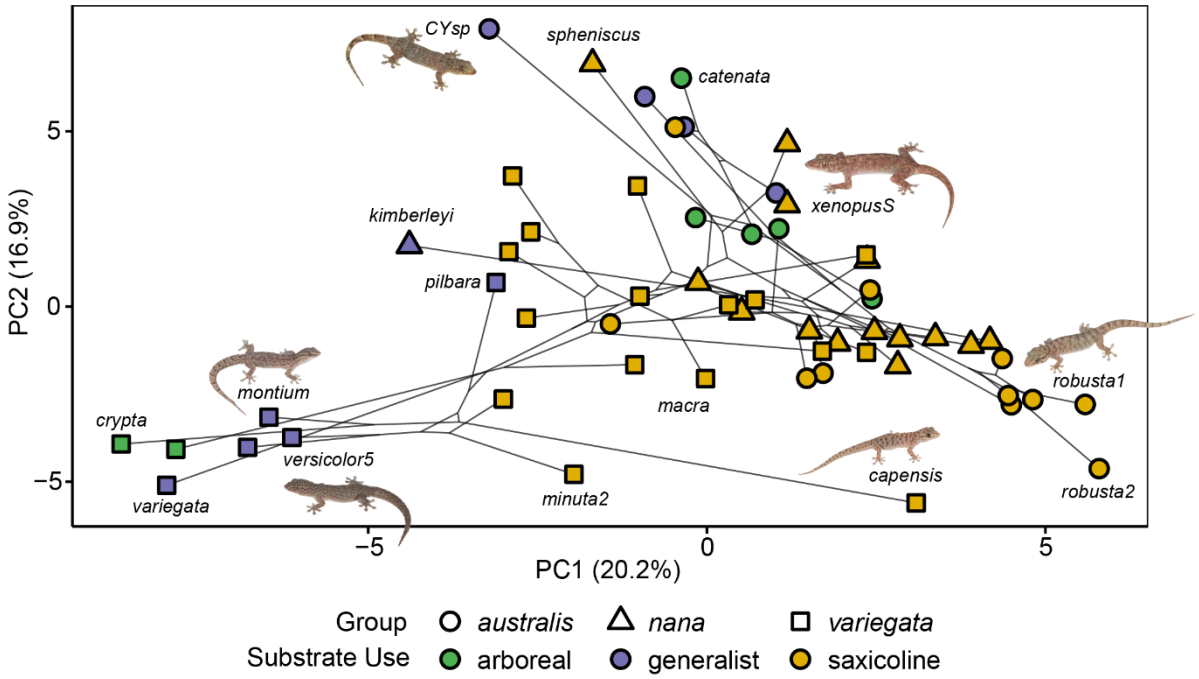


Figure 3. Phylomorphospace plot illustrating multivariate variation in chemical signal composition across *Gehyra* lineages using principal component analysis. Points represent lineage means projected onto the first two principal component axes, with phylogenetic relationships overlaid as connecting branches. The lineages are coloured by the substrate they use—arboreal species (green), generalist species (purple), and saxicoline species (orange)—and the shape corresponds to their clade—*australis* group (circles), *nana* group (triangles), and *variegata* group (squares).

The phylomorphospace plot was used to visualise among-lineage variation in chemical signal composition in relation to phylogenetic relationships in *Gehyra* and in relation to substrate use (Fig. 3). Along the first two axes (PC1 = 20.2%, PC2 = 16.9%), members of the *variegata* group generally occur towards the left of the ordination, whereas most *australis* and *nana* group lineages fall towards the right. This broad separation along PC1 reflects contrasting suites of chemical peaks, with strong positive loadings (e.g., peaks 29, 36, 42, 44, 45, 48) associated with lineages on the right-hand side of the plot and strong negative loadings (e.g., peaks 1, 2, 5–12, 24) associated with those on the left. Vertical separation along PC2 is driven by peaks with high positive loadings (e.g., peaks 3, 4, 14, 16,

18–20, 22, 30), which pull lineages upward, and peaks with negative loadings (e.g., peaks 43, 55, 60), which pull them downward. Substrate-associated clustering is also apparent: arboreal and generalist *variegata* group lineages cluster closely together in the lower-left region of the plot, while within the *australis* group, arboreal and generalist lineages occupy the upper region of the ordination and saxicoline lineages fall below them, towards the lower right. Together, these patterns illustrate broad multivariate structure in chemical signal composition across *Gehyra*, associated with both phylogenetic grouping and substrate use.

Chemical signal composition showed moderate phylogenetic signal (K_{mult} = 0.70, $p < 0.001$; λ = 0.69), indicating that closely related lineages tend to have more similar chemical profiles, though substantial variation remains unexplained by shared ancestry. Multivariate phylogenetic regressions revealed associations between chemical signal composition and both substrate use and climatic variation across *Gehyra* lineages. Substrate use, modelled as a three-level factor, was significantly associated with chemical signal composition (Pillai's trace = 1.224, p = 0.004; Fig. 4). Pairwise contrasts showed that saxicoline lineages differed from both arboreal (Pillai's trace = 0.682, p = 0.002) and generalist lineages (Pillai's trace = 0.684, p = 0.002), whereas arboreal and generalist lineages were not distinguishable (Pillai's trace = 0.489, p = 0.596). Substrate use changed repeatedly across the phylogeny: at least 12 transitions were required to explain its distribution among lineages (Fitch parsimony), and stochastic character mapping estimated 15 (95% interval 12–22; Fig. S8). The chemical contrast between saxicoline and other lineages therefore spans multiple independent shifts in substrate use rather than a single divergence between clades. Lineage-level projections of chemical signal composition onto the saxicoline contrast (the average of the saxicoline vs arboreal and saxicoline vs generalist contrasts) revealed a clear separation of substrate use categories, with arboreal and generalist lineages clustering at lower projected chemical signal scores and saxicoline lineages occupying higher values. This contrast was driven by a subset of chemical peaks with consistent directional effects (elevated or reduced in saxicoline lineages relative to both other categories), including peaks 6, 7, 24, 34, 37, 43–45 and 48 (Fig. 4; Table S6). The two underlying

contrasts were strongly correlated (r = 0.77; r = 0.94 with their average) and differed mainly in the magnitude of peak contributions rather than direction; only peak 26 was inconsistent, being strongly reduced in saxicoline lineages relative to arboreal (−1.02) but not generalist lineages (0.05; Table S6).

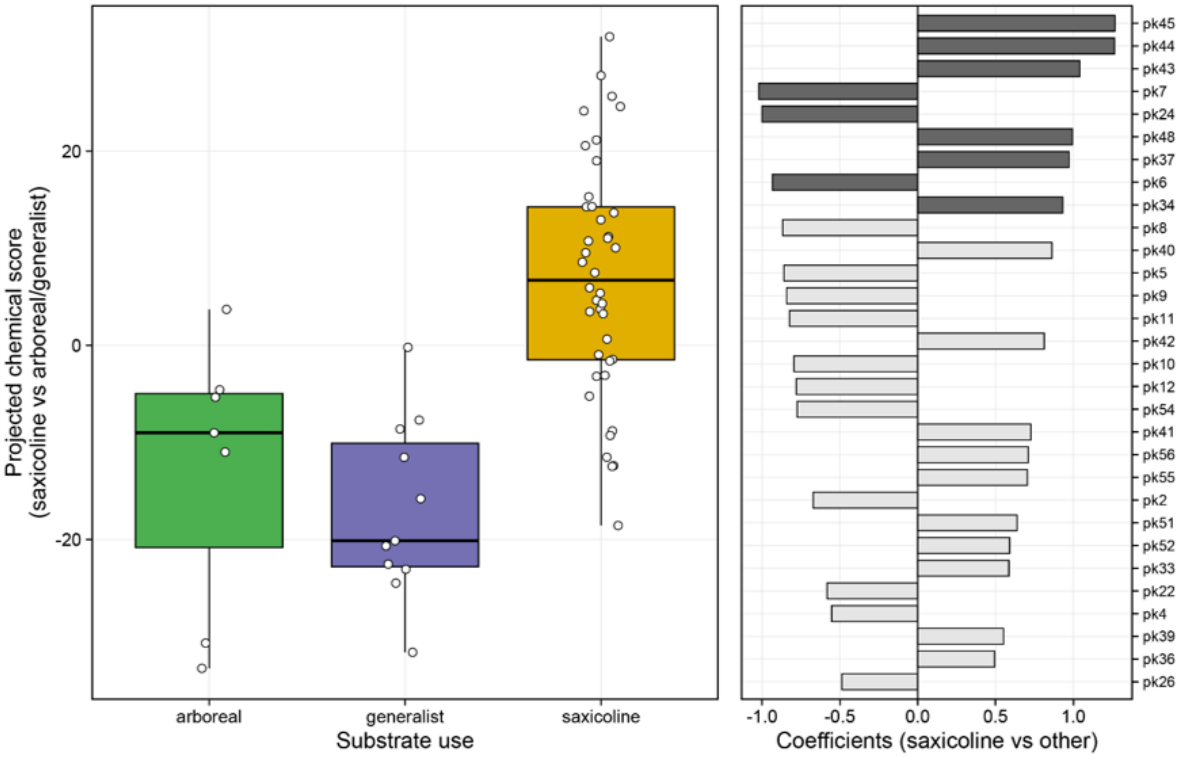


Figure 4. Chemical signal variation associated with substrate use. The left panel shows boxplots of lineage-level projected chemical scores derived from the multivariate phylogenetic regression (mvGLS) with substrate use plotted across three categories (arboreal, generalist, saxicoline). Scores are projections onto the coefficient vector contrasting saxicoline lineages with the mean of arboreal and generalist lineages; points show individual lineages. Colours are consistent with figures throughout the manuscript. The right panel shows mvGLS contrast coefficients (saxicoline vs arboreal and generalist) for the 30 chemical peaks with the largest absolute effects. Bars retain their original sign, indicating whether each peak is higher or lower in saxicoline lineages. Peaks with coefficients ≥ 70% of the maximum absolute coefficient are shaded darker.

Among the candidate climatic models (Table S4), the vapour pressure × maximum temperature and precipitation × maximum temperature models performed similarly, each with a significant main effect of the moisture variable; the interaction with maximum temperature was

404 significant for vapour pressure ($p = 0.046$) but not for precipitation ($p = 0.077$). When the two
405 moisture variables were modelled jointly, however, vapour pressure explained more multivariate
406 variation (Pillai's trace: 0.61 vs. 0.50) and retained significance ($p = 0.039$) while precipitation did not
407 ($p = 0.544$). We therefore selected the vapour pressure × maximum temperature model for all
408 subsequent analyses. In this final model, chemical signal composition was associated with vapour
409 pressure (Pillai's trace = 0.64, $p = 0.010$) and with the interaction between vapour pressure and
410 maximum temperature (Pillai's trace = 0.61, $p = 0.046$), but not detectably with maximum
411 temperature alone (Pillai's trace = 0.57, $p = 0.144$). After correction for multiple testing across the
412 three candidate models, the vapour pressure effect remained significant ($p = 0.026$), but the
413 interaction did not ($p = 0.116$; Table S4). These results suggest that maximum temperature may
414 modulate the association between chemical composition and vapour pressure rather than having an
415 independent association with chemical composition. Substrate use and climate were not
416 confounded. Across all lineages, vapour pressure ranged from 0.76 to 2.48 kPa and maximum
417 temperature from 30.4 to 38.6°C, and each substrate use category spanned most of this range (at
418 least 0.94–2.22 kPa and 32.5–37.4°C). In a joint model, both substrate use (Pillai's trace = 1.30, $p =$
419 0.001) and vapour pressure (Pillai's trace = 0.67, $p = 0.003$) remained associated with chemical
420 composition, with peak coefficients nearly identical to those from the separate models ($r \geq 0.98$;
421 Table S5).

422 Using coefficients from the vapour pressure × maximum temperature interaction model
423 (Table S6), we described the response of each peak to vapour pressure at low, mean, and high
424 maximum temperatures (±1 SD; Fig. 5). The resulting values across all 60 peaks form an effect vector
425 describing the multivariate response of the chemical blend to vapour pressure at each temperature.
426 Vector length represents the strength of the overall response, while its orientation represents the
427 combination of peaks contributing to that response. Response strength increased with temperature,
428 with effect vector lengths of 1.47, 1.55, and 2.32 at low, mean, and high maximum temperature,
429 respectively, so the effect of vapour pressure was approximately 50% stronger under the hottest

conditions than at mean maximum temperature. The angle between the low- and high-temperature effect vectors was 71.8° (cosine = 0.31), with more of this between low and mean (45.2°) than between mean and high (26.5°), although angles between vectors in 60 dimensions are inflated by estimation noise and should be interpreted cautiously.

As with substrate use, the response was concentrated in a relatively small subset of peaks, and descriptively became more so at higher maximum temperatures. At mean maximum temperature the five largest effects accounted for 44.9% of the squared vector length and the ten largest for 65.8%; at high maximum temperature these rose to 55.1% and 74.3%. Peak 38 alone carried 17.5% and 24.3%, respectively. The five largest at mean maximum temperature were peaks 38, 36, 26, 51, and 35, all of which retained the same sign across the maximum temperature range. Under high maximum temperature conditions, the dominant peaks changed to 38, 26, 39, 41, and 54. Some peaks were strongly amplified from low to high maximum temperatures, including peak 38 (0.15 to 1.15) and peak 26 (0.13 to 0.73), whereas others changed little, such as peak 36 (0.43 to 0.48). Peaks 39, 41, 54, and 32 contributed little under low maximum temperature conditions but substantially more under high maximum temperature conditions, whereas peaks 18, 8, 57, and 22 showed the opposite pattern. Thirty-one of the 60 peaks changed sign between the low and high maximum temperature conditions. In all cases at least one of the two values was small relative to the peaks driving the response, so these sign changes largely reflect peaks with near-zero coefficients rather than genuine reversals in the direction of response. Peak 39 was the only sign-changing peak to become a major contributor, shifting from −0.13 at low maximum temperature to +0.71 at high, and so contributed to the vapour-pressure response mainly under hot conditions.

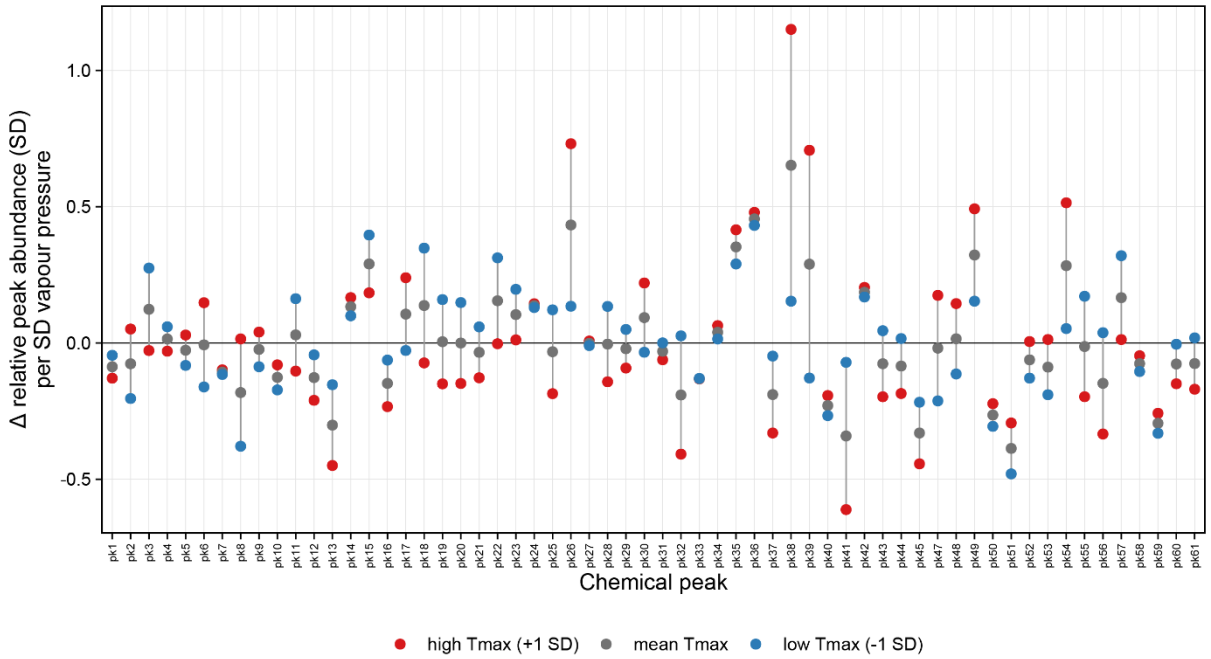


Figure 5. Effect of vapour pressure (Vap) on chemical signal composition across a gradient of maximum temperature (T_{max}). Each point is the conditional effect of Vap on one chemical peak, derived from mvGLS regression coefficients and expressed as the change in relative peak abundance (SD units) per +1 SD increase in Vap. Effects are shown at three levels of T_{max}: the mean (35.3°C; grey) and one standard deviation above (high; 37.3°C; red) and below (low; 33.3°C; blue) the mean. The grey segment spans the two extremes; its length represents the strength of the Vap × T_{max} interaction for that peak. The interaction was not significant after correction across candidate models (Table S4), so the figure describes the fitted pattern. Peaks are ordered by peak number.

Both resampling and Bayesian multivariate mixed models yielded results consistent with the mvGLS analyses. Resampled coefficients corresponded closely with lineage-mean estimates for all substrate use contrasts (Pearson's r = 0.98–0.99; Spearman ρ = 0.98–0.99) and all climatic terms (Pearson's r = 0.95, 0.90 and 0.91 for vapour pressure, maximum temperature and the interaction respectively; Spearman ρ = 0.92, 0.86 and 0.89). In the Bayesian models, all five focal peaks differed between saxicoline lineages and both arboreal and generalist lineages (95% credible intervals excluding zero; e.g. peak 45, saxicoline vs arboreal: 1.12 [0.65, 1.61]), whereas no peak differed

between arboreal and generalist lineages. The vapour pressure × maximum temperature interaction was credibly positive for peaks 38 (0.20 [0.12, 0.30]), 26 (0.11 [0.03, 0.20]) and 39 (0.10 [0.01, 0.20]), but not for peaks 36 and 41, whose intervals included zero. Together, these analyses indicate that the inferred environmental associations are not artefacts of aggregating to lineage means or of a single modelling framework (Methods S4 and Figs S9–S29; Methods S5 and Figs S30–S31).

Discussion

Analysing 754 individuals from 58 lineages of *Gehyra* across continental-scale climatic gradients, we show that chemical signal composition is structured by broad substrate use and climatic variables, particularly vapour pressure, with some evidence that its association with signal composition is stronger under hotter conditions. Together, these results are consistent with sensory drive as a mechanism shaping chemical signal evolution in *Gehyra.* Under this framework, signal design is expected to evolve in response to local environmental constraints that affect transmission, persistence, and detection (Endler, 1992). While sensory drive has been widely invoked to explain divergence in visual and acoustic signals, where environmental variation has repeatedly been shown to shape signal design through predictable effects on transmission and detectability under local conditions (Boughman, 2002; Seehausen et al., 2008; Boeckle et al., 2009; Goutte et al., 2016; Maan et al., 2017; Torres-Dowdall et al., 2017; Cummings & Endler, 2018; To et al., 2021), its applicability to chemical communication, particularly in vertebrates, has received comparatively little empirical attention despite the ubiquity of chemical signalling (Baeckens et al., 2018; Zozaya et al., 2022). By extending tests of sensory drive to chemical communication, we provide results consistent with environmentally mediated selection as a driver of signal divergence.

Substrate use represents a major axis of environmental variation that integrates microclimatic and substrate properties relevant to chemical signal transmission and persistence. Across *Gehyra* lineages, substrate use emerged as a significant predictor of chemical signal

composition. Saxicoline lineages occupied distinct multivariate chemical space, while arboreal and generalist lineages largely overlapped. Generalist lineages in *Gehyra* are predominantly arboreal, shifting onto rock or human structures largely where true saxicoline species are absent, so the overlap between arboreal and generalist lineages in chemical space is expected and the principal contrast falls between saxicoline lineages and the rest. Because substrate use changed at least 12 times across the phylogeny, the chemical divergence between saxicoline and other lineages reflects multiple independent shifts in substrate use rather than a single divergence between clades. This pattern was robust across mvGLS models, resampling analyses, and Bayesian multivariate mixed models incorporating individual-level variation. These findings parallel well-documented patterns of ecomorphological divergence in lizards, where substrate use repeatedly predicts trait evolution across clades and continents (Losos, 2009; Hagey et al., 2017; Vicent-Castelló et al., 2025).

Substrate use is expected to shape signal composition through both microclimate and the properties of the deposition surface itself, which determine the chemical background against which a signal must be detected and how well deposited compounds are retained (Regnier & Goodwin, 1977; Wilson et al., 2015). Rock and bark differ on both counts, and the divergence we found between saxicoline lineages and both arboreal and generalist lineages is consistent with these differences shaping blend composition. Divergence between saxicoline and other lineages was driven by a relatively small subset of chemical peaks (6, 7, 24, 34, 37, 43–45, and 48), suggesting that these compounds are especially responsive to substrate use, structure, or substrate-specific deposition. Similar substrate linked differences in chemical composition have been reported in other lizard systems, such as *Podarcis*, where terrestrial species exhibit higher proportions of waxy esters relative to saxicoline taxa (García-Roa et al., 2016). Interestingly, termite-mound specialists (*Gehyra kimberleyi* and *G. pilbara*), which occupy a distinctive but structurally intermediate substrate, clustered closely in PCA despite belonging to different taxonomic groups. Although represented by only two lineages and therefore conservatively classified as generalists in our analyses, their

proximity in chemical space is consistent with the role of substrate use-specific selective environments in shaping chemical signal composition.

Importantly, substrate use may not operate independently of broader climatic conditions: chemical signals deposited within specific microhabitats are simultaneously exposed to the surrounding thermal and atmospheric environment, including peak daytime temperatures despite the nocturnal activity of *Gehyra*, linking substrate-associated divergence with climate-mediated selective pressures. Among continuous climatic predictors, chemical signal composition was associated with vapour pressure, while maximum temperature showed no detectable association on its own. Instead, maximum temperature may modulate how strongly composition is associated with vapour pressure: the multivariate response was descriptively stronger under the hottest conditions (Fig. 5), although this interaction did not remain significant after correction across candidate models. Our sampling spans these climatic gradients across the northern half of the Australian continent (Fig. 1), with lineage mean maximum temperatures ranging from 30.4 to 38.6°C and vapour pressures from 0.76 to 2.48 kPa over the September to December period. Lineages from coastal and near-coastal areas of the monsoonal north, including *arnhemica*, *gemina*, *borroloola*, *nana4*, and *nana7*, experience elevated atmospheric moisture alongside high maximum temperatures during this period, while arid-zone lineages such as *micra2*, *fenestrula*, *polka*, and *pulingka* occupy consistently drier and cooler country. Chemical signals deposited in high-moisture environments, particularly lipophilic compounds deposited on substrates, may degrade more readily through interactions with water vapour, potentially selecting for blends that resist moisture-driven breakdown (Regnier & Goodwin, 1977; Alberts, 1992; Martín et al., 2015; Baeckens et al., 2018). Evaporative loss increases with temperature (McDonough et al., 1989), so atmospheric moisture has more influence over how fast a deposited chemical signal dries when conditions are hot (Regnier & Goodwin, 1977). Selection driven by relative humidity would predict the reverse, since a given change in vapour pressure shifts relative humidity further in cool air. Our results are consistent with selection on absolute moisture content, possibly moderated by temperature, rather than relative humidity.

A further notable pattern was that climatic associations were again driven by a limited subset of chemical peaks, with several compounds (peaks 26, 36, 38, 39, 41 and 51) consistently exhibiting large coefficients across interaction models and resampling analyses. This pattern suggests that particular compounds play disproportionate roles in mediating environmental responses. Though we have not yet characterised them chemically, these compounds may function as a stabilising matrix, protecting more volatile signal components under specific climatic regimes (Regnier & Goodwin, 1977; Escobar et al., 2003; Martín et al., 2015). Several of these peaks appeared amplified under hot conditions, with peak 39 contributing mainly there, consistent with what would be expected if their role is to offset faster degradation at higher temperatures. Similar climate-associated structuring of chemical signals has been documented in other squamate reptiles: lacertid lizards exhibit predictable shifts in signal chemistry across climatic gradients (Baeckens et al., 2018), and species recognition in Iberian wall lizards (*Podarcis hispanicus*) is closely tied to local adaptation in chemical signals (Martín & López, 2006). Comparable ecological and functional pressures are therefore likely to act on *Gehyra*, driving context-dependent divergence in chemical signal composition across both arid and humid abiotic environments.

While our analyses focus on substrate and climate-associated drivers of chemical signal divergence, sexual selection and other biotic interactions are also likely to contribute to chemical signal evolution in *Gehyra*. Chemical signals commonly function in territorial interactions, mate recognition and species discrimination. Hence, divergence in these traits may be shaped by assortative mating, signal interference from local chemical backgrounds, or selection for reliable species recognition in communities where multiple lineages co-occur, driven by reinforcement or reproductive character displacement (Higgie et al., 2000; Higgie & Blows, 2008; Ord & Stamps, 2009; Weber et al., 2016; Dyer et al., 2018; Zozaya et al., 2019b). This is potentially important for *Gehyra*, where local assemblages of up to six species are known (e.g. in the west Kimberley). Importantly, sensory drive and sexual selection are not mutually exclusive: environmental conditions may shape

568 the persistence and efficacy of chemical signals, while biotic interactions further refine signal
569 structure to ensure effective communication and species recognition (Hoskin & Higgie, 2010).

570 Determining the contributing roles of abiotic and biotic factors requires interpreting the
571 functional roles of individual compounds, but this remains challenging. Epidermal pore secretions are
572 complex mixtures, and not all components necessarily function as signalling molecules. Some
573 compounds may represent metabolic by-products or structural constituents of glandular secretions
574 rather than chemical signals per se. Relatedly, the associations we detected may not reflect selection
575 on signalling alone: substrate use and climate may covary with diet or with skin physiology, such as
576 the regulation of cutaneous water loss, which is likely to respond to atmospheric moisture.
577 Identifying which compounds actively influence receiver behaviour—and under what environmental
578 conditions—will require targeted behavioural and experimental assays. Nevertheless, by combining
579 multivariate phylogenetic regression with robustness checks and individual-level modelling, this
580 study narrows the field of candidate compounds likely to play important ecological and evolutionary
581 roles. Future work integrating chemical identification, behavioural assays, and experimental
582 manipulation of environmental conditions will be critical for resolving how chemical signals
583 contribute to adaptation and diversification in *Gehyra* and other animals.

584

585 ## Acknowledgements

586 We thank Naomi Laven, Anders Zimny, Sofia Hayden, Jordan Mulder, Kimberley Day, Kade Skelton,
587 Keith Christian, Ian Bool, Jake Barker, Joe Porter, and Diane Chanut for assistance with fieldwork;
588 Elizabeth Broady and Rhiannon Schembri for assistance with laboratory work; Eridani Mulder and the
589 Australian Wildlife Conservancy for access to several properties; Cecilia Myers for access to Theda
590 Station; and Rebecca Moss and Shane Askew for assistance with Gas Chromatography. We also thank
591 members of the Adaptation and Biodiversity Conservation lab at James Cook University and the
592 Moritz Lab and Keogh Lab at the Australian National University for advice and support. This work was

593 funded by Australian Research Council Discovery Project DP210102267 to C.M., M.H., and C.J.H., and
594 an Australian Society of Herpetologists student grant to S.A.M. We acknowledge the contribution of
595 the Australian Amphibian and Reptile Genomics (AusARG) initiative in the generation of data used in
596 this publication. AusARG is supported by funding from Bioplatforms Australia, enabled by the
597 Commonwealth Government National Collaborative Research Infrastructure Strategy (NCRIS).

Literature Cited

Adams, D. C. (2014). A generalized K statistic for estimating phylogenetic signal from shape and other high-dimensional multivariate data. *Systematic Biology, 63*(5), 685-697. https://doi.org/10.1093/sysbio/syu030

Adams, D. C., & Otárola-Castillo, E. (2013). geomorph: an R package for the collection and analysis of geometric morphometric shape data. *Methods in Ecology and Evolution, 4*(4), 393-399. https://doi.org/10.1111/2041-210X.12035

Agashe, M., Biswas, A., & Karanth, P. (2025). Nested effects of climate and substrate in functional trait investment: insights from chemical communication in geckos. bioRxiv. https://doi.org/10.1101/2025.10.23.684092

Aitchison, J. (1982). The statistical analysis of compositional data. *Journal of the Royal Statistical Society: Series B, 44*(2), 139-177.

Alberts, A. C. (1992). Constraints on the design of chemical communication systems in terrestrial vertebrates. *The American Naturalist, 139*, S62-S89. http://www.jstor.org/stable/2462428

Alberts, A. C. (1993). Chemical and behavioral studies of femoral gland secretions in iguanid lizards. *Brain, Behavior and Evolution, 41*(3-5), 255-260. https://doi.org/10.1159/000113847

Apps, P. J., Weldon, P. J., & Kramer, M. (2015). Chemical signals in terrestrial vertebrates: search for design features. *Natural Product Reports, 32*(7), 1131-1153. https://doi.org/10.1039/c5np00029g

Ashman, L. G., Bragg, J. G., Doughty, P., Hutchinson, M. N., Bank, S., Matzke, N. J., Oliver, P. M., & Moritz, C. (2018). Diversification across biomes in a continental lizard radiation. *Evolution, 72*(8), 1553-1569. https://doi.org/10.1111/evo.13541

Baeckens, S., Edwards, S., Huyghe, K., & Van Damme, R. (2015). Chemical signalling in lizards: an interspecific comparison of femoral pore numbers in Lacertidae. *Biological Journal of the Linnean Society, 114*(1), 44-57. https://doi.org/10.1111/bij.12414

623 Baeckens, S., Martín, J., García-Roa, R., Pafilis, P., Huyghe, K., & Van Damme, R. (2018).
624 Environmental conditions shape the chemical signal design of lizards. *Functional Ecology,*
625 *32*(2), 566-580. https://doi.org/10.1111/1365-2435.12984
626 Barbosa, D., Font, E., Desfilis, E., & Carretero, M. A. (2006). Chemically mediated species recognition
627 in closely related *Podarcis* wall lizards. *Journal of Chemical Ecology, 32*(7), 1587-1598.
628 https://doi.org/10.1007/s10886-006-9072-5
629 Benjamini, Y., & Hochberg, Y. (1995). Controlling the false discovery rate: a practical and powerful
630 approach to multiple testing. *Journal of the Royal Statistical Society: Series B, 57*(1), 289-300.
631 https://doi.org/10.1111/j.2517-6161.1995.tb02031.x
632 Blomberg, S. P., Garland, T., & Ives, A. R. (2003). Testing for phylogenetic signal in comparative data:
633 behavioral traits are more labile. *Evolution, 57*(4), 717-745. https://doi.org/10.1111/j.0014-
634 3820.2003.tb00285.x
635 Boeckle, M., Preininger, D., & Hödl, W. (2009). Communication in noisy environments I: acoustic
636 signals of *Staurois latopalmatus* Boulenger 1887. *Herpetologica, 65*(2), 154-165.
637 https://doi.org/10.1655/07-071R1.1
638 Borowiec, M. L. (2016). AMAS: a fast tool for alignment manipulation and computing of summary
639 statistics. *PeerJ, 4*, e1660. https://doi.org/10.7717/peerj.1660
640 Bouckaert, R., Heled, J., Kühnert, D., Vaughan, T., Wu, C.-H., Xie, D., Suchard, M. A., Rambaut, A., &
641 Drummond, A. J. (2014). BEAST 2: a software platform for Bayesian evolutionary analysis.
642 *PLoS Computational Biology, 10*(4), e1003537. https://doi.org/10.1371/journal.pcbi.1003537
643 Boughman, J. W. (2002). How sensory drive can promote speciation. *Trends in Ecology & Evolution,*
644 *17*(12), 571-577. https://doi.org/10.1016/S0169-5347(02)02595-8
645 Brennan, I. G., Chapple, D. G., Keogh, J. S., & Donnellan, S. (2024a). Evolutionary bursts drive
646 morphological novelty in the world's largest skinks. *Current Biology, 34*(17), 3905-3916.e5.
647 https://doi.org/10.1016/j.cub.2024.07.039

Brennan, I. G., Singhal, S., & Al Bkhetan, Z. (2024b). pipesnake: generalized software for the assembly and analysis of phylogenomic datasets from conserved genomic loci. *Bioinformatics, 40*(5), btae195. https://doi.org/10.1093/bioinformatics/btae195

Clavel, J., Aristide, L., & Morlon, H. (2019). A penalized likelihood framework for high-dimensional phylogenetic comparative methods and an application to New-World monkeys brain evolution. *Systematic Biology, 68*(1), 93-116. https://doi.org/10.1093/sysbio/syy045

Clavel, J., Escarguel, G., & Merceron, G. (2015). mvMORPH: an R package for fitting multivariate evolutionary models to morphometric data. *Methods in Ecology and Evolution, 6*(11), 1311-1319. https://doi.org/10.1111/2041-210x.12420

Clavel, J., & Morlon, H. (2020). Reliable phylogenetic regressions for multivariate comparative data: illustration with the MANOVA and application to the effect of diet on mandible morphology in phyllostomid bats. *Systematic Biology, 69*(5), 927-943. https://doi.org/10.1093/sysbio/syaa010

Collyer, M. L., & Adams, D. C. (2018). RRPP: an R package for fitting linear models to high-dimensional data using residual randomization. *Methods in Ecology and Evolution, 9*, 1772-1779. https://doi.org/10.1111/2041-210X.13029

Cooper, W. E., Van Wyk, J. H., & Mouton, P. L. F. N. (1996). Pheromonal detection and sex discrimination of conspecific substrate deposits by the rock-dwelling cordylid lizard *Cordylus cordylus*. *Copeia, 1996*(4), 839-845. https://doi.org/10.2307/1447645

Cummings, M. E., & Endler, J. A. (2018). 25 years of sensory drive: the evidence and its watery bias. *Current Zoology, 64*(4), 471-484. https://doi.org/10.1093/cz/zoy043

Daza, J. D., Bauer, A. M., & Snively, E. D. (2014). On the fossil record of the Gekkota. *The Anatomical Record, 297*(3), 433-462. https://doi.org/10.1002/ar.22856

delBarco-Trillo, J., Sacha, C. R., Dubay, G. R., & Drea, C. M. (2012). *Eulemur*, me lemur: the evolution of scent-signal complexity in a primate clade. *Philosophical Transactions of the Royal Society B: Biological Sciences, 367*(1597), 1909-1922. https://doi.org/10.1098/rstb.2011.0225

674 Doughty, P., Bauer, A. M., Pepper, M., & Keogh, J. S. (2018a). Spots before the eyes: revision of the
675 saxicoline geckos of the *Gehyra punctata* (Squamata: Gekkonidae) species complex in the
676 Pilbara region of Western Australia. *Records of the Western Australian Museum, 33*(1), 1-50.
677 https://doi.org/10.18195/issn.0312-3162.33(1).2018.001-050
678 Doughty, P., Bourke, G., Tedeschi, L. G., Pratt, R. C., Oliver, P. M., Palmer, R. A., & Moritz, C. (2018b).
679 Species delimitation in the *Gehyra nana* (Squamata: Gekkonidae) complex: cryptic and
680 divergent morphological evolution in the Australian Monsoonal Tropics, with the description
681 of four new species. *Zootaxa, 4403*(2), 201-244. https://doi.org/10.11646/zootaxa.4403.2.1
682 Doughty, P., Palmer, R., Sistrom, M. J., Bauer, A. M., & Donnellan, S. C. (2012). Two new species of
683 *Gehyra* (Squamata: Gekkonidae) geckos from the north-west Kimberley region of Western
684 Australia. *Records of the Western Australian Museum, 27*(2), 117-134.
685 Dyer, K. A., Bewick, E. R., White, B. E., Bray, M. J., & Humphreys, D. P. (2018). Fine-scale geographic
686 patterns of gene flow and reproductive character displacement in *Drosophila subquinaria*
687 and *Drosophila recens*. *Molecular Ecology, 27*(18), 3655-3670.
688 https://doi.org/10.1111/mec.14825
689 Endler, J. A. (1992). Signals, signal conditions, and the direction of evolution. *The American*
690 *Naturalist, 139*, S125-S153. http://www.jstor.org/stable/2462431
691 Escobar, C. M., Escobar, C. A., Labra, A., & Niemeyer, H. M. (2003). Chemical composition of
692 precloacal secretions of two *Liolaemus fabiani* populations: are they different? *Journal of*
693 *Chemical Ecology, 29*(3), 629-638. https://doi.org/10.1023/a:1022858919037
694 Fick, S. E., & Hijmans, R. J. (2017). WorldClim 2: new 1-km spatial resolution climate surfaces for
695 global land areas. *International Journal of Climatology, 37*(12), 4302-4315.
696 https://doi.org/10.1002/joc.5086
697 Fitch, W. M. (1971). Toward defining the course of evolution: minimum change for a specific tree
698 topology. *Systematic Zoology, 20*(4), 406-416. https://doi.org/10.1093/sysbio/20.4.406

García-Roa, R., Cabido, C., López, P., & Martín, J. (2016). Interspecific differences in chemical composition of femoral gland secretions between two closely related wall lizard species, *Podarcis bocagei* and *Podarcis carbonelli*. *Biochemical Systematics and Ecology, 64*, 105-110. https://doi.org/10.1016/j.bse.2015.11.012

García-Roa, R., Jara, M., Baeckens, S., López, P., Van Damme, R., Martín, J., & Pincheira-Donoso, D. (2017). Macroevolutionary diversification of glands for chemical communication in squamate reptiles. *Scientific Reports, 7*(1), 9288. https://doi.org/10.1038/s41598-017-09083-7

Goutte, S., Dubois, A., Howard, S. D., Márquez, R., Rowley, J. J. L., Dehling, J. M., Grandcolas, P., Xiong, R., & Legendre, F. (2016). Environmental constraints and call evolution in torrent-dwelling frogs. *Evolution, 70*(4), 811-826. https://doi.org/10.1111/evo.12903

Hadfield, J. D. (2010). MCMC methods for multi-response generalized linear mixed models: the MCMCglmm R package. *Journal of Statistical Software, 33*(2), 1-22. https://doi.org/10.18637/jss.v033.i02

Hagey, T. J., Harte, S., Vickers, M., Harmon, L. J., & Schwarzkopf, L. (2017). There's more than one way to climb a tree: limb length and microhabitat use in lizards with toe pads. *PLOS ONE, 12*(9), e0184641. https://doi.org/10.1371/journal.pone.0184641

Halpern, M., & Martínez-Marcos, A. (2003). Structure and function of the vomeronasal system: an update. *Progress in Neurobiology, 70*(3), 245-318. https://doi.org/10.1016/s0301-0082(03)00103-5

Higgie, M., & Blows, M. W. (2008). The evolution of reproductive character displacement conflicts with how sexual selection operates within a species. *Evolution, 62*(5), 1192-1203. https://doi.org/10.1111/j.1558-5646.2008.00357.x

Higgie, M., Chenoweth, S., & Blows, M. W. (2000). Natural selection and the reinforcement of mate recognition. *Science, 290*(5491), 519-521. https://doi.org/10.1126/science.290.5491.519

Hoang, D. T., Chernomor, O., von Haeseler, A., Minh, B. Q., & Vinh, L. S. (2018). UFBoot2: improving the ultrafast bootstrap approximation. *Molecular Biology and Evolution, 35*(2), 518-522. https://doi.org/10.1093/molbev/msx281

Holm, S. (1979). A simple sequentially rejective multiple test procedure. *Scandinavian Journal of Statistics, 6*(2), 65-70.

Hopkins, C. D., & Bass, A. H. (1981). Temporal coding of species recognition signals in an electric fish. *Science, 212*(4490), 85-87. https://doi.org/10.1126/science.7209524

Hoskin, C. J., & Goosem, M. W. (2010). Road impacts on abundance, call traits, and body size of rainforest frogs in northeast Australia. *Ecology and Society, 15*(3), 15. https://doi.org/10.5751/ES-03272-150315

Hoskin, C. J., & Higgie, M. (2010). Speciation via species interactions: the divergence of mating traits within species. *Ecology Letters, 13*(4), 409-420. https://doi.org/10.1111/j.1461-0248.2010.01448.x

Huelsenbeck, J. P., Nielsen, R., & Bollback, J. P. (2003). Stochastic mapping of morphological characters. *Systematic Biology, 52*(2), 131-158. https://doi.org/10.1080/10635150390192780

Ibáñez, A., Menke, M., Quezada, G., Jiménez-Uzcátegui, G., Schulz, S., & Steinfartz, S. (2017). Diversity of compounds in femoral secretions of Galápagos iguanas (genera: *Amblyrhynchus* and *Conolophus*), and their potential role in sexual communication in lek-mating marine iguanas (*Amblyrhynchus cristatus*). *PeerJ, 5*, e3689. https://doi.org/10.7717/peerj.3689

Joshi, M., Ellsworth, B., & Thaker, M. (2022). Single components of complex chemical signals convey sex identity and individual variation. *Animal Behaviour, 187*, 1-13. https://doi.org/10.1016/j.anbehav.2022.02.013

Kalyaanamoorthy, S., Minh, B. Q., Wong, T. K. F., von Haeseler, A., & Jermiin, L. S. (2017). ModelFinder: fast model selection for accurate phylogenetic estimates. *Nature Methods, 14*(6), 587-589. https://doi.org/10.1038/nmeth.4285

Katoh, K., & Standley, D. M. (2013). MAFFT multiple sequence alignment software version 7: improvements in performance and usability. *Molecular Biology and Evolution, 30*(4), 772-780. https://doi.org/10.1093/molbev/mst010

Kealley, L., Doughty, P., Pepper, M., Keogh, J. S., Hillyer, M., & Huey, J. (2018). Conspicuously concealed: revision of the arid clade of the *Gehyra variegata* (Gekkonidae) group in Western Australia using an integrative molecular and morphological approach, with the description of five cryptic species. *PeerJ, 6*, e5334. https://doi.org/10.7717/peerj.5334

Khannoon, E. R., El-Gendy, A., & Hardege, J. D. (2011). Scent marking pheromones in lizards: cholesterol and long chain alcohols elicit avoidance and aggression in male *Acanthodactylus boskianus* (Squamata: Lacertidae). *Chemoecology, 21*(3), 143-149. https://doi.org/10.1007/s00049-011-0076-4

Lau, C. C., Christian, K., Fenker, J., Laver, R. J., O'Hara, K., Zozaya, S. M., Moritz, C., & Roycroft, E. (2025). Range size variably predicts genetic diversity in *Gehyra* geckos. *Evolution, 79*(6), 1086-1095. https://doi.org/10.1093/evolut/qpaf057

Lemmon, A. R., Emme, S. A., & Lemmon, E. M. (2012). Anchored hybrid enrichment for massively high-throughput phylogenomics. *Systematic Biology, 61*(5), 727-744. https://doi.org/10.1093/sysbio/sys049

López, P., Amo, L., & Martín, J. (2006). Reliable signaling by chemical cues of male traits and health state in male lizards, *Lacerta monticola*. *Journal of Chemical Ecology, 32*(2), 473-488. https://doi.org/10.1007/s10886-005-9012-9

Losos, J. B. (2009). *Lizards in an evolutionary tree: ecology and adaptive radiation of anoles*. University of California Press. https://doi.org/10.1525/california/9780520255913.001.0001

Maan, M. E., & Seehausen, O. (2011). Ecology, sexual selection and speciation. *Ecology Letters, 14*(6), 591-602. https://doi.org/10.1111/j.1461-0248.2011.01606.x

774 Maan, M. E., Seehausen, O., & Groothuis, T. G. G. (2017). Differential survival between visual
775 environments supports a role of divergent sensory drive in cichlid fish speciation. *The*
776 *American Naturalist, 189*(1), 78-85. https://doi.org/10.1086/689605
777 Mangiacotti, M., Baeckens, S., Scali, S., Martín, J., Van Damme, R., & Sacchi, R. (2021). Evolutionary
778 and biogeographical support for species-specific proteins in lizard chemical signals.
779 *Biological Journal of the Linnean Society, 134*(4), 912-928.
780 https://doi.org/10.1093/biolinnean/blab131
781 Mardia, K. V., Bibby, J. M., & Kent, J. T. (1979). *Multivariate analysis*. Academic Press.
782 Martín, J., & López, P. (2006). Interpopulational differences in chemical composition and
783 chemosensory recognition of femoral gland secretions of male lizards *Podarcis hispanica*:
784 implications for sexual isolation in a species complex. *Chemoecology, 16*(1), 31-38.
785 https://doi.org/10.1007/s00049-005-0326-4
786 Martín, J., & López, P. (2010). Condition-dependent pheromone signaling by male rock lizards: more
787 oily scents are more attractive. *Chemical Senses, 35*(4), 253-262.
788 https://doi.org/10.1093/chemse/bjq009
789 Martín, J., & López, P. (2011). Pheromones and reproduction in reptiles. In D. O. Norris & K. H. Lopez
790 (Eds.), *Hormones and reproduction of vertebrates, Vol. 3: Reptiles* (pp. 141-167). Academic
791 Press. https://doi.org/10.1016/b978-0-12-374930-7.10006-8
792 Martín, J., & López, P. (2013). Effects of global warming on sensory ecology of rock lizards: increased
793 temperatures alter the efficacy of sexual chemical signals. *Functional Ecology, 27*(6), 1332-
794 1340. https://doi.org/10.1111/1365-2435.12128
795 Martín, J., & López, P. (2014). Pheromones and chemical communication in lizards. In J. L. Rheubert,
796 D. S. Siegel, & S. E. Trauth (Eds.), *Reproductive biology and phylogeny of lizards and tuatara*
797 (pp. 43-77). CRC Press. https://doi.org/10.1201/b17961-6

798 Martín, J., Ortega, J., & López, P. (2015). Interpopulational variations in sexual chemical signals of
799 Iberian wall lizards may allow maximizing signal efficiency under different climatic
800 conditions. *PLOS ONE, 10*(6), e0131492. https://doi.org/10.1371/journal.pone.0131492
801 Mason, R. T., & Parker, M. R. (2010). Social behavior and pheromonal communication in reptiles.
802 *Journal of Comparative Physiology A, 196*(10), 729-749. https://doi.org/10.1007/s00359-
803 010-0551-3
804 McDonough, L. M., Brown, D. F., & Aller, W. C. (1989). Insect sex pheromones: effect of temperature
805 on evaporation rates of acetates from rubber septa. *Journal of Chemical Ecology, 15*(3), 779-
806 790. https://doi.org/10.1007/BF01015176
807 Minh, B. Q., Schmidt, H. A., Chernomor, O., Schrempf, D., Woodhams, M. D., von Haeseler, A., &
808 Lanfear, R. (2020). IQ-TREE 2: new models and efficient methods for phylogenetic inference
809 in the genomic era. *Molecular Biology and Evolution, 37*(5), 1530-1534.
810 https://doi.org/10.1093/molbev/msaa015
811 Moritz, C., Pratt, R. C., Bank, S., Bourke, G., Bragg, J. G., Doughty, P., Keogh, J. S., Laver, R. J., Potter,
812 S., Teasdale, L. C., Tedeschi, L. G., & Oliver, P. M. (2018). Cryptic lineage diversity, body size
813 divergence, and sympatry in a species complex of Australian lizards (*Gehyra*). *Evolution,*
814 *72*(1), 54-66. https://doi.org/10.1111/evo.13380
815 Müller-Schwarze, D. (2006). *Chemical ecology of vertebrates*. Cambridge University Press.
816 Noble, C., Laver, R. J., Rosauer, D. F., Ferrier, S., & Moritz, C. (2018). Phylogeographic evidence for
817 evolutionary refugia in the Gulf sandstone ranges of northern Australia. *Australian Journal of*
818 *Zoology, 65*(6), 408-416. https://doi.org/10.1071/ZO17079
819 Oksanen, J., Simpson, G. L., Blanchet, F. G., Kindt, R., Legendre, P., Minchin, P. R., O'Hara, R. B.,
820 Solymos, P., Stevens, M. H. H., Szoecs, E., Wagner, H., Bedward, M., Bolker, B., Borcard, D.,
821 Carvalho, G., De Caceres, M., Durand, S., Evangelista, H. B. A., Hannigan, G., … Weedon, J.
822 (2026). *vegan: Community ecology package* (R package version 2.7-5).
823 https://doi.org/10.32614/CRAN.package.vegan

824 Oliver, P. M., Ashman, L. G., Bank, S., Laver, R. J., Pratt, R. C., Tedeschi, L. G., & Moritz, C. (2019). On
825 and off the rocks: persistence and ecological diversification in a tropical Australian lizard
826 radiation. *BMC Evolutionary Biology, 19*(1), 81. https://doi.org/10.1186/s12862-019-1408-1
827 Oliver, P. M., Laver, R. J., Lee, M. S. Y., Kraus, F., Matzke, N. J., Austin, C. C., Fisher, R. N., & Moritz, C.
828 (2026). Limited dispersal leads to differing evolutionary trajectories between adjacent
829 continental and insular lineages in a widespread lizard radiation (*Gehyra*: Gekkonidae).
830 *Biological Journal of the Linnean Society, 147*(3), blag004.
831 https://doi.org/10.1093/biolinnean/blag004
832 Oliver, P. M., Prasetya, A. M., Tedeschi, L. G., Fenker, J., Ellis, R. J., Doughty, P., & Moritz, C. (2020).
833 Crypsis and convergence: integrative taxonomic revision of the *Gehyra* australis group
834 (Squamata: Gekkonidae) from northern Australia. *PeerJ, 8*, e7971.
835 https://doi.org/10.7717/peerj.7971
836 Ord, T. J., & Stamps, J. A. (2009). Species identity cues in animal communication. *The American*
837 *Naturalist, 174*(4), 585-593. https://doi.org/10.1086/605372
838 Pagel, M. (1999). Inferring the historical patterns of biological evolution. *Nature, 401*(6756), 877-
839 884. https://doi.org/10.1038/44766
840 Rambaut, A., Drummond, A. J., Xie, D., Baele, G., & Suchard, M. A. (2018). Posterior summarization in
841 Bayesian phylogenetics using Tracer 1.7. *Systematic Biology, 67*(5), 901-904.
842 https://doi.org/10.1093/sysbio/syy032
843 Rannala, B., & Yang, Z. (2007). Inferring speciation times under an episodic molecular clock.
844 *Systematic Biology, 56*(3), 453-466. https://doi.org/10.1080/10635150701420643
845 Read, W. J., Laver, R. J., Lau, C. C., Moritz, C., & Zozaya, S. M. (2025). Repeated mitochondrial
846 capture with limited genomic introgression in a lizard group. *Molecular Ecology, 34*(10),
847 e17766. https://doi.org/10.1111/mec.17766

Read, W. J., Laver, R. J., & Zozaya, S. M. (2026). *Gehyra woondagoom* sp. nov. (Squamata; Gekkonidae), a new gecko from the Yampi Peninsula and Buccaneer Archipelago of Western Australia. *Australian Journal of Taxonomy, 135*, 1-13. https://doi.org/10.54102/ajt.berkw

Regnier, F. E., & Goodwin, M. (1977). On the chemical and environmental modulation of pheromone release from vertebrate scent marks. In D. Müller-Schwarze & M. M. Mozell (Eds.), *Chemical signals in vertebrates* (pp. 115-133). Springer US. https://doi.org/10.1007/978-1-4684-2364-8_8

Revell, L. J. (2012). phytools: an R package for phylogenetic comparative biology (and other things). *Methods in Ecology and Evolution, 3*(2), 217-223. https://doi.org/10.1111/j.2041-210x.2011.00169.x

Roberts, S. A., Simpson, D. M., Armstrong, S. D., Davidson, A. J., Robertson, D. H., McLean, L., Beynon, R. J., & Hurst, J. L. (2010). Darcin: a male pheromone that stimulates female memory and sexual attraction to an individual male's odour. *BMC Biology, 8*(1), 75. https://doi.org/10.1186/1741-7007-8-75

Schliep, K. P. (2011). phangorn: phylogenetic analysis in R. *Bioinformatics, 27*(4), 592-593. https://doi.org/10.1093/bioinformatics/btq706

Scott, M. L., Llewelyn, J., Higgie, M., Hoskin, C. J., Pike, K., & Phillips, B. L. (2015). Chemoreception and mating behaviour of a tropical Australian skink. *Acta Ethologica, 18*(3), 283-293. https://doi.org/10.1007/s10211-015-0213-0

Seehausen, O., Terai, Y., Magalhaes, I. S., Carleton, K. L., Mrosso, H. D. J., Miyagi, R., Van Der Sluijs, I., Schneider, M. V., Maan, M. E., Tachida, H., Imai, H., & Okada, N. (2008). Speciation through sensory drive in cichlid fish. *Nature, 455*(7213), 620-626. https://doi.org/10.1038/nature07285

Singhal, S., Colston, T. J., Grundler, M. R., Smith, S. A., Costa, G. C., Colli, G. R., Moritz, C., Pyron, R. A., & Rabosky, D. L. (2021). Congruence and conflict in the higher-level phylogenetics of

873 squamate reptiles: an expanded phylogenomic perspective. *Systematic Biology, 70*(3), 542-
874 557. https://doi.org/10.1093/sysbio/syaa054
875 Singhal, S., Grundler, M. R., Colli, G. R., & Rabosky, D. L. (2017). Squamate Conserved Loci (SqCL): a
876 unified set of conserved loci for phylogenomics and population genetics of squamate
877 reptiles. *Molecular Ecology Resources, 17*(6), e12-e24. https://doi.org/10.1111/1755-
878 0998.12681
879 Sistrom, M., Hutchinson, M. N., Hutchinson, R., & Donnellan, S. (2009). Molecular phylogeny of
880 Australian *Gehyra* (Squamata: Gekkonidae) and taxonomic revision of *Gehyra variegata* in
881 south-eastern Australia. *Zootaxa, 2277*, 14-32. https://doi.org/10.5281/zenodo.191131
882 Smadja, C., & Butlin, R. K. (2009). On the scent of speciation: the chemosensory system and its role
883 in premating isolation. *Heredity, 102*(1), 77-97. https://doi.org/10.1038/hdy.2008.55
884 Srivathsan, A., Lee, L., Katoh, K., Hartop, E., Kutty, S. N., Wong, J., Yeo, D., & Meier, R. (2021).
885 ONTbarcoder and MinION barcodes aid biodiversity discovery and identification by
886 everyone, for everyone. *BMC Biology, 19*, 217. https://doi.org/10.1186/s12915-021-01141-x
887 Steenwyk, J. L., Buida, T. J., Li, Y., Shen, X.-X., & Rokas, A. (2020). ClipKIT: a multiple sequence
888 alignment trimming software for accurate phylogenomic inference. *PLOS Biology, 18*(12),
889 e3001007. https://doi.org/10.1371/journal.pbio.3001007
890 Symonds, M. R. E., & Elgar, M. A. (2008). The evolution of pheromone diversity. *Trends in Ecology &*
891 *Evolution, 23*(4), 220-228. https://doi.org/10.1016/j.tree.2007.11.009
892 Tiatragul, S., Brennan, I. G., Skeels, A., Esquerré, D., Zozaya, S. M., Keogh, J. S., & Pepper, M. (2026).
893 Aridification and habitat shifts are associated with diversification in Australian diplodactylid
894 geckos. *Systematic Biology*, syag066. https://doi.org/10.1093/sysbio/syag066
895 To, A. W. Y., Dingle, C., & Collins, S. A. (2021). Multiple constraints on urban bird communication:
896 both abiotic and biotic noise shape songs in cities. *Behavioral Ecology, 32*(5), 1042-1053.
897 https://doi.org/10.1093/beheco/arab058

898 Torres-Dowdall, J., Pierotti, M. E. R., Härer, A., Karagic, N., Woltering, J. M., Henning, F., Elmer, K. R.,
899 & Meyer, A. (2017). Rapid and parallel adaptive evolution of the visual system of Neotropical
900 Midas cichlid fishes. *Molecular Biology and Evolution, 34*(10), 2469-2485.
901 https://doi.org/10.1093/molbev/msx143
902 Uetz, P., Freed, P., Aguilar, R., Reyes, F., Kudera, J., & Hošek, J. (2026). *The Reptile Database*.
903 http://www.reptile-database.org
904 Van Bocxlaer, I., Maex, M., Treer, D., Janssenswillen, S., Janssens, R., Vandebergh, W., Proost, P., &
905 Bossuyt, F. (2016). Beyond sodefrin: evidence for a multi-component pheromone system in
906 the model newt *Cynops pyrrhogaster* (Salamandridae). *Scientific Reports, 6*(1), 21880.
907 https://doi.org/10.1038/srep21880
908 Vicent-Castelló, P., Herrel, A., Harris, D. J., & Kaliontzopoulou, A. (2025). Walking or hanging: the role
909 of habitat use for body shape evolution in lacertid lizards. *Journal of Evolutionary Biology,*
910 *38*(3), 353-366. https://doi.org/10.1093/jeb/voaf003
911 Weber, M. G., Cacho, N. I., Phan, M. J. Q., Disbrow, C., Ramírez, S. R., & Strauss, S. Y. (2018). The
912 evolution of floral signals in relation to range overlap in a clade of California Jewelflowers
913 (*Streptanthus* s.l.). *Evolution, 72*(4), 798-807. https://doi.org/10.1111/evo.13456
914 Weber, M. G., Mitko, L., Eltz, T., & Ramírez, S. R. (2016). Macroevolution of perfume signalling in
915 orchid bees. *Ecology Letters, 19*(11), 1314-1323. https://doi.org/10.1111/ele.12667
916 Weldon, P. J., Flachsbarth, B., & Schulz, S. (2008). Natural products from the integument of nonavian
917 reptiles. *Natural Product Reports, 25*(4), 738-756. https://doi.org/10.1039/b509854h
918 Wilson, J. K., Kessler, A., & Woods, H. A. (2015). Noisy communication via airborne infochemicals.
919 *BioScience, 65*(7), 667-677. https://doi.org/10.1093/biosci/biv062
920 Wilson, S., & Swan, G. (2025). *A complete guide to reptiles of Australia* (7th ed.). New Holland
921 Publishers.
922 Wong, T. K. F., Ly-Trong, N., Ren, H., Demotte, P., Baños, H., Roger, A. J., Susko, E., Bielow, C., De
923 Maio, N., Goldman, N., Hahn, M. W., dos Reis, M., Vinh, L. S., Huttley, G., Lanfear, R., &

924 Minh, B. Q. (2025). IQ-TREE 3: phylogenomic inference software using complex evolutionary
925 models. EcoEvoRxiv. https://doi.org/10.32942/X2P62N
926 Wyatt, T. D. (2003). *Pheromones and animal behaviour: communication by smell and taste*.
927 Cambridge University Press. https://doi.org/10.1017/CBO9780511615061
928 Zhang, C., & Mirarab, S. (2022). Weighting by gene tree uncertainty improves accuracy of quartet-
929 based species trees. *Molecular Biology and Evolution, 39*(12), msac215.
930 https://doi.org/10.1093/molbev/msac215
931 Zozaya, S. M., Fenker, J., & Macdonald, S. L. (2019a). A new species of rock-dwelling gecko
932 (Gekkonidae: *Gehyra*) from the Mt Surprise region of northern Queensland, Australia.
933 *Zootaxa, 4688*(4), 503-518. https://doi.org/10.11646/zootaxa.4688.4.3
934 Zozaya, S. M., Higgie, M., Moritz, C., & Hoskin, C. J. (2019b). Are pheromones key to unlocking cryptic
935 lizard diversity? *The American Naturalist, 194*(2), 168-182. https://doi.org/10.1086/704059
936 Zozaya, S. M., Macor, S. A., Schembri, R., Higgie, M., Hoskin, C. J., O'Hara, K., Lau, C. C., Read, W. J., &
937 Moritz, C. (2025). Contact zones reveal restricted introgression despite frequent
938 hybridization across a recent lizard radiation. *Evolution, 79*(3), 411-422.
939 https://doi.org/10.1093/evolut/qpae174
940 Zozaya, S. M., Teasdale, L. C., Moritz, C., Higgie, M., & Hoskin, C. J. (2022). Composition of a chemical
941 signalling trait varies with phylogeny and precipitation across an Australian lizard radiation.
942 *Journal of Evolutionary Biology, 35*(7), 919-933. https://doi.org/10.1111/jeb.14031
943 Zozaya, S. M., Teasdale, L. C., Tedeschi, L. G., Higgie, M., Hoskin, C. J., & Moritz, C. (2023). Initiation
944 of speciation across multiple dimensions in a rock-restricted, tropical lizard. *Molecular*
945 *Ecology, 32*(3), 680-695. https://doi.org/10.1111/mec.16787

Supplementary Material

Methods S1. Mitochondrial DNA sampling, sequencing, and phylogenetics

Some *Gehyra* are difficult or impossible to identify based on morphology. Because of this, we performed mitochondrial DNA (mtDNA) sequencing on a subset of sampled individuals. These included both a subset of individuals sampled for chemical signals and sometimes other individuals, such as females, from the same sampling sites. Where morphologically indistinguishable species/lineages were found to occur in sympatry or at contact zones, all individuals were sequenced to confirm species/lineage assignment. Where species identification by morphology was more tractable, only a few samples were sequenced to confirm that morphology-based identification was correct and consistent. A few species are unmistakable in the field and, for these, few to no samples were sequenced; these include the following *Gehyra*: *einasleighensis*, *minuta* (minuta1 & minuta2), *occidentalis*-OR, *spheniscus*, and *xenopus*. The identification of samples belonging to some species could be based on previous studies: genome-wide DArTseq data in Lau et al. (2025) included 79 of the individuals analysed here, from 13 lineages, and confirmed *G. lapistola* sampled within 1 km of our *G. lapistola* site. Similarly, all individuals of the nanamulti lineage sampled here—and some individuals of nana1, nana4, *paranana*, *occidentalis*-OR, and *occidentalis*-KL—were confirmed through genome-wide DArTseq in Read et al. (2025); genomic identification for nanamulti is crucial because of repeated mitochondrial capture from *G. multiporosa* (not sampled here). Some mtDNA data from Read et al. (2025) were included here (see below).

We sequenced *ca.* 1,041 bp of the mitochondrial *NADH dehydrogenase subunit 2* (*ND2*) locus using the Oxford Nanopore Technologies MinION method presented in Srivathsan et al. (2021); methods followed those presented in Zozaya et al. (2025) except using the primers M112F (5'-AAGCTTTCGGGGCCCATACC-3') and M1123R (5'-GCTTAATTAAAGTGTYTGAGTTGC-3') (Sistrom et al., 2009). We sequenced 532 new individuals and combined these with 207 published sequences from nine other studies (Doughty et al., 2012, 2018a; Ashman et al., 2018; Kealley et al., 2018; Moritz et al., 2018; Noble et al., 2018; Oliver et al., 2019; Zozaya et al., 2019a; Read et al., 2025). Published sequences were included either because they represent geckos sampled for chemical signals or else originating from the same sites, or because they provide reference sequences for assigning newly sequenced individuals to species (1–3 representatives per species/lineage). All 739 samples included in mtDNA phylogenetic analysis, and the studies each sequence originated from, are given in Table S1; the source of genetic data for each individual sampled for chemical signals is given in Table S2.

Sequences were aligned using ClustalW with default settings in Geneious Prime v2021.2.2. The alignment was then manually checked for gaps, unexpected stop codons, or frame shifts. This yielded a final ND2 alignment of 1,044 bp across 739 samples. Phylogenetic analysis was done using IQ-TREE v3.0.0 (Wong et al., 2025); the alignment was partitioned by codon position, with the final partition scheme and substitution models chosen using ModelFinder (Kalyaanamoorthy et al., 2017), and with 1,000 ultrafast bootstrap replicates (UFBoot2; Hoang et al., 2018). Model selection maintained each codon position as a separate partition with the following substitution models, in order of codon position: TVM+F+I+R4; GTR+F+R4; GTR+F+R5. The resulting phylogeny is shown in Figure S1.

Table S1. Individuals included in the mitochondrial *ND2* phylogeny (739 sequences), with lineage assignment and the source of each sequence (new or published study), provided as a separate CSV file.



Figure S1. Maximum-likelihood phylogeny of mitochondrial *ND2* sequences (739 individuals, 1,044 bp) inferred in IQ-TREE with a codon-position partitioned model. Tip labels give specimen ID and species or lineage. Lineages are ordered as in Figures S2 and S3 where the topology allows. Ultrafast bootstrap (UFBoot) values below 95 are shown for nodes among and at the base of lineages. Scale bar in substitutions per site.

Figure S1. (continued)

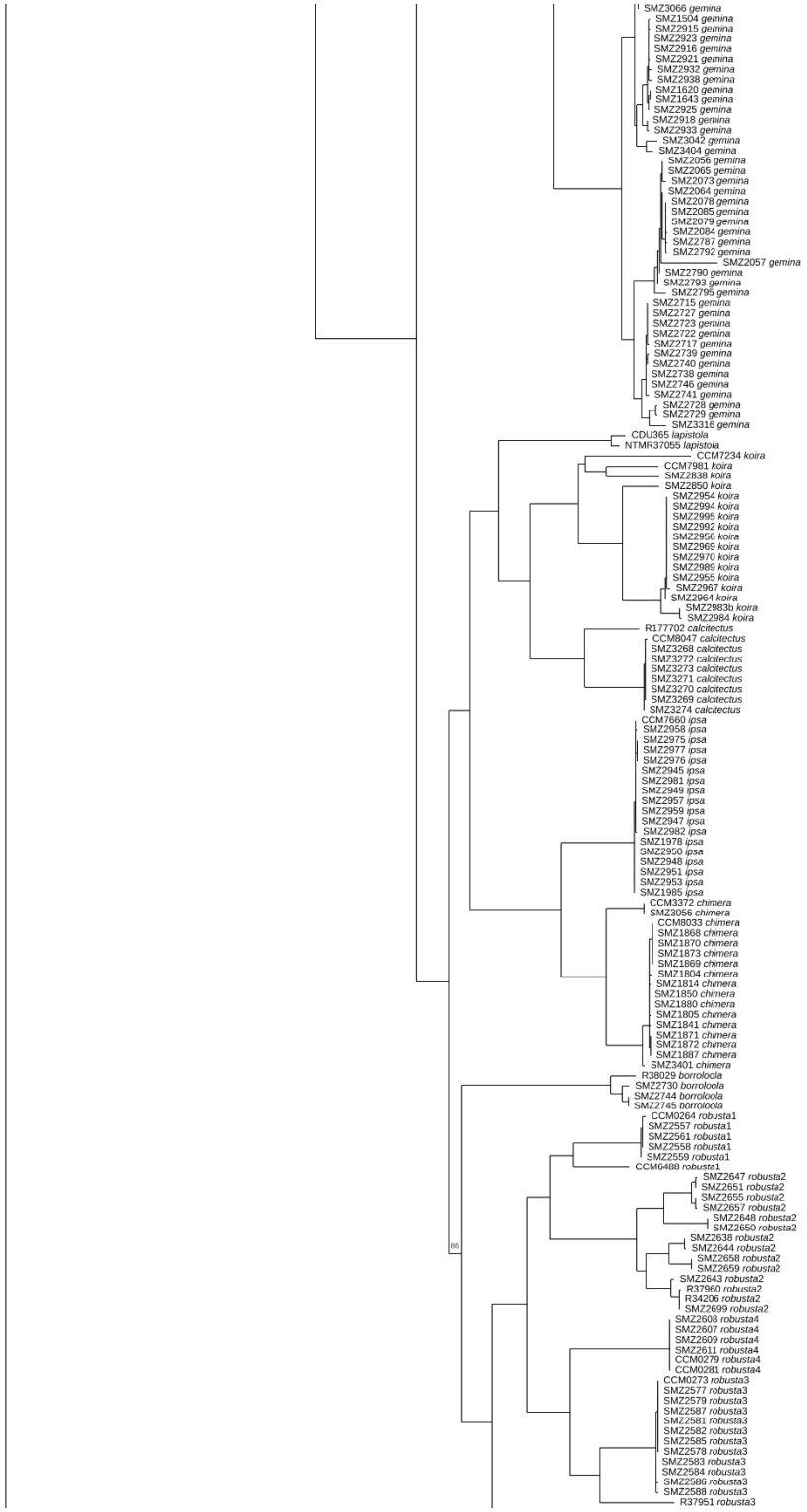


Fig. S1 (2 of 5)

Figure S1. (continued)



Fig. S1 (3 of 5)

Figure S1. (continued)



Fig. S1 (4 of 5)

Figure S1. (continued)

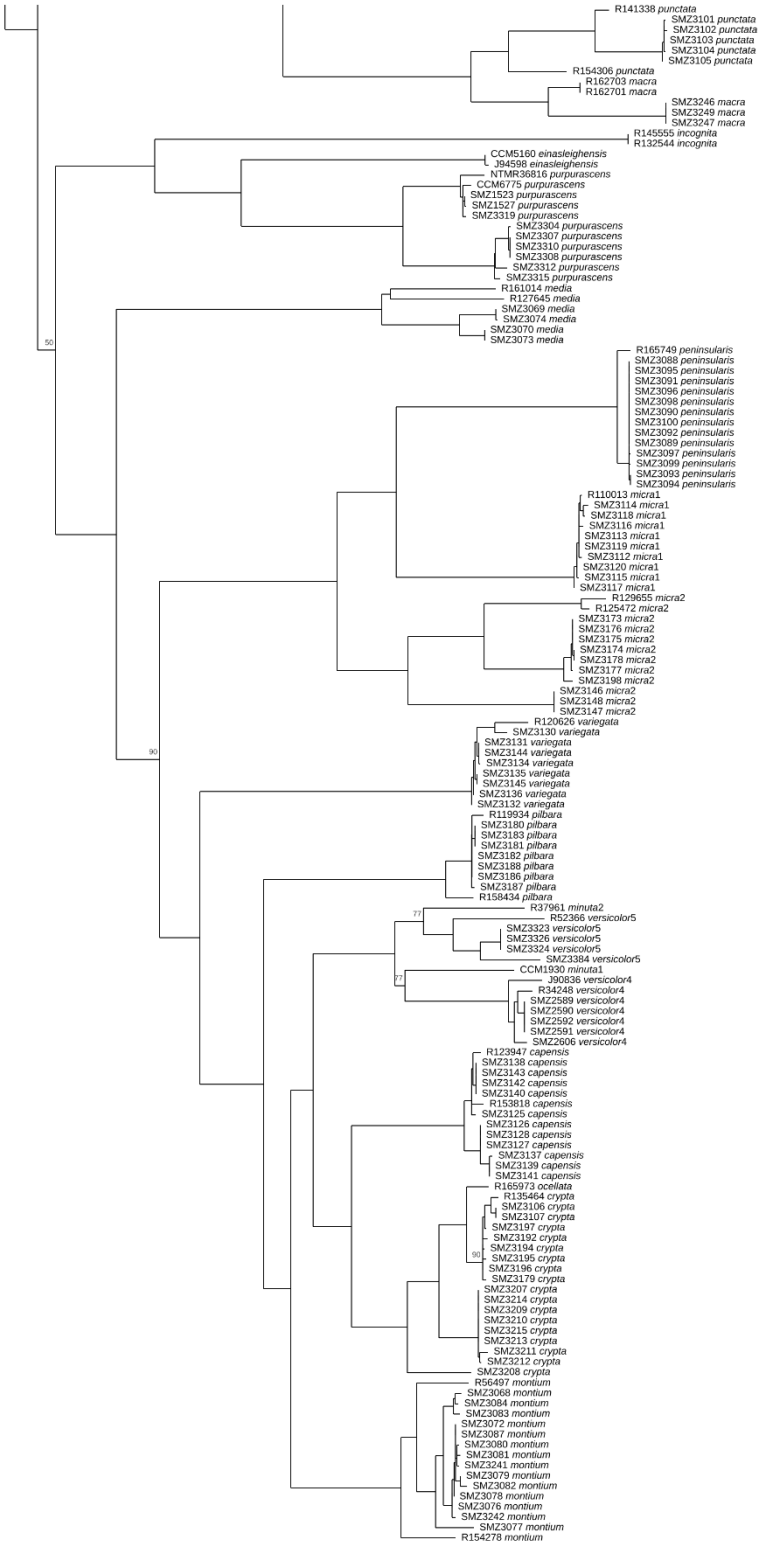


Fig. S1 (5 of 5)

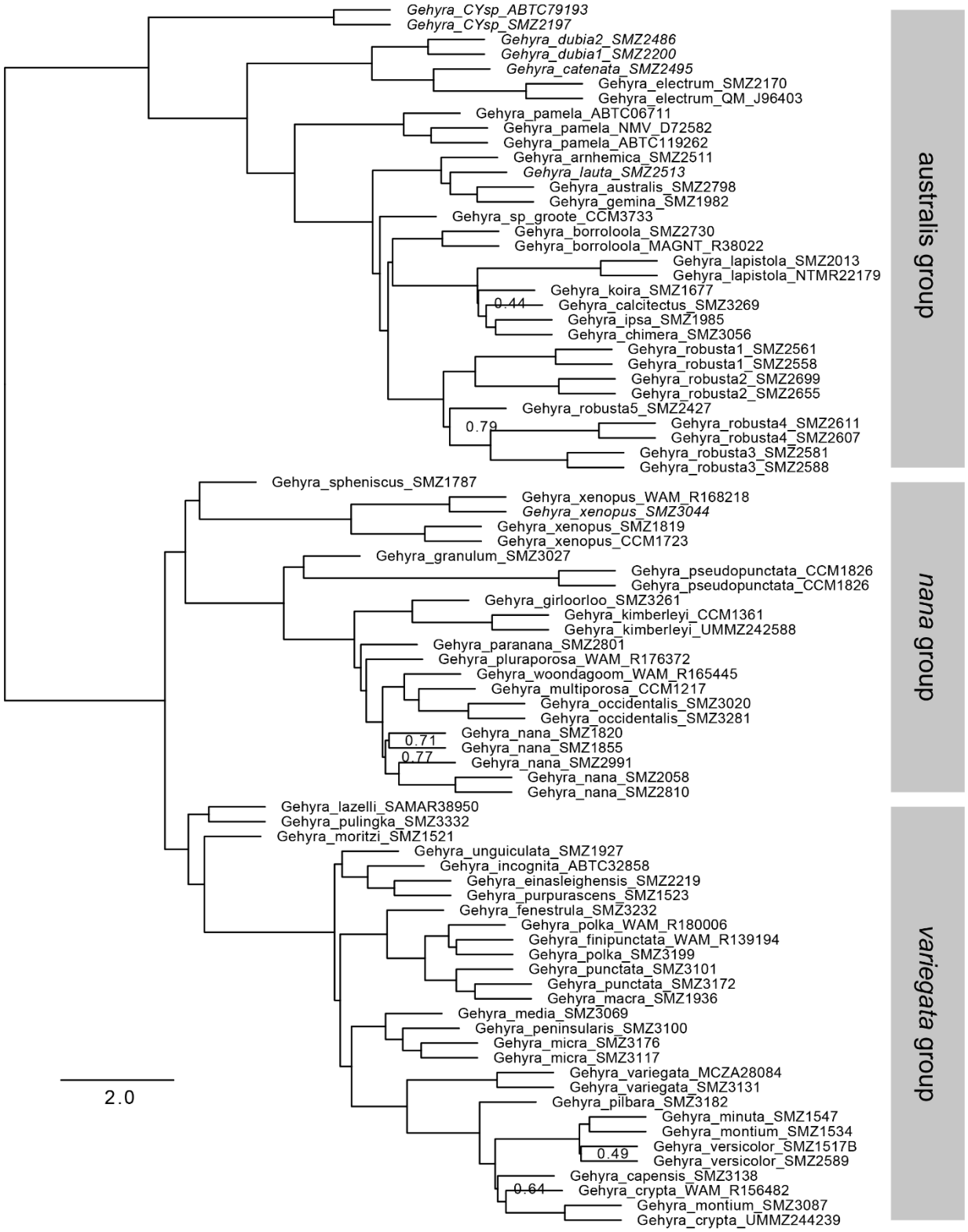


Figure S2. Species tree inferred with weighted ASTRAL using 374 Anchored Hybrid Enrichment loci and used to inform the topology for the MCMCTree analysis (Fig. S3). Local posterior probability (pp) values are shown only where pp < 0.95. Scale bar shows branch length in coalescent units. Tree file available as part of the online repository.

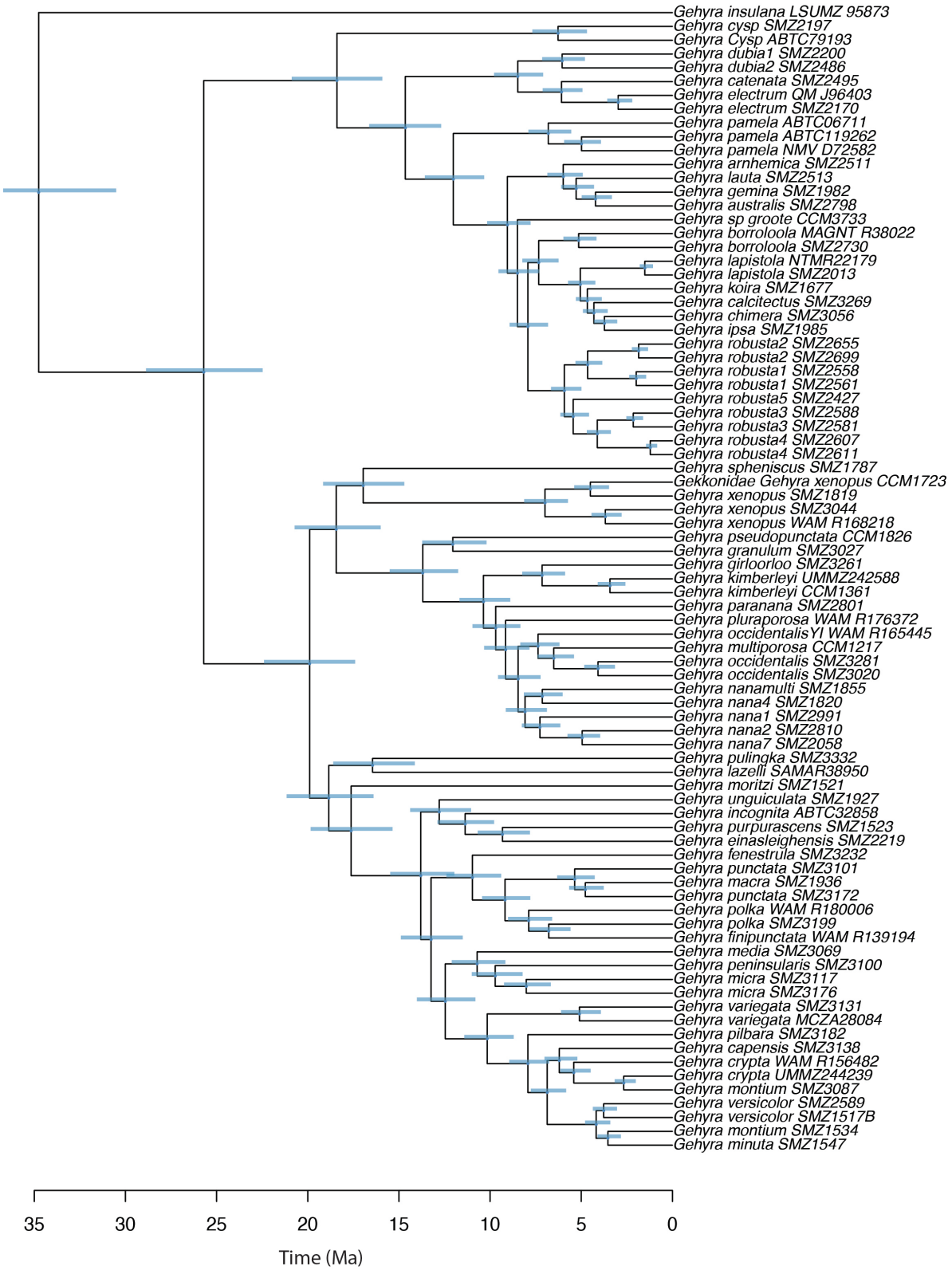


Figure S3. Time calibrated phylogenetic tree of Australian *Gehyra* displayed in Figure 1 and used for downstream analyses. Tree constructed using MCMCTree with 374 Anchored Hybrid Enrichment (AHE) loci and four secondary calibration points. Node error bars represent 95% highest posterior density (HPD) interval from MCMC chain. Tree file available as part of the online repository.

Table S2. Specimen data for all *Gehyra* samples collected for chemical signal analysis (827 samples: 768 successfully integrated, 22 failed integrations and 37 field controls), provided as a separate CSV file. Lineage matches lineage names in the main text and phylogenies; Group is the species group. Coordinates are decimal degrees (WGS84). integration_status gives the outcome of chromatogram integration (successful, failed or control), and outlier marks the 14 individuals excluded as outliers before analysis. mtDNA_data and SNP_data give the source of the mitochondrial and genome-wide SNP data used to confirm each individual's identity ("New" = sequenced in this study; Methods S1). Blank cells denote data not applicable or not recorded.

Methods S2. Data processing and transformations

After removing the contaminant peak, each individual was characterised by 61 peaks. We converted peak areas to proportions of each individual's summed peak area (each peak area divided by the summed area of all 61 peaks), so the proportions summed to one within each sample. Because proportions that sum to one are not free to vary independently (the unit-sum constraint), they must be transformed before analysis (Aitchison, 1982). We applied a centred log-ratio (CLR) transformation, expressing each peak as the log of its proportion divided by the geometric mean of all 61 peak proportions for that individual.

CLR values sum to zero within each individual, so one peak is fully determined by the others and only 60 carry independent information. We therefore removed one peak before fitting multivariate models. Rather than dropping a peak at random, we chose the one whose removal would lose the least biological signal. We ran a principal component analysis (PCA) on the full 61-peak CLR matrix and retained the PC axes needed to capture 60% of the variance (nine axes in the final dataset). For each peak we calculated its mean absolute loading across these axes; peaks with low scores contribute little to the main axes of variation and so make the best candidates for removal. To avoid dropping peaks with unusually high or low abundance, we restricted candidates to those whose mean raw abundance fell between the 10th and 90th percentiles and removed the lowest-scoring candidate (peak 46; Fig. S4).

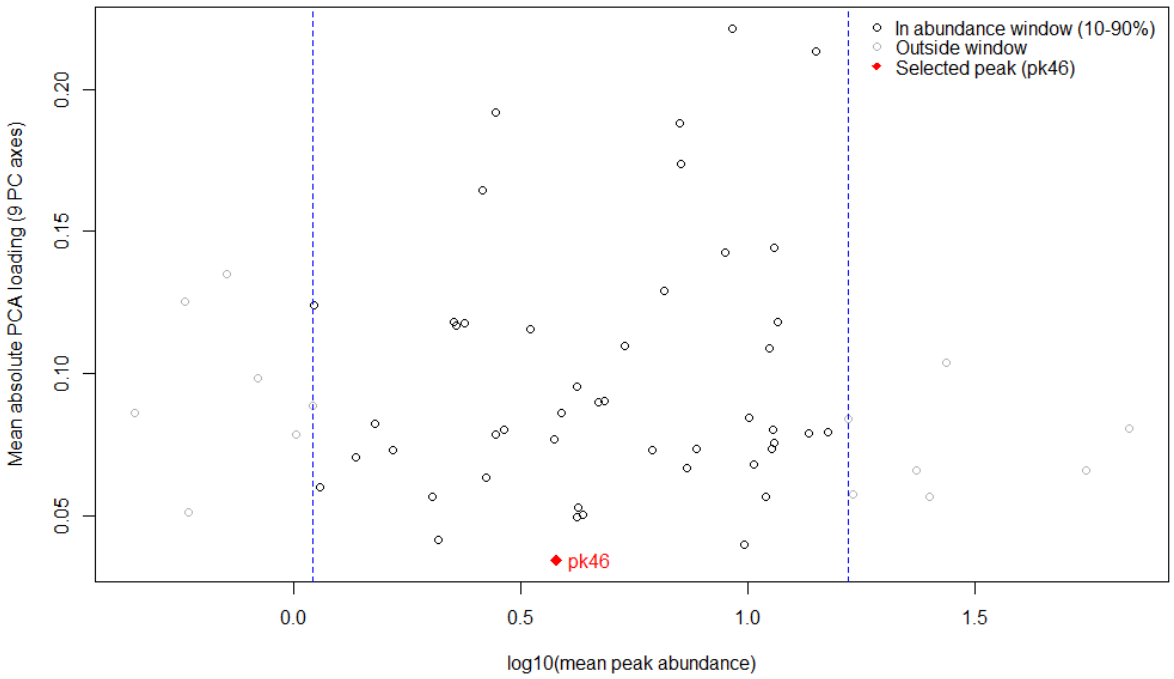


Figure S4. Peak selection criterion. Mean absolute PCA loading (across the nine axes capturing 60% of variance) plotted against log10 mean peak abundance for all 61 peaks. Black circles fall within the 10th–90th percentile abundance window (dashed vertical lines) and were eligible for selection; grey circles fall outside this window and were excluded. Within the eligible window, peak 46 (red diamond) had the lowest loading and was removed.

We considered the additive log-ratio (ALR) transformation instead, but ALR depends heavily on which peak is used as the reference, and our dataset has no obvious internal standard or biologically meaningful reference compound. CLR followed by removal of a low-information peak avoids this problem, since it uses the geometric mean of all peaks as the denominator and selects

the removed peak through a clear, repeatable criterion. To check that this selection was robust, we repeated it while retaining enough PC axes to capture between 50% and 80% of the variance (Table S3). Peak 46 was selected from 50% up to 70%, with a different peak (peak 48) chosen only at 80%. Capturing 80% pulls in lower-variance axes that weight the criterion toward minor rather than major chemical variation. Our choice was therefore stable across a sensible range.

Table S3. Sensitivity of peak selection to the number of principal component (PC) axes retained. For each number of axes (chosen to capture increasing proportions of total variance), the table shows the cumulative variance captured and the peak identified for removal by the loading-based criterion. Peak 46 was selected across the 50–70% range (6–14 axes); a different peak (peak 48) was selected only when 21 axes were retained (80% variance).

PC axes retained	Cumulative variance (%)	Peak selected
6	52.2	46
9	60.3	46
14	70.6	46
21	80.8	48

Methods S3. Correcting for sample concentration

Converting peak areas to proportions removes variation in injection volume, but the flame-ionisation detector (FID) response is not perfectly linear across the full range of signal intensities, so relative peak abundances can still vary systematically with summed peak area even after proportional normalisation. We saw this in our data: PC1 of the CLR-transformed matrix, which captured 24.4% of total variance, was strongly correlated with log-transformed summed peak area ($\beta = -3.35$, $p < 0.001$; Fig. S5, top left). This is partially because secretion volume scales with body size: larger lizards deposit more secretion, raising the total signal recorded by the FID, so that trace compounds falling below detection in smaller samples become quantifiable in larger ones. In studies with smaller sample sizes this is often dealt with by drying and weighing a standardised amount of secretion per individual before analysis, but with 790 samples (754 retained for analysis) this was not feasible, so we corrected for this statistically. Because volume scales with size, snout–vent length (SVL) and summed peak area were themselves strongly correlated ($r = 0.82$), and PC1 of the uncorrected matrix tracked both (PC1 vs SVL, $r = -0.74$; Fig. S6, left).

We corrected for summed peak area rather than SVL because summed peak area directly measures how much signal was detected, and SVL may carry genuine biological information: larger or higher-condition males can differ in the proportions of steroids and fatty acids they secrete (López et al., 2006; Martín & López, 2010). Correcting on SVL would therefore risk removing real size-related variation in signal composition. Because SVL and summed peak area are so closely correlated, correcting on summed peak area removed most of the size-associated variation as well (PC1 vs SVL fell from $r = -0.74$ to $r = 0.18$ after correction; Fig. S6, right), but it better preserves any size-related biology that is independent of secretion volume. To apply the correction, we regressed the 60-peak CLR matrix on log-transformed summed peak area using a multivariate RRPP model in the RRPP package (Collyer & Adams, 2018) and used the residuals as the response in subsequent analyses. After correction, PC1 captured 13.5% of the variance and was independent of summed peak area ($\beta \approx 0$, $p = 1$; Fig. S5, bottom left), while PC2 was largely unaffected (8.6% before, 10.1% after). Individual corrected profiles were then aggregated to lineage means by averaging across individuals

within each of the 58 lineages, aligning the dataset with the tips of the phylogeny. Lineage means were then standardised to zero mean and unit variance for each peak, so that abundant compounds did not dominate the analyses.

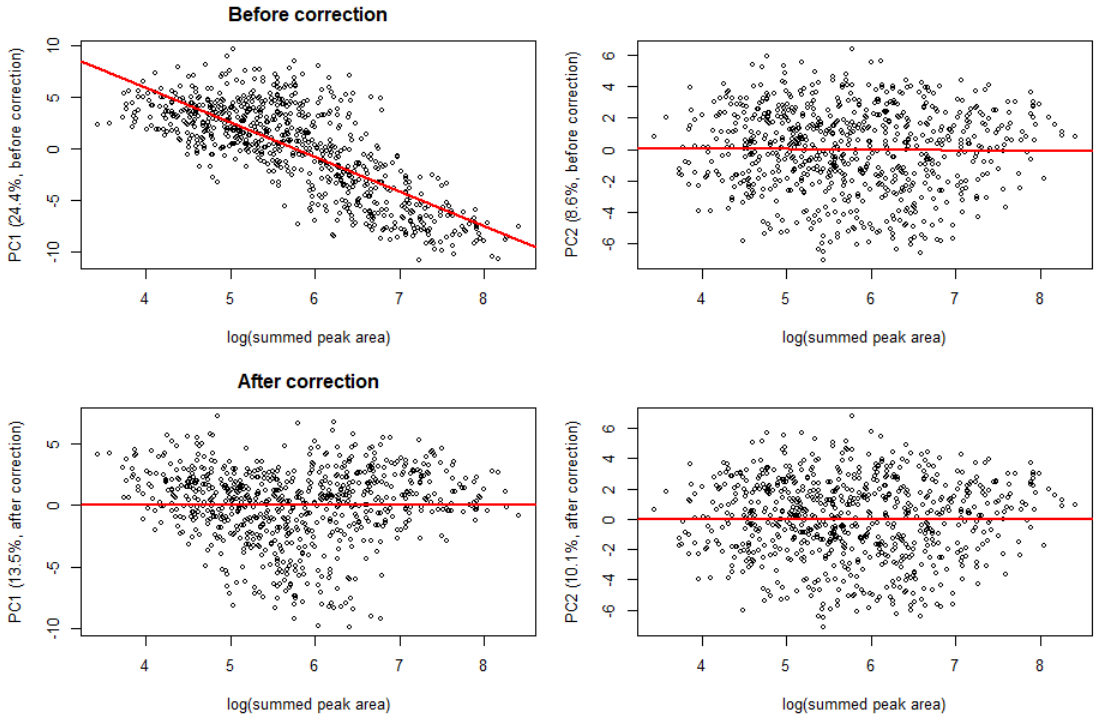


Figure S5. Justification for correcting CLR-transformed chemical signal data for summed peak area. Top row: PC1 (24.4% of variance) and PC2 (8.6%) of the CLR-transformed peak matrix plotted against log-transformed summed peak area, before correction. PC1 shows a strong negative dependence on log(summed peak area) ($\beta = -3.35$, $p < 0.001$), indicating that the dominant axis of chemical variation was confounded with sample concentration; PC2 shows no such dependence. Bottom row: the same axes after regressing the 60-peak CLR matrix on log(summed peak area) and retaining residuals. PC1 (13.5% of variance) is now independent of summed peak area ($\beta \approx 0$, $p = 1$), and PC2 (10.1%) is unaffected. Each point is one individual *Gehyra*; the red line is a linear fit.

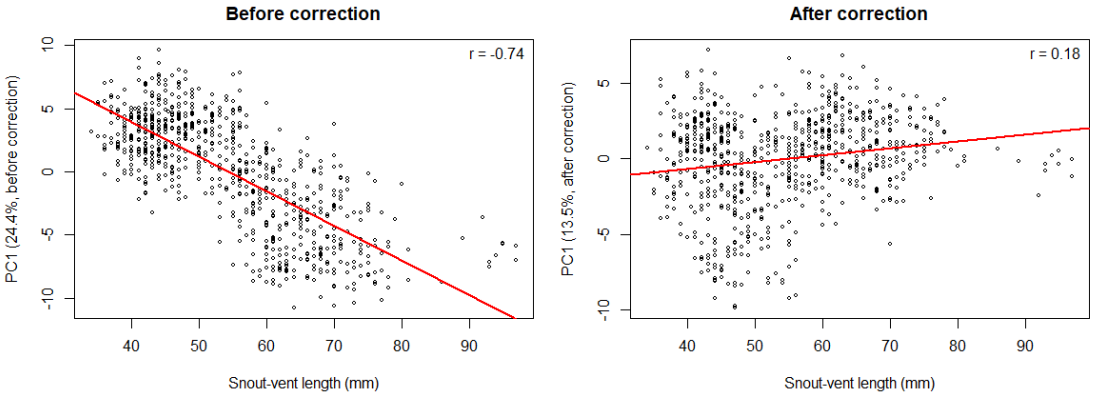


Figure S6. PC1 of the CLR-transformed chemical matrix plotted against snout–vent length (SVL), before (left) and after (right) correction for summed peak area. SVL and summed peak area were strongly correlated ($r = 0.82$), so PC1 of the uncorrected data tracked body size ($r = -0.74$). After correction, most of this relationship was removed ($r = 0.18$), as expected given the close correlation between SVL and summed peak area. Each point is one individual *Gehyra*; the red line is a linear fit. Five individuals lacking SVL measurements were excluded.

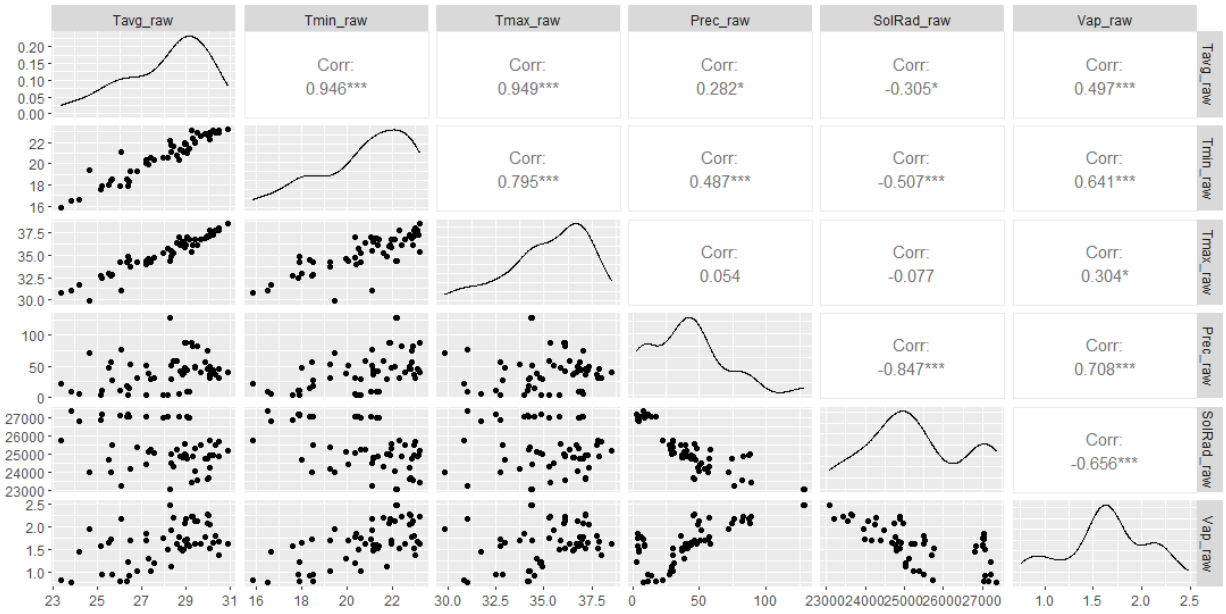


Figure S7. Pairwise correlations among environmental variables extracted from WorldClim data. Variables include mean temperature (T_{avg}), minimum temperature (T_{min}), maximum temperature (T_{max}), precipitation (Prec), solar radiation (SolRad), and vapour pressure (Vap). The upper triangle reports Pearson's correlation coefficients, with asterisks indicating significance levels (* $p < 0.05$; ** $p < 0.01$; *** $p < 0.001$). The diagonal panels show the univariate distributions of each variable. The lower triangle displays scatterplots of raw values for each pairwise comparison. Strong linear relationships indicate high collinearity among variables, whereas diffuse point clouds indicate weaker correlations. This correlation structure informed variable selection and model specification in subsequent analyses.

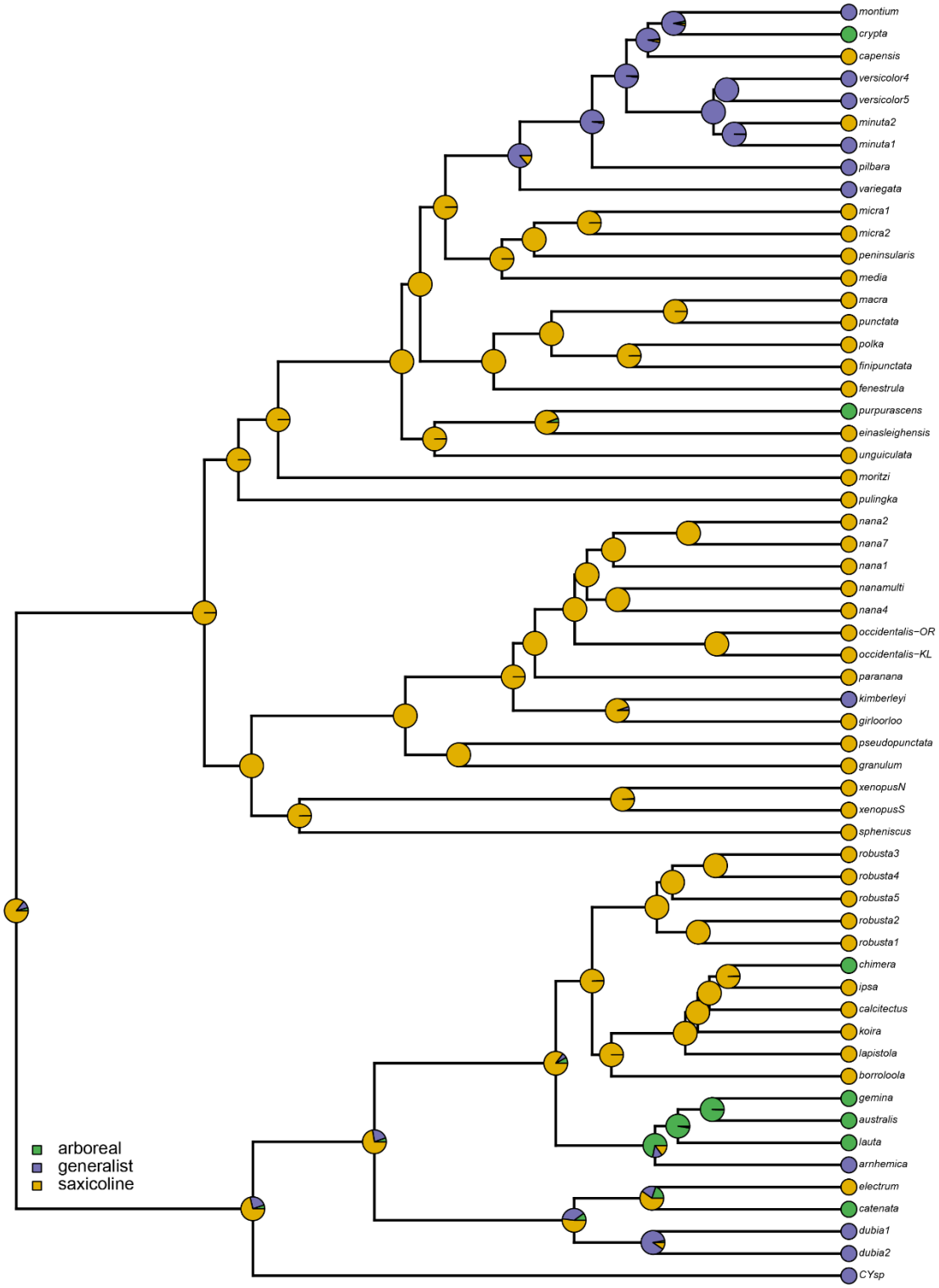


Figure S8. History of substrate use across the *Gehyra* phylogeny, reconstructed by stochastic character mapping (1,000 simulations) under an equal-rates Mk model, selected over symmetric and all-rates-different models by AICc, with the transition rate sampled from its posterior distribution. Pie charts at nodes show the proportion of simulations in which each substrate use state occurred; tip colours show observed substrate use (green = arboreal, purple = generalist, orange = saxicoline). A minimum of 12 transitions was required to explain the distribution of substrate use among lineages (Fitch parsimony); stochastic character mapping estimated 15 transitions (95% interval 12–22).

Table S4. Results of multivariate phylogenetic regressions (mvGLS) testing all pairwise interaction models among the three retained climatic predictors: vapour pressure (Vap), maximum temperature (T_{max}), and precipitation (Prec). These variables were retained after removing highly collinear predictors (see Methods and Fig. S7). Each model includes an interaction term and was evaluated using Type III permutation-based MANOVA (Pillai's trace, 10,000 permutations). Corrected p-values are adjusted for multiple testing across the three models, separately for each term (Benjamini & Hochberg, 1995); inference on the selected Vap × T_{max} model uses uncorrected values (see Methods).

Model	Effect	Stat	p	p (corrected)
Vap × T_{max}	Vap	0.640	0.010	**0.026**
	T_{max}	0.573	0.144	0.433
	Vap:T_{max}	0.610	0.046	0.116
Prec × T_{max}	Prec	0.631	0.017	**0.026**
	T_{max}	0.530	0.370	0.544
	Prec:T_{max}	0.593	0.077	0.116
Vap × Prec	Vap	0.609	0.039	**0.039**
	Prec	0.499	0.544	0.544
	Vap:Prec	0.543	0.278	0.278

Table S5. Joint mvGLS model including substrate use and climate (substrate use + Vap × T_{max}), fitted with the same phylogeny and model structure as the main analyses and evaluated with Type III permutation-based MANOVA (Pillai's trace, 10,000 permutations). r is the correlation across peaks between coefficients from the joint model and from the corresponding separate model (for substrate use, the saxicoline vs other contrast). Substrate use and climate were not confounded: each substrate use category spanned nearly the full range of lineage-mean vapour pressure (arboreal 0.94–2.22 kPa, generalist 0.79–2.27 kPa, saxicoline 0.76–2.48 kPa) and maximum temperature (32.5–37.4°C, 30.4–37.7°C, 30.8–38.6°C).

Effect	Stat	p	r
Substrate use	1.300	**0.001**	0.997
Vap	0.674	**0.003**	0.982
T_{max}	0.584	0.162	0.998
Vap:T_{max}	0.617	0.059	0.988

Table S6. Chemical signal peak loadings from PCA, together with regression coefficients from multivariate phylogenetic regressions (mvGLS) for substrate use, vapour pressure (Vap), maximum temperature (T_{max}), and the Vap × T_{max} interaction. Substrate use was modelled as a three-level factor (arboreal, Arb; generalist, Gen; saxicoline, Sax). Substrate columns give coefficients for each pairwise contrast (Sax–Arb and Sax–Gen significant; Gen–Arb not significant) and for the contrast between saxicoline lineages and the unweighted mean of arboreal and generalist lineages (Sax–Other; see Fig. 4). Climate coefficients are per standard deviation of the predictor. Loadings and coefficients indicate the relative contribution of each chemical peak to the corresponding multivariate axis or predictor, and are comparable within but not across columns. For each column, peaks with values ≥ 70% of the largest absolute loading or coefficient are highlighted in bold to identify dominant contributors to multivariate chemical divergence.

			Substrate use						
Peak	PCA1	PCA2	Sax–Arb	Sax–Gen	Gen–Arb	Sax–Other	Vap	T_{max}	Vap x T_{max}
1	**-0.202**	-0.074	-0.131	-0.802	0.671	-0.467	-0.087	0.226	-0.042
2	**-0.201**	-0.108	-0.617	-0.725	0.108	-0.671	-0.076	0.067	0.127
3	-0.062	**0.192**	0.117	-0.495	0.612	-0.189	0.123	0.119	-0.151
4	-0.074	**0.185**	-0.390	-0.715	0.325	-0.552	0.015	0.027	-0.045
5	**-0.207**	0.026	-0.617	**-1.100**	0.483	-0.859	-0.027	0.076	0.056
6	**-0.236**	-0.051	-0.789	**-1.077**	0.288	**-0.933**	-0.007	0.035	0.155
7	**-0.226**	-0.131	**-1.072**	-0.970	-0.102	**-1.021**	-0.107	-0.005	0.009
8	**-0.192**	-0.011	-0.677	**-1.058**	0.382	-0.867	-0.182	-0.026	0.197
9	**-0.240**	-0.070	-0.839	-0.846	0.007	-0.842	-0.024	-0.014	0.064
10	**-0.216**	-0.099	-0.872	-0.718	-0.155	-0.795	-0.126	-0.004	0.046
11	**-0.194**	-0.047	-0.706	-0.941	0.235	-0.823	0.030	0.080	-0.133
12	**-0.211**	-0.144	-0.748	-0.810	0.062	-0.779	-0.127	0.146	-0.083
13	0.002	0.084	-0.086	-0.166	0.080	-0.126	-0.301	-0.198	-0.148
14	0.065	**0.217**	0.515	0.018	0.497	0.266	0.133	-0.058	0.033
15	-0.056	0.096	-0.280	-0.190	-0.090	-0.235	0.290	-0.285	-0.106
16	0.004	**0.232**	0.285	-0.469	**0.754**	-0.092	-0.148	0.039	-0.085
17	-0.051	0.178	-0.065	-0.287	0.222	-0.176	0.106	-0.026	0.134
18	0.071	**0.221**	0.247	-0.338	0.585	-0.045	0.137	0.165	-0.211
19	0.084	**0.255**	0.509	-0.081	0.590	0.214	0.005	0.151	-0.155
20	0.010	**0.225**	-0.073	-0.443	0.371	-0.258	-0.000	0.193	-0.148
21	0.028	0.031	-0.111	-0.324	0.213	-0.218	-0.034	0.129	-0.093
22	0.025	**0.263**	-0.787	-0.377	-0.411	-0.582	0.155	-0.237	-0.158
23	0.015	0.079	-0.625	-0.253	-0.372	-0.439	0.104	0.017	-0.093
24	**-0.186**	0.018	**-1.198**	-0.802	-0.396	**-1.000**	0.137	-0.059	0.007
25	-0.067	0.167	-0.008	-0.807	**0.799**	-0.407	-0.032	-0.257	-0.154
26	-0.089	0.106	**-1.022**	0.048	**-1.070**	-0.487	0.433	**-0.437**	0.298
27	-0.026	0.001	-0.436	0.253	-0.689	-0.092	-0.001	**-0.370**	0.008
28	0.025	-0.003	0.001	0.389	-0.388	0.195	-0.004	-0.077	-0.138
29	**0.169**	-0.005	0.004	0.749	-0.745	0.376	-0.021	-0.102	-0.071
30	0.148	0.184	0.452	0.389	0.062	0.420	0.093	-0.156	0.127
31	0.076	0.011	0.462	0.455	0.007	0.459	-0.031	-0.165	-0.031
32	0.067	-0.094	0.052	0.509	-0.457	0.281	-0.191	-0.151	-0.217
33	0.073	-0.162	0.697	0.474	0.224	0.585	-0.131	-0.010	-0.001
34	0.158	-0.054	0.541	**1.323**	**-0.781**	**0.932**	0.039	-0.114	0.025
35	0.163	-0.004	-0.164	0.871	**-1.035**	0.354	0.352	-0.100	0.063
36	**0.183**	0.044	0.383	0.606	-0.223	0.494	0.455	-0.205	0.024
37	0.142	-0.147	**1.122**	0.823	0.300	**0.973**	-0.189	-0.021	-0.141
38	0.047	0.012	-0.489	0.023	-0.512	-0.233	**0.652**	-0.260	**0.499**
39	0.156	-0.019	0.254	0.848	-0.594	0.551	0.289	-0.108	**0.418**
40	0.142	-0.027	0.851	0.873	-0.022	0.862	-0.230	-0.047	0.037
41	0.140	0.017	0.736	0.717	0.019	0.727	-0.341	0.152	-0.270
42	**0.174**	-0.098	0.601	**1.023**	-0.422	0.812	0.186	-0.131	0.018
43	0.132	**-0.201**	**1.112**	0.972	0.140	**1.042**	-0.076	0.039	-0.121
44	**0.168**	-0.165	**1.134**	**1.394**	-0.261	**1.264**	-0.085	0.192	-0.101

			Substrate use						
Peak	**PCA1**	**PCA2**	**Sax–Arb**	**Sax–Gen**	**Gen–Arb**	**Sax–Other**	**Vap**	**T_{max}**	**Vap x T_{max}**
45	**0.207**	-0.086	**1.459**	**1.077**	0.382	**1.268**	-0.331	0.134	-0.113
47	0.121	0.030	0.468	0.208	0.260	0.338	-0.019	0.042	0.194
48	**0.178**	-0.141	**1.250**	0.738	0.512	**0.994**	0.015	0.014	0.129
49	0.086	0.008	-0.398	-0.254	-0.144	-0.326	0.323	-0.109	0.169
50	0.064	-0.029	0.660	0.299	0.360	0.479	-0.264	-0.008	0.042
51	0.026	-0.112	0.823	0.453	0.370	0.638	-0.387	0.168	0.093
52	0.112	-0.079	0.639	0.543	0.096	0.591	-0.062	-0.064	0.067
53	-0.081	-0.153	-0.149	-0.117	-0.033	-0.133	-0.089	0.025	0.101
54	-0.103	0.071	**-1.128**	-0.419	-0.709	-0.774	0.283	0.024	0.231
55	0.075	**-0.217**	0.576	0.832	-0.256	0.704	-0.013	0.216	-0.184
56	0.088	-0.166	0.675	0.746	-0.071	0.711	-0.148	0.236	-0.186
57	-0.010	-0.112	-0.219	0.165	-0.384	-0.027	0.166	0.008	-0.154
58	-0.019	-0.111	0.636	0.053	0.583	0.344	-0.076	0.245	0.029
59	-0.071	-0.125	0.517	0.180	0.337	0.349	-0.295	**0.353**	0.037
60	-0.020	**-0.211**	-0.365	0.230	-0.595	-0.067	-0.077	0.180	-0.073
61	0.017	-0.120	-0.039	-0.025	-0.014	-0.032	-0.076	0.284	-0.094

Methods S4. Sensitivity to Intraspecific Variation—Resampling approach

To assess the robustness of the lineage-means approach used in mvGLS analyses, we implemented a resampling procedure that explicitly incorporated individual-level variation. For this comparison, all chemical peaks were standardised at the individual level prior to analysis, ensuring that coefficient estimates derived from resampling and lineage-mean mvGLS models were directly comparable. This differs from the main analyses presented in the manuscript, where predictors and responses were standardised at the lineage level to maximise robustness for phylogenetic comparative inference.

Instead of analysing lineage means directly, we randomly selected one individual per lineage and refitted the mvGLS model using the same phylogeny and model structure. We repeated this procedure 10,000 times for both the substrate use model (three-level factor) and the Vap × T_{max} interaction model, generating distributions of regression coefficients for each chemical peak. For substrate use, we retained coefficients for all four contrasts (saxicoline vs arboreal, saxicoline vs generalist, generalist vs arboreal, and saxicoline vs other). We then calculated mean resampled coefficients for each peak and compared these values to coefficients obtained from the corresponding lineage-means mvGLS models. Coefficients from the two approaches showed a near 1:1 correspondence (Figs S9–S15). For substrate use, resampled and lineage-level coefficients were strongly correlated for all four contrasts (Pearson r = 0.977–0.993; Spearman ρ = 0.977–0.989). For the Vap × T_{max} model, correlations were r = 0.95, 0.90 and 0.91 for vapour pressure, maximum temperature and their interaction (Spearman ρ = 0.92, 0.86 and 0.89).

Frequency distributions of resampled coefficients further showed that lineage-means estimates closely matched the central tendency of the resampled distributions (Figs S16–S22). The dominant peaks were also stable across iterations: the nine dominant peaks for the saxicoline vs other contrast (Table S6) retained the same sign in 97.6–100% of iterations, with 95% resampling intervals excluding zero, and the strongest contributors were largely shared between the lineage-means and resampling analyses (Figs S23–S29). The generalist vs arboreal contrast was the least stable (sign retention of dominant peaks 89.8–98.2%), consistent with its non-significance in the main analysis. Dominant climate peaks (Table S6) also retained their sign in most iterations: peak 38 for vapour pressure (98.9%), peaks 26, 27 and 59 for maximum temperature (94.4–99.0%), and peaks 38 and 39 for the vapour pressure × maximum temperature interaction (95.2–97.1%). The top five peaks for each climate term were largely shared between approaches (three of five for vapour pressure, five of five for maximum temperature and for the interaction). However, 95% resampling intervals for the dominant interaction peaks overlapped zero, indicating that interaction coefficients are more sensitive to within-lineage variation than the main effects. These results indicate that the peaks used for the Bayesian MCMCglmm analyses (Methods S5), which were selected from the main mvGLS results, reflect patterns that are robust to within-lineage variation.

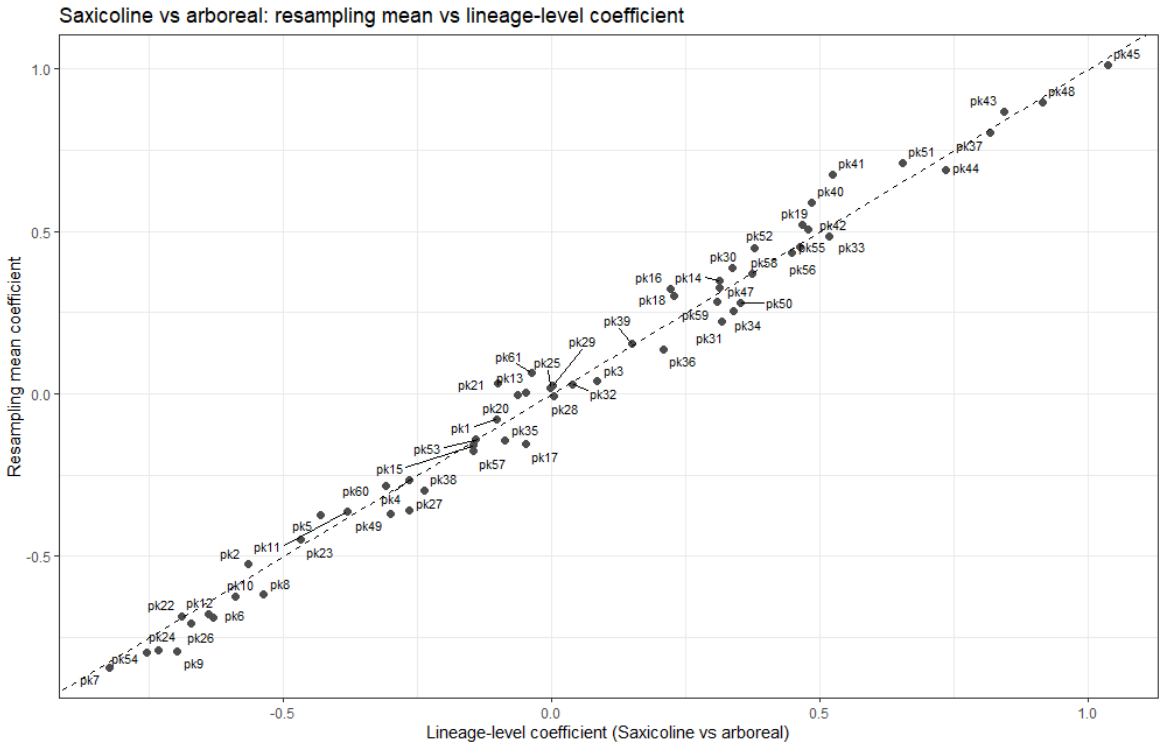


Figure S9. Scatter plot of mvGLS regression coefficients for the saxicoline vs arboreal substrate use contrast for each chemical signal peak, estimated using the resampling approach (y-axis), against coefficients estimated from the lineage-mean mvGLS model (x-axis). The dashed line represents a 1:1 relationship between methods (Pearson r = 0.993; Spearman ρ = 0.989).

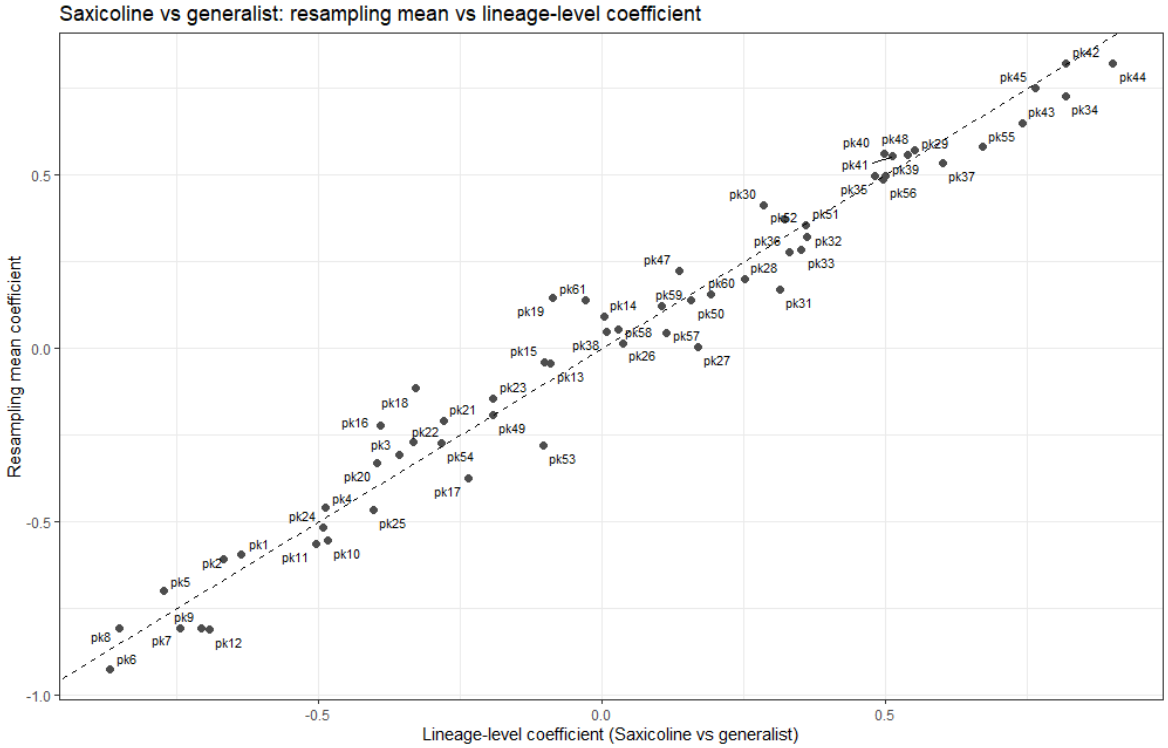


Figure S10. Scatter plot of mvGLS regression coefficients for the saxicoline vs generalist substrate use contrast for each chemical signal peak, estimated using the resampling approach (y-axis), against coefficients estimated from the lineage-mean mvGLS model (x-axis). The dashed line represents a 1:1 relationship between methods (Pearson r = 0.984; Spearman ρ = 0.982).

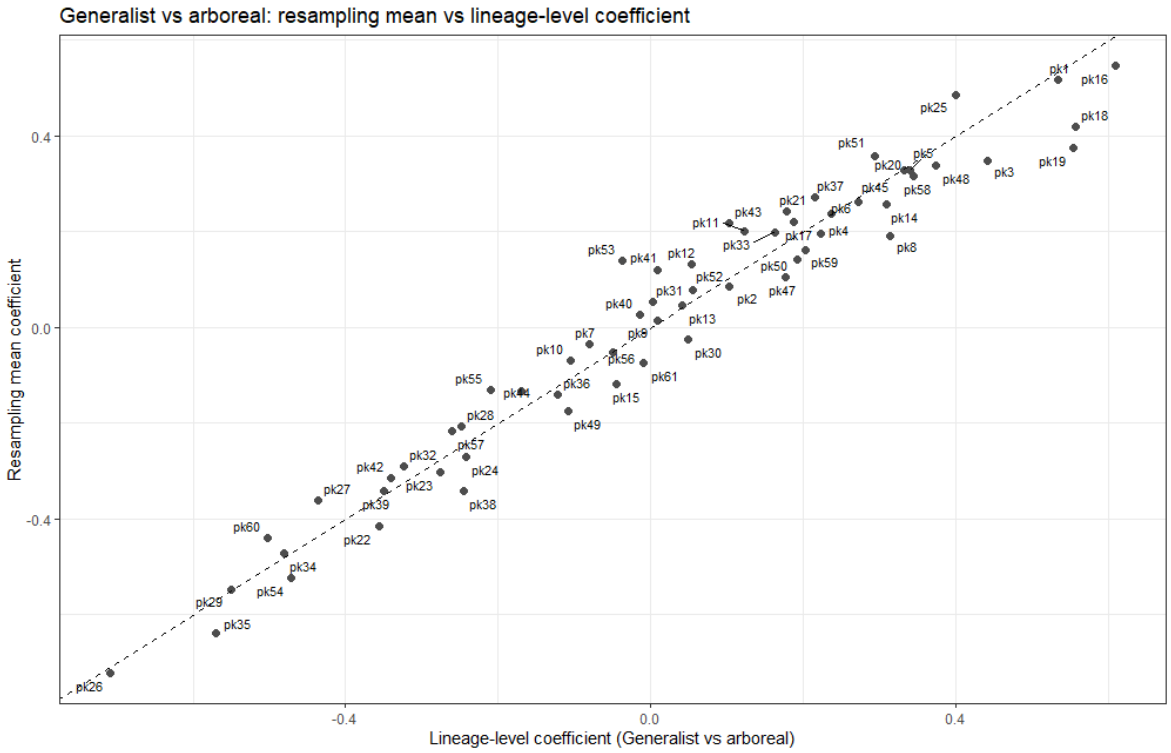


Figure S11. Scatter plot of mvGLS regression coefficients for the generalist vs arboreal substrate use contrast for each chemical signal peak, estimated using the resampling approach (y-axis), against coefficients estimated from the lineage-mean mvGLS model (x-axis). The dashed line represents a 1:1 relationship between methods (Pearson r = 0.977; Spearman ρ = 0.977).

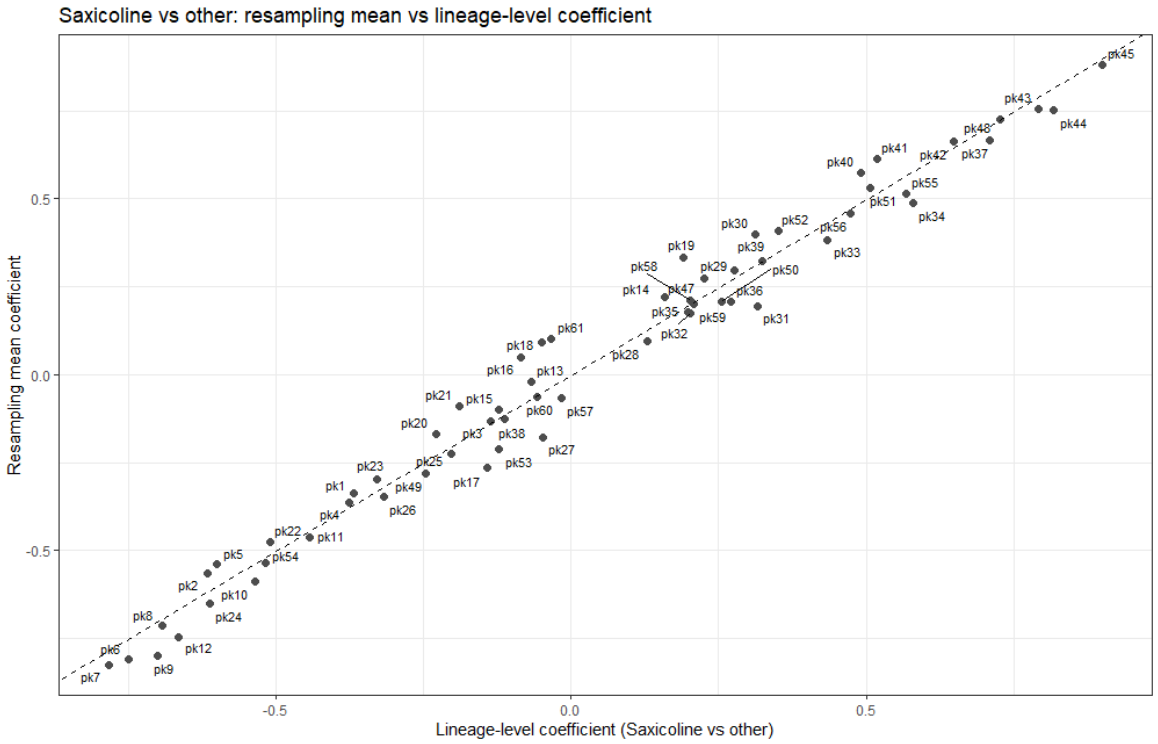
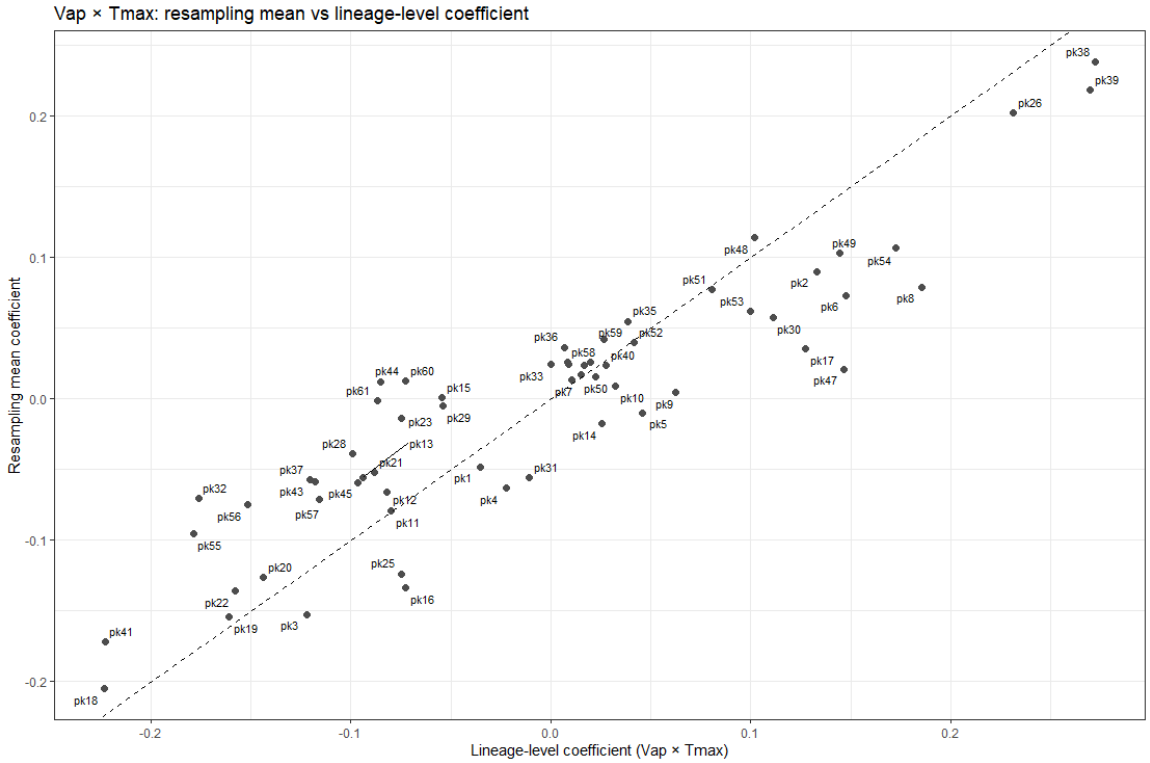
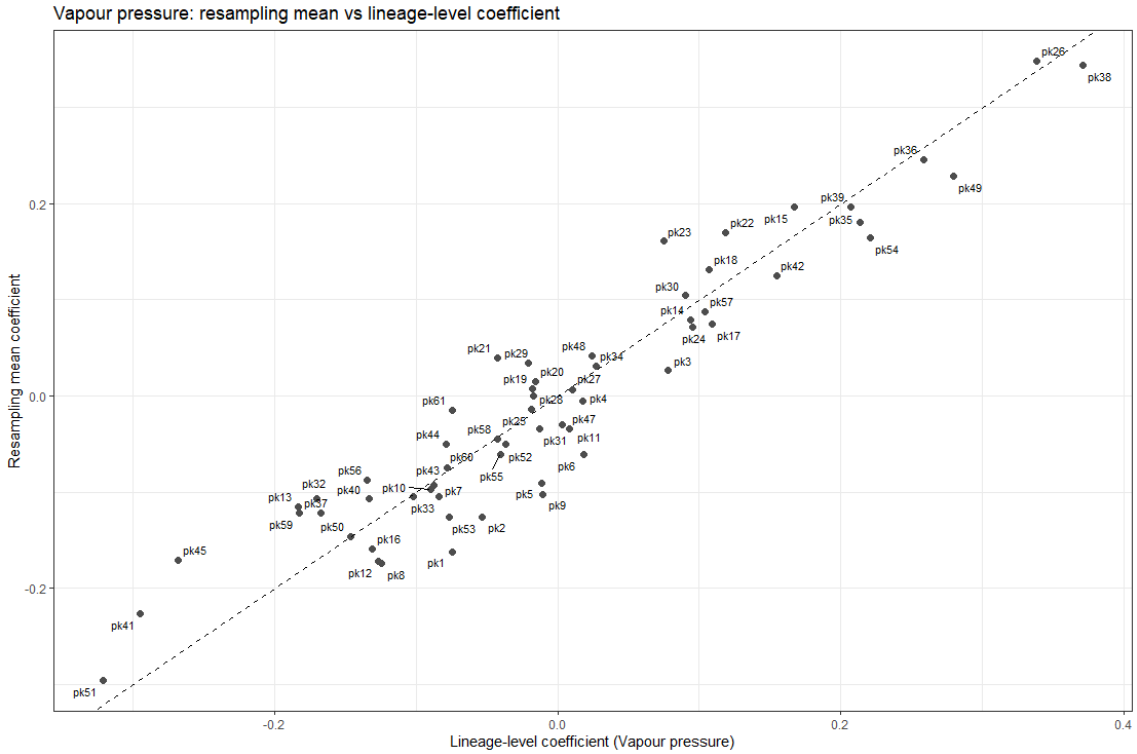


Figure S12. Scatter plot of mvGLS regression coefficients for the saxicoline vs other substrate use contrast (saxicoline vs the mean of arboreal and generalist) for each chemical signal peak, estimated using the resampling approach (y-axis), against coefficients estimated from the lineage-mean mvGLS model (x-axis). The dashed line represents a 1:1 relationship between methods (Pearson r = 0.990; Spearman ρ = 0.984).

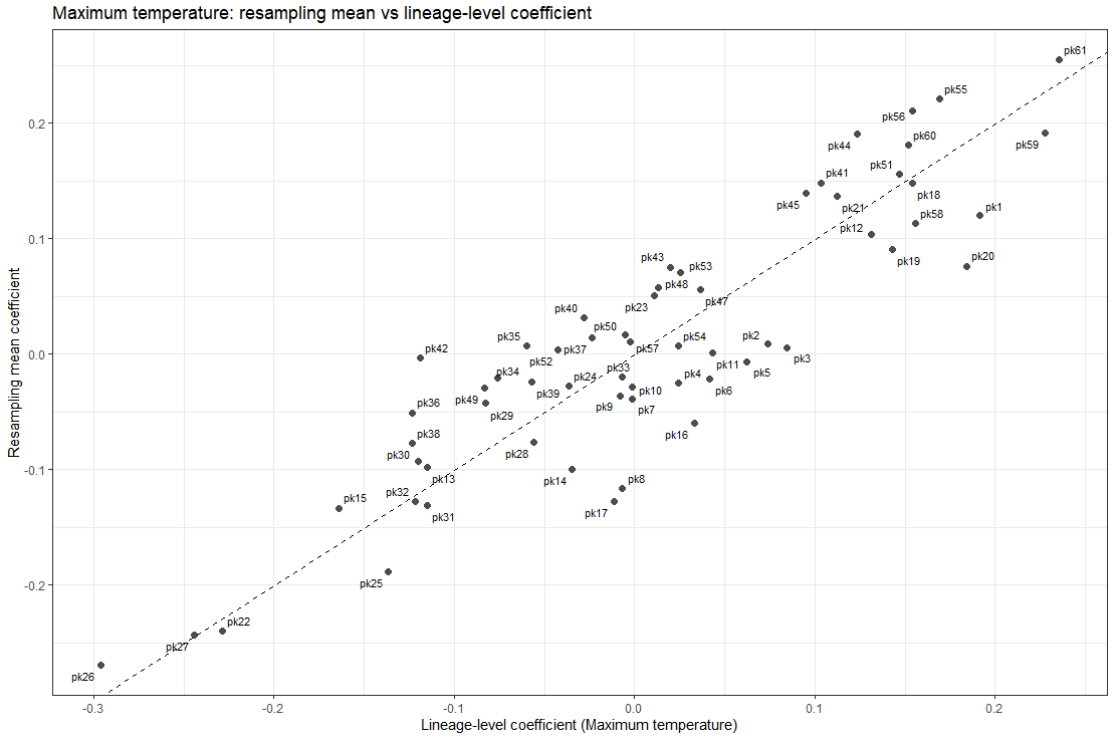


255 **Figure S13.** Scatter plot of mvGLS regression coefficients for the Vap × Tmax interaction for each chemical signal
256 peak, estimated using the resampling approach (y-axis), against coefficients estimated from the lineage-mean
257 mvGLS model (x-axis). The dashed line represents a 1:1 relationship between methods (Pearson r = 0.910;
258 Spearman ρ = 0.894).

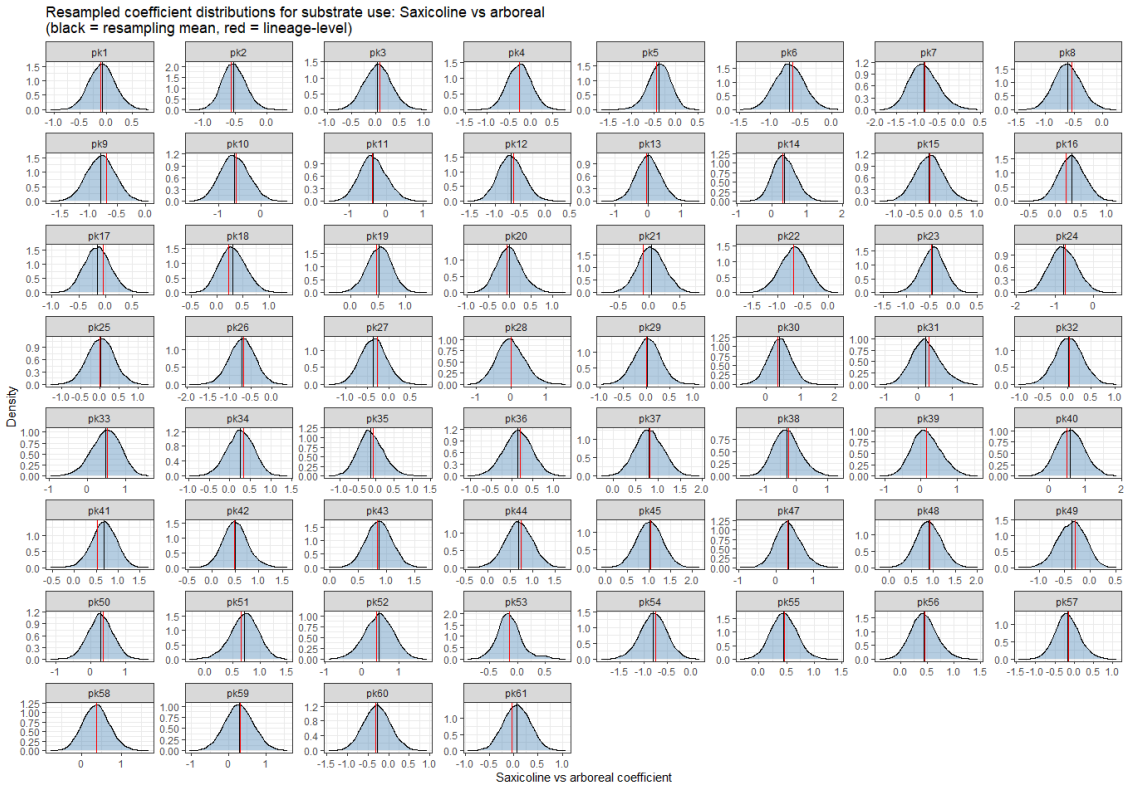


259 **Figure S14.** Scatter plot of mvGLS regression coefficients for vapour pressure (Vap) for each chemical signal
260 peak, estimated using the resampling approach (y-axis), against coefficients estimated from the lineage-mean
261 mvGLS model (x-axis). The dashed line represents a 1:1 relationship between methods (Pearson r = 0.950;
262 Spearman ρ = 0.917).

263



264 **Figure S15.** Scatter plot of mvGLS regression coefficients for maximum temperature (Tmax) for each chemical
265 signal peak, estimated using the resampling approach (y-axis), against coefficients estimated from the lineage-
266 mean mvGLS model (x-axis). The dashed line represents a 1:1 relationship between methods (Pearson r =
267 0.900; Spearman ρ = 0.859).



268 **Figure S16.** Frequency distributions of regression coefficients for each chemical signal peak estimated from the
269 resampling approach for the saxicoline vs arboreal substrate use contrast. Density curves show the distribution
270 of coefficients for each peak across 10,000 iterations. The red vertical line indicates the coefficient estimated
271 from the lineage-mean mvGLS model, and the black vertical line indicates the mean coefficient across
272 resampling iterations.

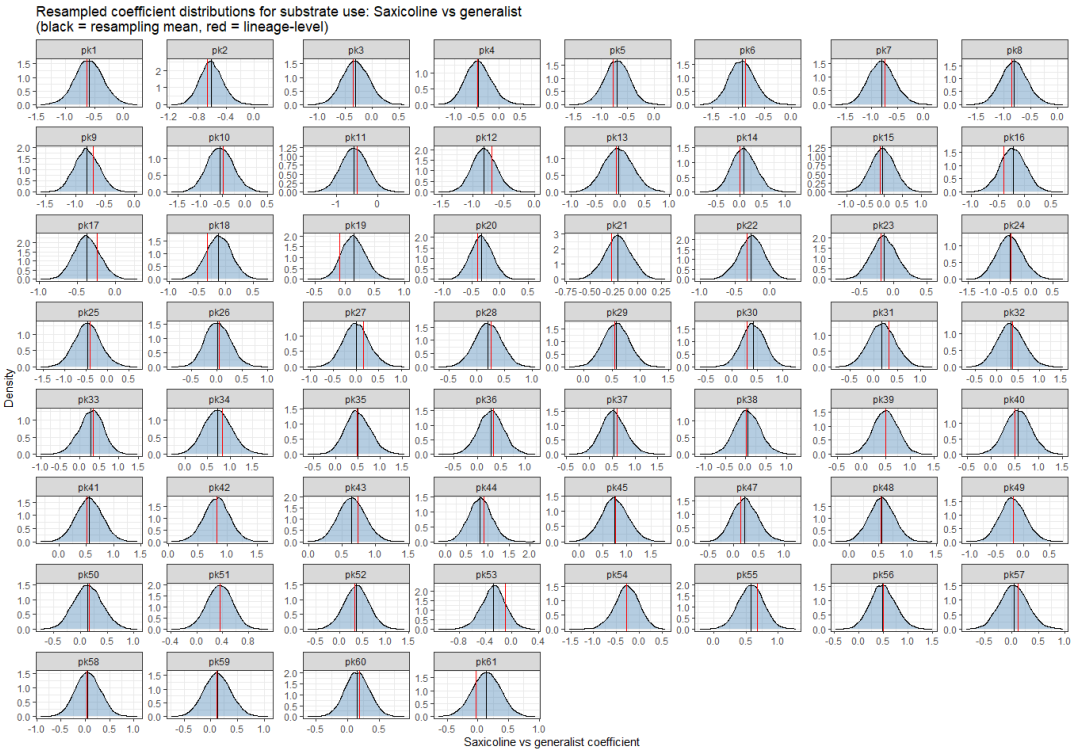


Figure S17. Frequency distributions of regression coefficients for each chemical signal peak estimated from the resampling approach for the saxicoline vs generalist substrate use contrast. Density curves show the distribution of coefficients for each peak across 10,000 iterations. The red vertical line indicates the coefficient estimated from the lineage-mean mvGLS model, and the black vertical line indicates the mean coefficient across resampling iterations.

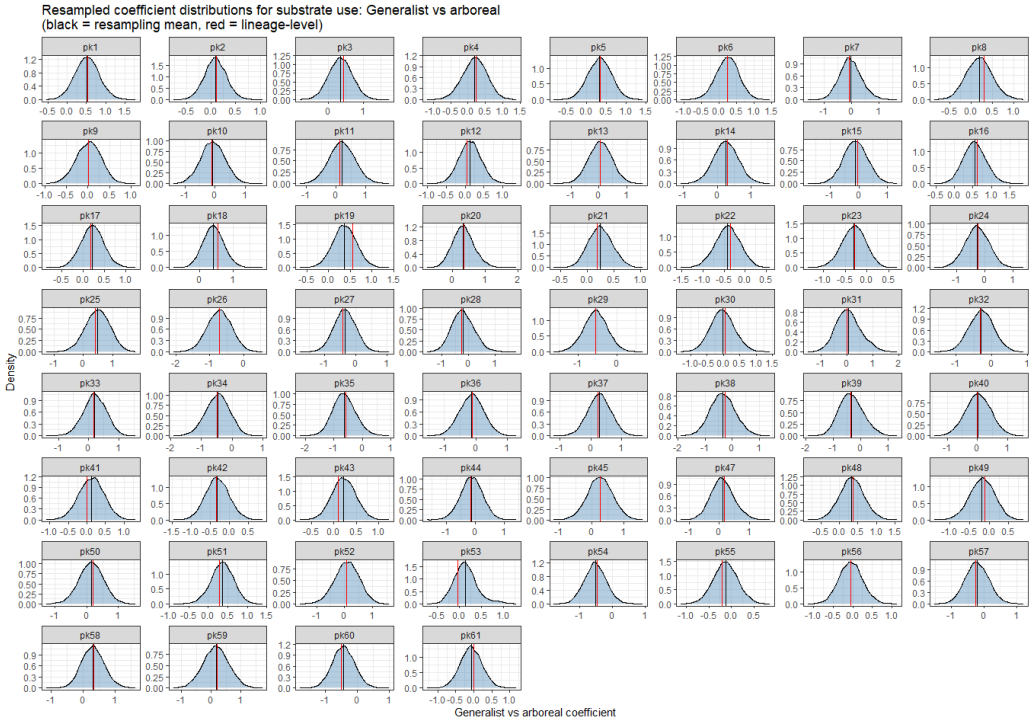


Figure S18. Frequency distributions of regression coefficients for each chemical signal peak estimated from the resampling approach for the generalist vs arboreal substrate use contrast. Density curves show the distribution of coefficients for each peak across 10,000 iterations. The red vertical line indicates the coefficient estimated from the lineage-mean mvGLS model, and the black vertical line indicates the mean coefficient across resampling iterations.

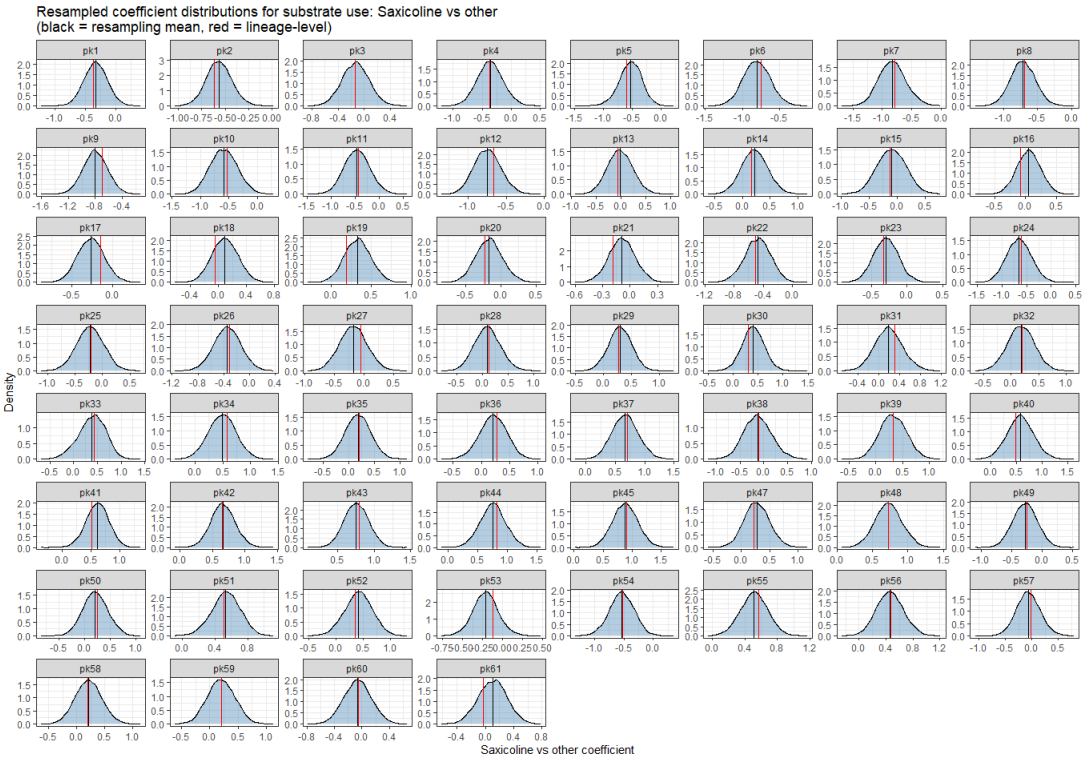


Figure S19. Frequency distributions of regression coefficients for each chemical signal peak estimated from the resampling approach for the saxicoline vs other substrate use contrast (saxicoline vs the mean of arboreal and generalist). Density curves show the distribution of coefficients for each peak across 10,000 iterations. The red vertical line indicates the coefficient estimated from the lineage-mean mvGLS model, and the black vertical line indicates the mean coefficient across resampling iterations.

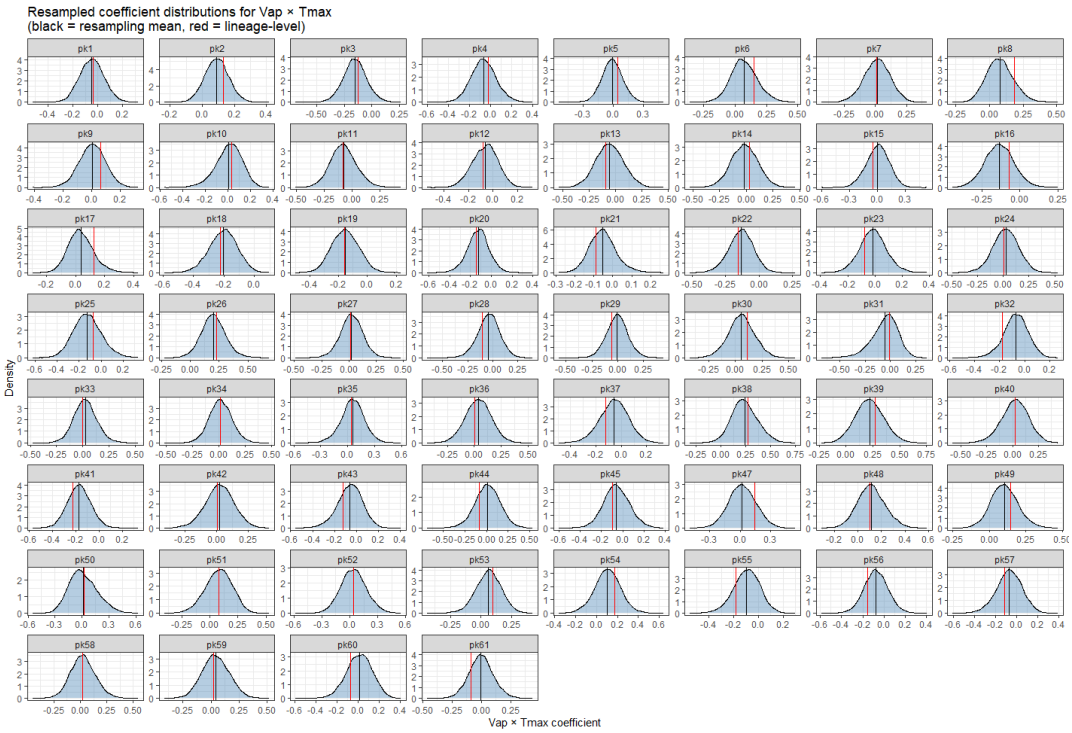
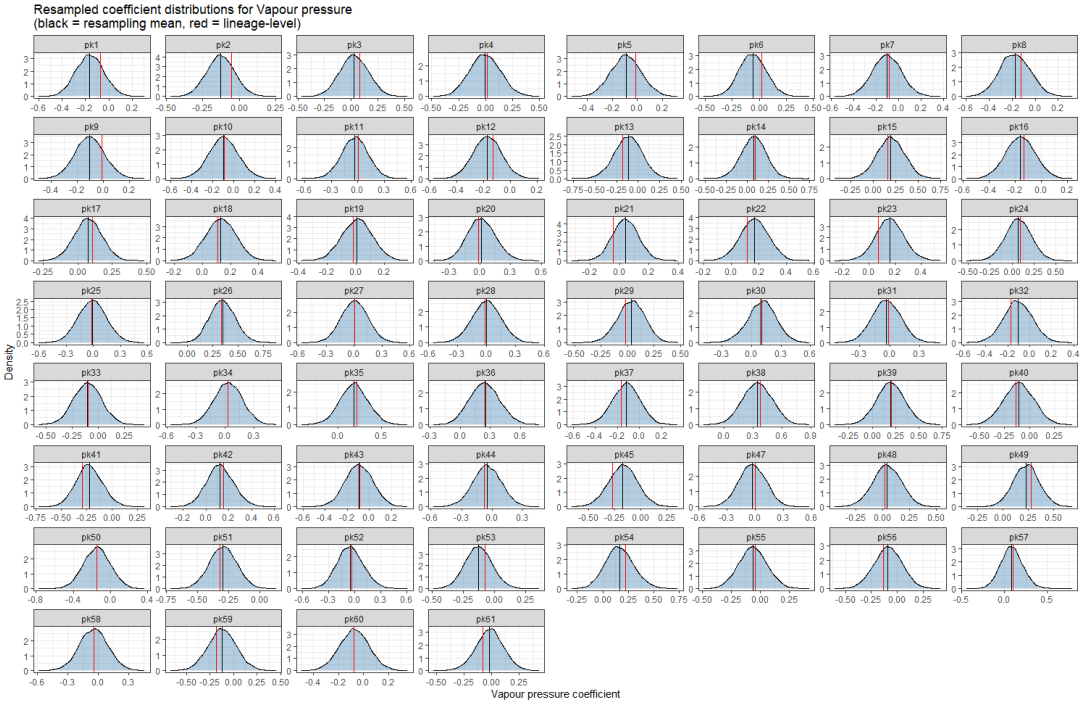
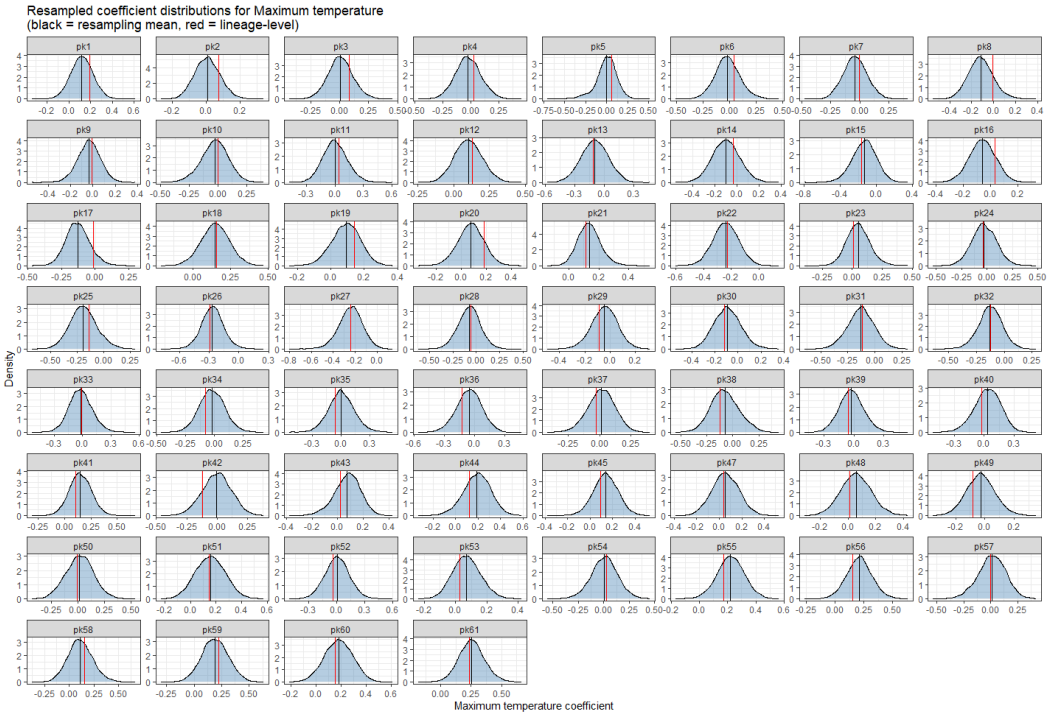


Figure S20. Frequency distributions of regression coefficients for each chemical signal peak estimated from the resampling approach for the Vap × T_{max} interaction model. Density curves show the distribution of coefficients for each peak across 10,000 iterations. The red vertical line indicates the coefficient estimated from the lineage-mean mvGLS model, and the black vertical line indicates the mean coefficient across resampling iterations.



293 **Figure S21.** Frequency distributions of regression coefficients for each chemical signal peak estimated from the
294 resampling approach for Vap from the Vap × T_{max} interaction model. Density curves show the distribution of
295 coefficients for each peak across 10,000 iterations. The red vertical line indicates the coefficient estimated from
296 the lineage-mean mvGLS model, and the black vertical line indicates the mean coefficient across resampling
297 iterations.



298 **Figure S22.** Frequency distributions of regression coefficients for each chemical signal peak estimated from the
299 resampling approach for T_{max} from the Vap × T_{max} interaction model. Density curves show the distribution of
300 coefficients for each peak across 10,000 iterations. The red vertical line indicates the coefficient estimated from
301 the lineage-mean mvGLS model, and the black vertical line indicates the mean coefficient across resampling
302 iterations.

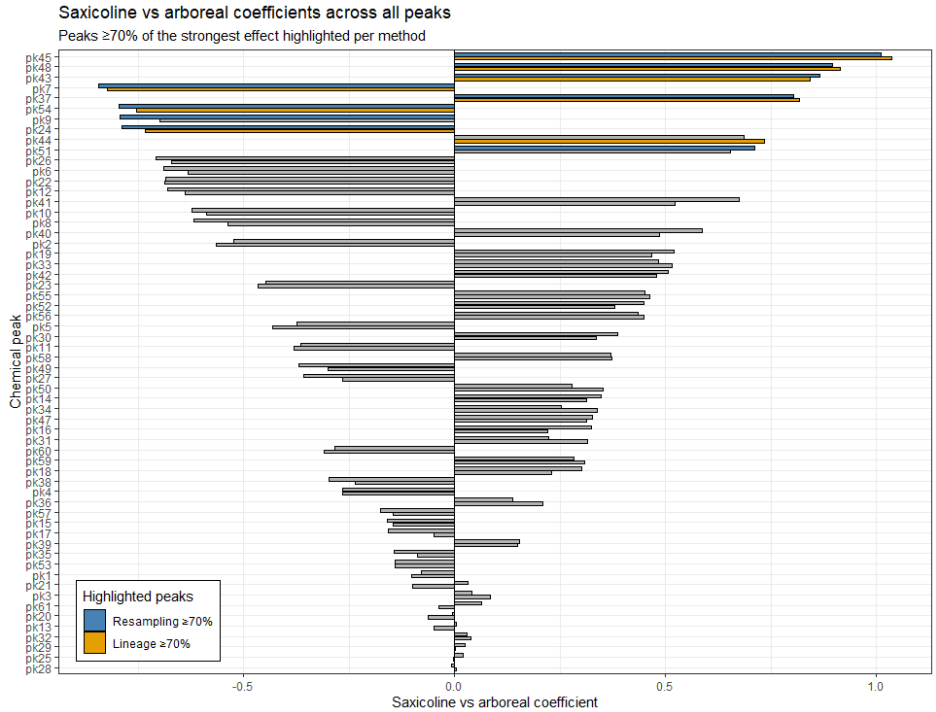


Figure S23. Coefficients for the saxicoline vs arboreal substrate use contrast for all chemical peaks, estimated using two approaches: resampling of individuals within lineages and lineage-mean models. Bars show regression coefficients for each peak; peaks ≥ 70% of the largest absolute coefficient per method are highlighted (blue, resampling; orange, lineage-mean), with remaining peaks in grey. Both approaches identified the same five top-ranking peaks.

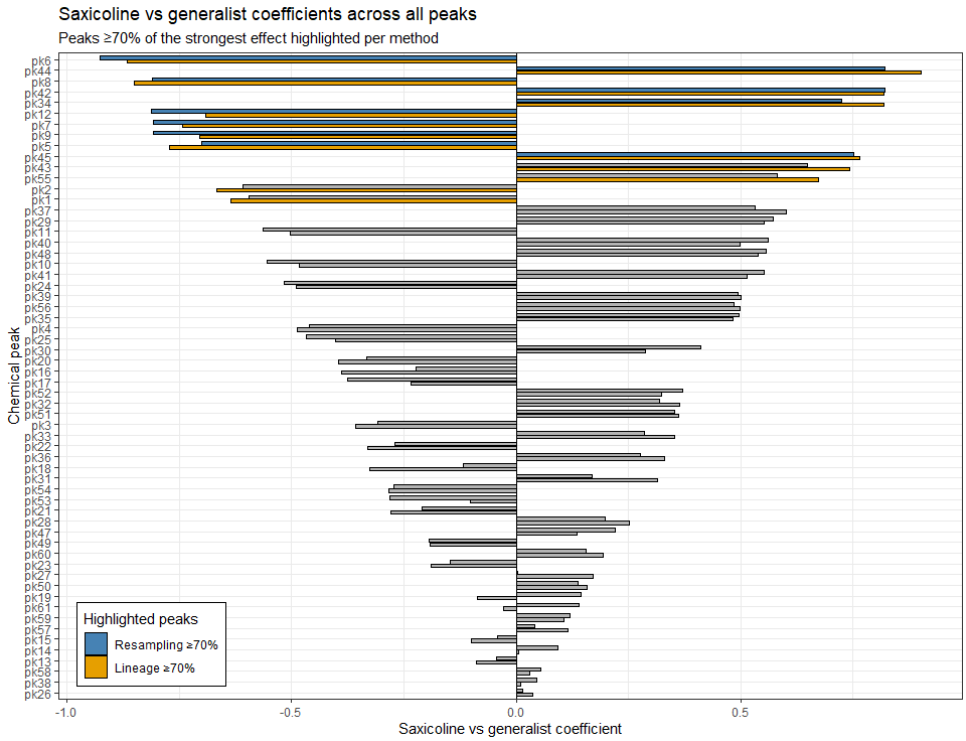


Figure S24. Coefficients for the saxicoline vs generalist substrate use contrast for all chemical peaks, estimated using two approaches: resampling of individuals within lineages and lineage-mean models. Bars show regression coefficients for each peak; peaks ≥ 70% of the largest absolute coefficient per method are highlighted (blue, resampling; orange, lineage-mean), with remaining peaks in grey. Four of the five top-ranking peaks were shared between approaches.

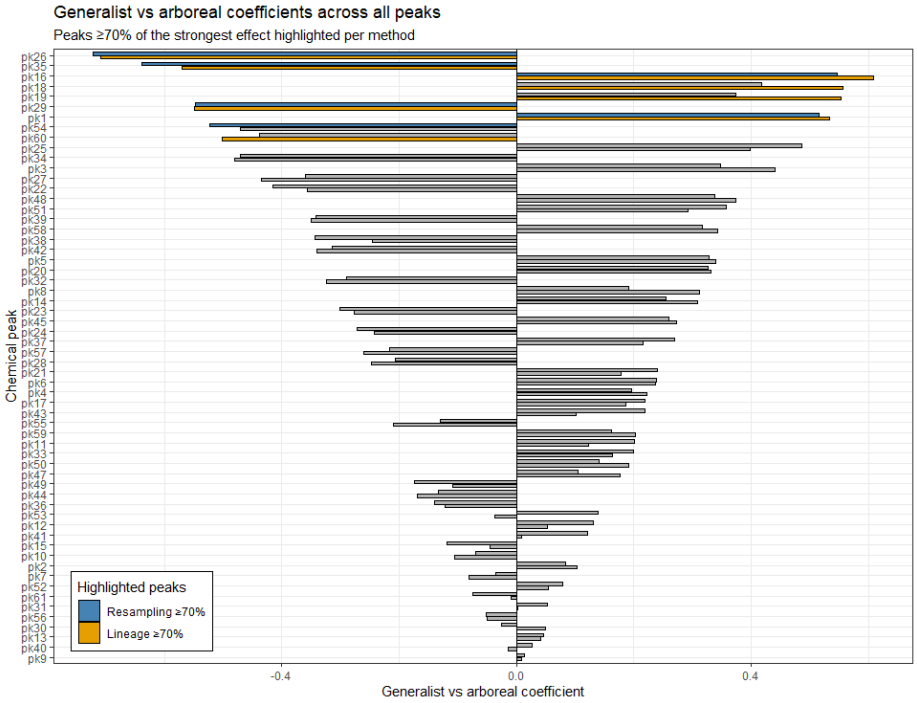


Figure S25. Coefficients for the generalist vs arboreal substrate use contrast for all chemical peaks, estimated using two approaches: resampling of individuals within lineages and lineage-mean models. Bars show regression coefficients for each peak; peaks ≥ 70% of the largest absolute coefficient per method are highlighted (blue, resampling; orange, lineage-mean), with remaining peaks in grey. Three of the five top-ranking peaks were shared between approaches, consistent with the non-significance of this contrast in the main analysis.

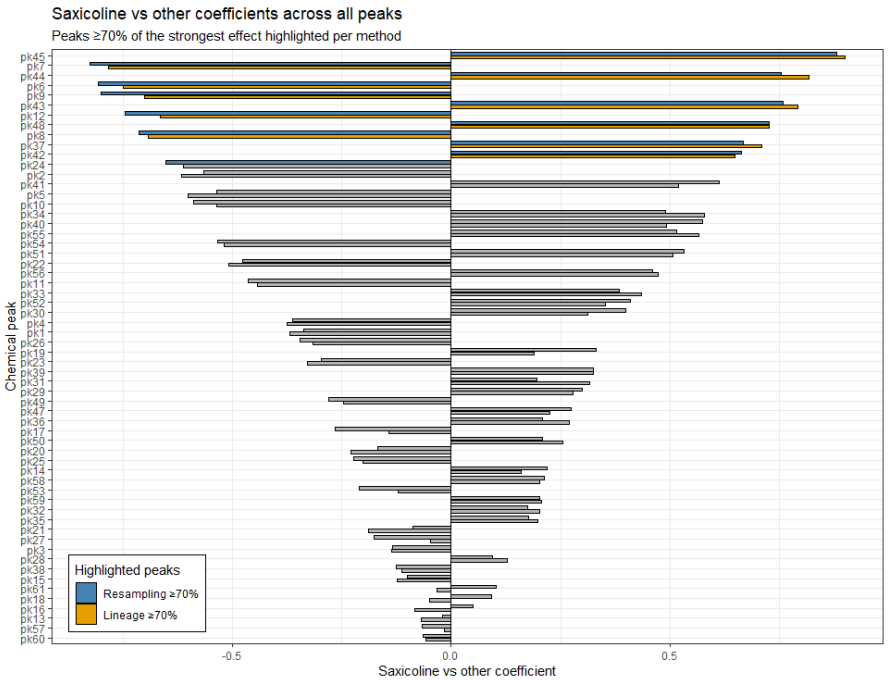


Figure S26. Coefficients for the saxicoline vs other substrate use contrast (saxicoline vs the mean of arboreal and generalist) for all chemical peaks, estimated using two approaches: resampling of individuals within lineages and lineage-mean models. Bars show regression coefficients for each peak; peaks ≥ 70% of the largest absolute coefficient per method are highlighted (blue, resampling; orange, lineage-mean), with remaining peaks in grey. Four of the five top-ranking peaks were shared between approaches.

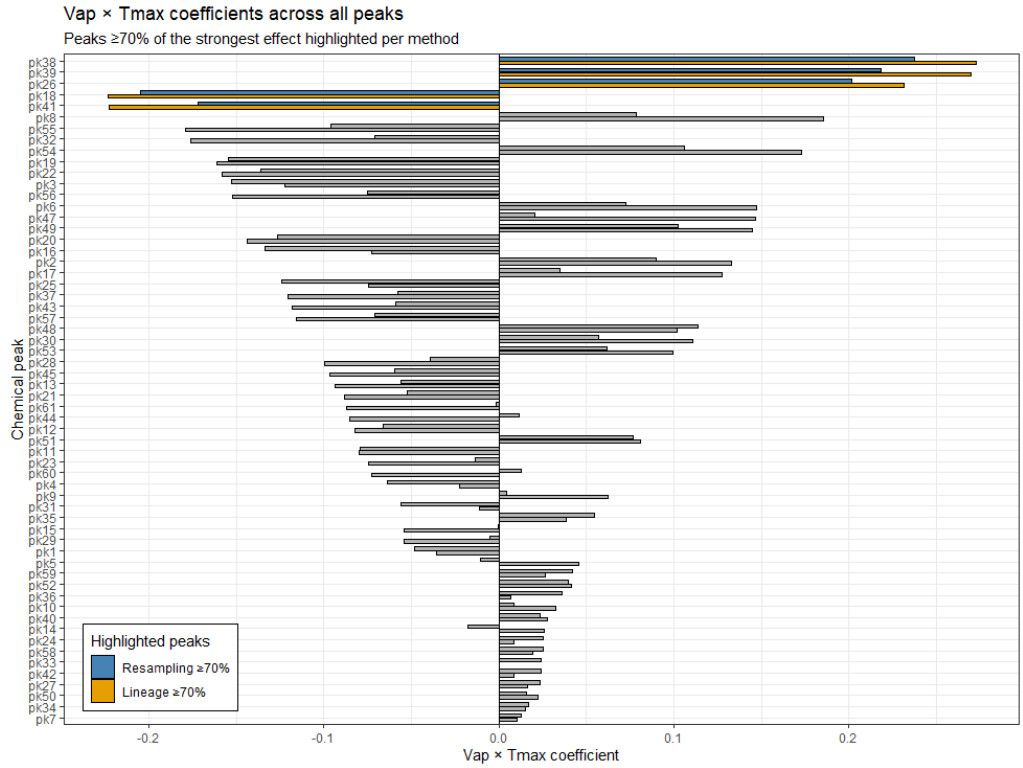


Figure S27. Coefficients for the Vap × T_{max} interaction for all chemical peaks, estimated using two approaches: resampling of individuals within lineages and lineage-mean models. Bars show regression coefficients for each peak; peaks ≥ 70% of the largest absolute coefficient per method are highlighted (blue, resampling; orange, lineage-mean), with remaining peaks in grey. Both approaches identified the same five top-ranking peaks.

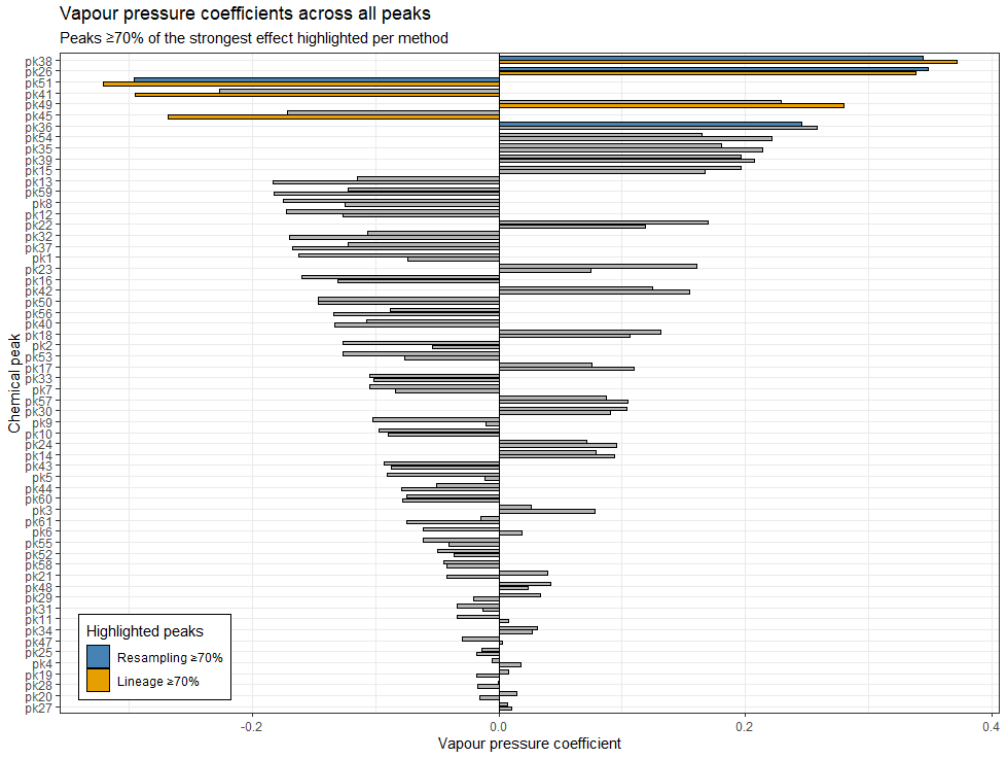


Figure S28. Coefficients for vapour pressure (Vap) from the Vap × T_{max} model for all chemical peaks, estimated using two approaches: resampling of individuals within lineages and lineage-mean models. Bars show regression coefficients for each peak; peaks ≥ 70% of the largest absolute coefficient per method are highlighted (blue, resampling; orange, lineage-mean), with remaining peaks in grey. Three of the five top-ranking peaks were shared between approaches.

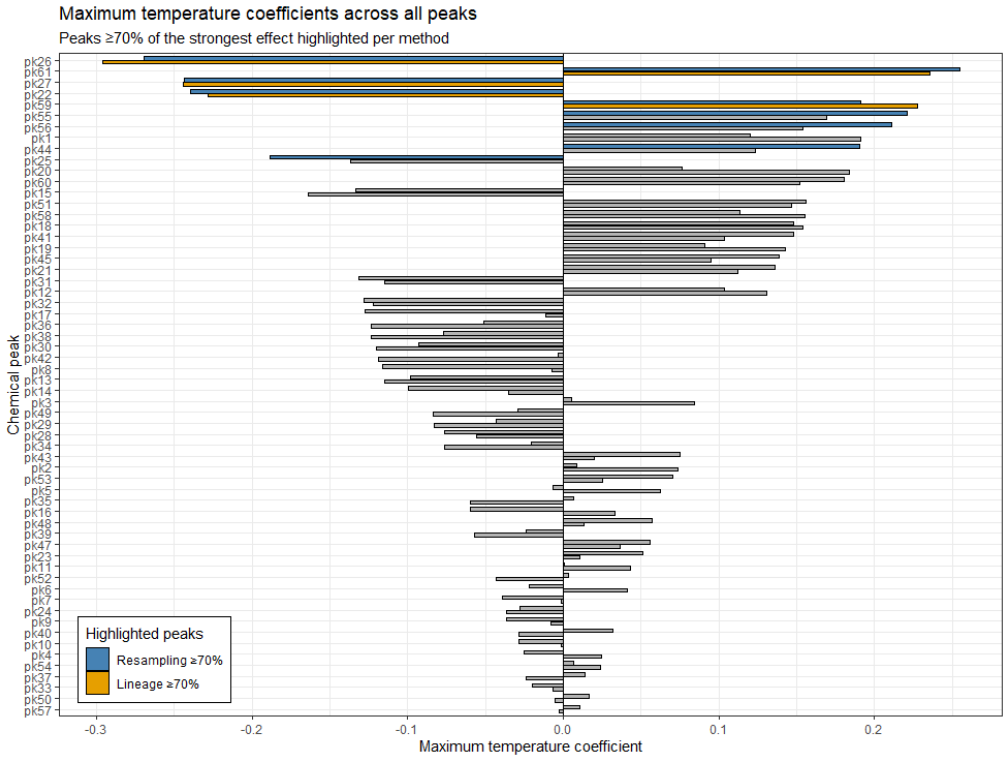


Figure S29. Coefficients for maximum temperature (T_{max}) from the Vap × T_{max} model for all chemical peaks, estimated using two approaches: resampling of individuals within lineages and lineage-mean models. Bars show regression coefficients for each peak; peaks ≥ 70% of the largest absolute coefficient per method are highlighted (blue, resampling; orange, lineage-mean), with remaining peaks in grey. Five of the five top-ranking peaks were shared between approaches.

Methods S5. Sensitivity to Intraspecific Variation—Bayesian models

To further assess the robustness of mvGLS results while explicitly modelling individual-level variation and phylogenetic non-independence, we fitted Bayesian multivariate mixed models using MCMCglmm (Hadfield, 2010). These analyses complement the phylogenetic mvGLS models by retaining individual-level observations rather than lineage means, estimating uncertainty in effects using posterior distributions, and explicitly modelling covariance among chemical traits. All analyses were conducted on individual-level chemical signal data. To ensure stable estimation of within-lineage variance, we retained only lineages represented by at least five individuals, reducing the dataset from 58 to 54 lineages (excluding *G. electrum*, *G. spheniscus*, *G. xenopusN*, and *G. xenopusS*).

Based on the phylogenetic mvGLS results, we selected five chemical signal peaks a priori for Bayesian modelling. For substrate use, these were the five peaks with the largest absolute coefficients for the saxicoline vs other contrast (Table S6): 45, 44, 43, 7, and 24. For the climate analysis, peaks were ranked separately by their vapour pressure and Vap × T_{max} coefficients, and the five with the highest single rank across the two terms were selected, with ties resolved by the peak's rank on the other term: 38, 39, 36, 26, and 41. Because the Bayesian model cannot accommodate all ~60 peaks while simultaneously estimating individual-level variance and inter-peak covariance, we restricted it to five peaks per analysis. This selection is deliberately not independent of the mvGLS: the analysis is a sensitivity check asking whether the lineage-level associations persist once intraspecific variation is modelled, not an independent test of their existence. Selecting the most strongly associated peaks necessarily favours detecting the same associations, so we interpret agreement as evidence of consistency rather than as independent corroboration. We standardised all selected peaks to mean zero and unit variance across individuals prior to analysis. To account for phylogenetic non-independence among lineages, we incorporated an inverse relatedness matrix derived from the time-calibrated phylogeny, pruned to include only the relevant tips.

We fitted Bayesian mixed models that analysed all five chemical peaks together while accounting for shared ancestry among lineages. For the substrate use analysis, we asked whether chemical profiles differed among the three substrate use groups (arboreal, generalist, saxicoline), using arboreal as the comparison baseline. We treated the three substrate uses as distinct groups rather than as points along a gradient, consistent with the mvGLS analysis (after filtering; arboreal: 7, generalist: 10, saxicoline: 37 lineages). For the climate analysis, we tested the effects of Vap, T_{max}, and their interaction. In both analyses, every peak was allowed its own response to each predictor, so that peaks could shift in opposite directions. Closely related lineages were expected to have similar chemistry simply through common descent, so we used the phylogeny to model this similarity directly. For the residual (within-lineage) variation we additionally allowed the five peaks to co-vary with one another, as is expected for chemical blend data where peaks are not independent. Because we had only 54 lineages, we estimated the ancestry-related (phylogenetic) variance for each peak separately rather than estimating every pairwise phylogenetic relationship among peaks. We used inverse-Wishart priors with V = I and ν = 5.002 for both the residual and phylogenetic variance components, placing minimal constraint on the estimated variances. Each model was run for 300,000 iterations, discarding the first 50,000 as burn-in and keeping every 50th sample. Model convergence was assessed using Heidelberger and Welch stationarity tests, effective sample sizes for all fixed effects and variance components (minimum ESS = 4062), and visual inspection of trace plots.

To visualise the substrate use results, we projected each individual's chemical profile onto the axis along which substrate use most strongly shifted the chemical blend (the saxicoline vs other contrast, i.e. saxicoline vs the mean of arboreal and generalist, matching Fig. 4), ensuring that peaks moving in opposite directions did not cancel each other out as they would in a simple average.

Because this axis is derived from the fitted contrast, it is a visualisation of the modelled relationship rather than an independent test of it. We show the predicted position of each substrate use group along this axis, with individuals plotted to show the spread within each group (Fig. S30). For the climate analysis we present the per-peak coefficients directly, since the interaction is a per-peak effect that no single summary axis can represent (Fig. S31).

Both analyses showed clear chemical divergence associated with substrate use and with climate. Saxicoline lineages had markedly different chemical profiles from both arboreal lineages (posterior mean difference = 1.979, 95% credible interval [1.477, 2.490], pMCMC < 0.001) and generalist lineages (1.709, [1.242, 2.159], pMCMC < 0.001), whereas arboreal and generalist lineages did not differ detectably (0.269, [−0.259, 0.813], pMCMC = 0.329). All five peaks differed between saxicoline and arboreal lineages in directions consistent with the mvGLS results: 45 (1.122, [0.652, 1.607], pMCMC < 0.001), 44 (0.876, [0.439, 1.322], pMCMC < 0.001), and 43 (0.786, [0.278, 1.287], pMCMC < 0.01) were higher in saxicoline lineages, while 7 (−0.796, [−1.260, −0.323], pMCMC < 0.01) and 24 (−0.822, [−1.225, −0.402], pMCMC < 0.001) were lower. All five also differed between saxicoline and generalist lineages: 45 (0.786, [0.335, 1.237], pMCMC < 0.001), 44 (1.000, [0.585, 1.409], pMCMC < 0.001), 43 (0.753, [0.287, 1.217], pMCMC < 0.01), 7 (−0.693, [−1.116, −0.251], pMCMC < 0.001), and 24 (−0.540, [−0.923, −0.163], pMCMC < 0.01), whereas none differed between arboreal and generalist lineages. For climate, vapour pressure had a clear positive effect on chemical composition, with 38 (0.295, [0.171, 0.419], pMCMC < 0.001) and 36 (0.194, [0.066, 0.315], pMCMC < 0.01) responding positively and 41 negatively (−0.211, [−0.334, −0.089], pMCMC < 0.001), while 39 (0.113, [−0.016, 0.244], pMCMC = 0.085) and 26 (0.102, [−0.021, 0.226], pMCMC = 0.116) were positive in the posterior mean but their credible intervals included zero. Maximum temperature had heterogeneous effects across peaks: 26 showed a clear negative response (−0.203, [−0.311, −0.093], pMCMC < 0.001), while the remaining peaks showed no credible T_{max} effect. Vapour pressure and maximum temperature interacted across multiple peaks, with 38 (0.204, [0.115, 0.296], pMCMC < 0.001), 26 (0.113, [0.026, 0.200], pMCMC < 0.05), and 39 (0.102, [0.009, 0.195], pMCMC < 0.05) all showing stronger vapour-pressure effects at higher temperatures, consistent with the descriptive pattern in the mvGLS (Fig. 5). Notably, 36 showed a clear vapour-pressure effect but no credible interaction (0.043, [−0.049, 0.133], pMCMC = 0.35), indicating that the model distinguished peaks whose response to vapour pressure depends on temperature from those that respond independently of it. The interaction for 41 was negative and fell just short of credibility (−0.083, [−0.166, 0.002], pMCMC = 0.057), in the opposite direction to 38, 39, and 26. These Bayesian results closely matched those from the mvGLS analyses of lineage means, indicating that the patterns are robust to modelling individual-level variation.

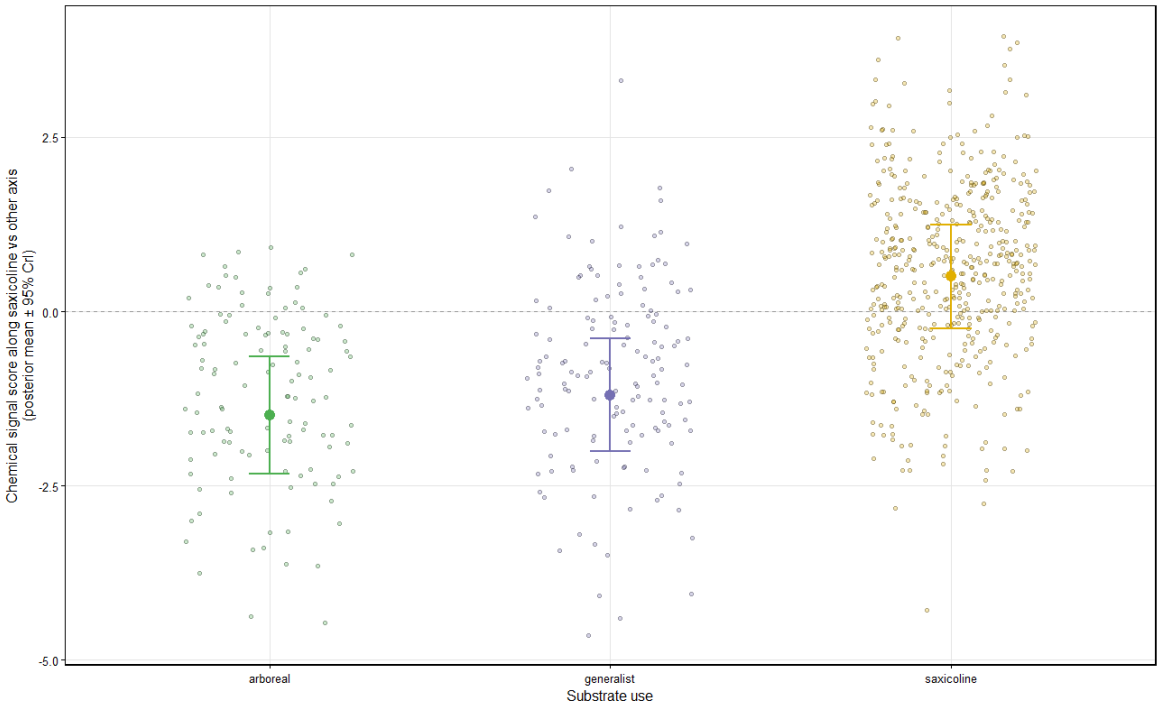


Figure S30. Posterior mean and 95% credible intervals of chemical signal score along the saxicoline vs other chemical axis for each substrate use category (arboreal, generalist, saxicoline), derived from a Bayesian multivariate mixed model (MCMCglmm). The chemical signal score is computed by projecting each individual's five standardised focal peaks (45, 44, 43, 7, 24) onto the unit-normalised posterior mean of the saxicoline vs other contrast vector (saxicoline vs the mean of arboreal and generalist) estimated by the model, weighting peaks by the direction and magnitude of their estimated effect so that 7 and 24 (which shift negatively for saxicoline) contribute appropriately. Points show individual observations projected onto the same axis, illustrating within-substrate use variation, though statistical inference is based on the posterior distributions of the fixed effects rather than on these points. Substrate use colours correspond to those used throughout the main text (green = arboreal, purple = generalist, orange = saxicoline).

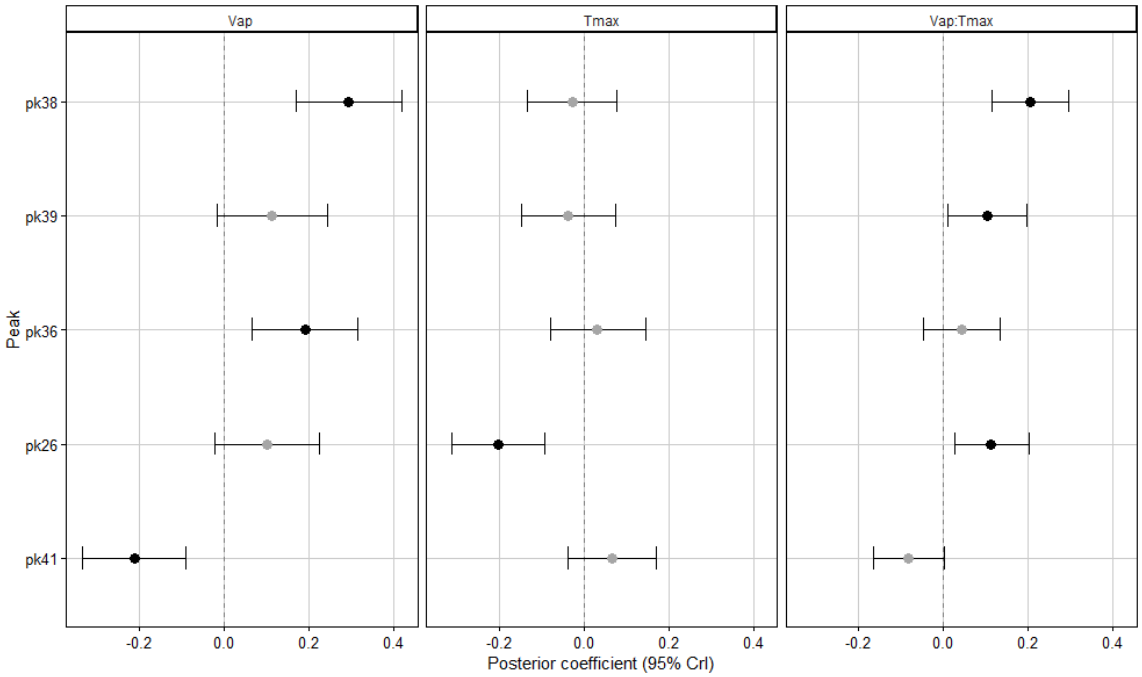


Figure S31. Per-peak posterior coefficients from the Bayesian multivariate mixed model (MCMCglmm) of chemical signal on vapour pressure (Vap), maximum temperature (T_{max}), and their interaction (Vap × T_{max}), for the five climate-associated peaks. Points are posterior means and horizontal bars 95% credible intervals; predictors were standardised, so coefficients are on a common scale. Black points indicate coefficients whose 95% credible interval excludes zero (dashed line); grey points indicate intervals overlapping zero. Each peak was modelled with its own response to every predictor, and the panels show these per-peak effects directly. Vapour pressure shifted composition at several peaks (positive for 38 and 36, negative for 41), the interaction was credible for 38, 39, and 26 (indicating stronger vapour-pressure effects at higher temperatures), and a credible main effect of maximum temperature was confined to 26. Note that 36 responded to vapour pressure but showed no credible interaction, indicating that the model distinguished peaks whose vapour-pressure response depends on temperature from those that respond independently of it.